NASA CR-166,147

NASA CONTRACTOR REPORT 166147

NASA-CR-166147
19820023426

Axisymmetric & Non-Axisymmetric Exhaust Jet Induced
Effects on a V/STOL Vehicle Design
(Part III: Experimental Technique)

W. C. Schnell

CONTRACT NAS2–9887
June 1982

NASA

N82-31302

Axisymmetric & Non-Axisymmetric Exhaust Jet Induced
Effects on a V/STOL Vehicle Design
(Part III: Experimental Technique)

W. C. Schnell
Grumman Aerospace Corp.
Bethpage, NY

NASA

This Page Intentionally Left Blank

CONTENTS

CONTENTS (contd)

ILLUSTRATIONS

ILLUSTRATIONS (contd)

ILLUSTRATIONS (contd)

SYMBOLS & ABBREVIATIONS

ADEN	Augmented Deflector Exhaust Nozzle
AEDC	Arnold Engineering Development Center
AF	Axial Force
AFB	Net axial force after bellows pressure tare force correction
ALBEN	Asymmetric Load Balanced Exhaust Nozzle
ASME	American Society of Mechanical Engineers
A/C	Aircraft
A_t	Nozzle throat area
A_{tL}	Left nozzle throat area
A_{tR}	Right nozzle throat area
A_x	Applied load on balance axial gauge, positive aft
BAL	Balance
BAF	Bellows axial force tare
BIAS. EXINT	Bias weight after interactions
BNF	Bellows normal force tare
C.G.	Center of gravity
CDTR	Thrust-removed drag coefficient
CLTR	Thrust-removed lift coefficient
CNF	Normal cavity tare force
CNTR	Thrust-removed normal force coefficient
CORR	Corrected
CTTR	Thrust-removed axial force coefficient

C_{DIS}	Discharge coefficient
EUBAL	Actual load (including bias) on balance gauge
EXINT	Gauge load after interactions
EXBIAS	Gauge load after biases removed
EXRESOLVED	Gauge loads in same direction summed
EXTARE	Net load after static weight tare removed
F.S.	Fuselage station
F_i	Isentropic ideal thrust
F_{iM}	Isentropic ideal thrust for main balance
F_{iN}	Isentropic ideal thrust for nozzle balance
geom	Geometric
INSTL	Installed
K	Balance primary constant
M	Mach number
MBTP	Data reduction procedure to determine T/R parameters using main balance and P_o-Method
MNF	Normal momentum tare force
NBTF	Data reduction procedure to determine T/R parameters using nozzle balance and F_i-Method
NBTP	Data reduction procedure to determine T/R parameters using nozzle balance and P_o-Method
NFB	Net normal force after bellows pressure tare force correction
NFBC	Net normal force after bellows pressure and cavity tare force corrections
NFBCM	Net normal force after bellows pressure, cavity, and momentum tare force corrections
NOZ	Nozzle
NPR	Nozzle pressure ratio
N_1	Forward normal force gauge output

N_2	Aft normal force gauge output
PMB	Bellows pressure
P_o	Tunnel static pressure
P_T	Nozzle total pressure
P_{TL}	Left nozzle total pressure
P_{TR}	Right nozzle total pressure
P_{TV}	Venturi total pressure
Re	Reynolds number
S	Slope of installed balance calibration curve
T/R	Thrust-removed
T_{SM}	Main balance measured static thrust, negative forward
T_{SN}	Nozzle balance measured static thrust, negative forward
T_T	Total temperature
T_{TV}	Venturi total temperature
UNCORR	Uncorrected
UNINSTL	Uninstalled
VFP	Venturi flow parameter
W	Model weight
W.L.	Water Line
$\dot{W}$	Mass flow
$\dot{W}_L$	Left nozzle mass flow
$\dot{W}_R$	Right nozzle mass flow
$\dot{W}_{TOT}$	Model total mass flow
$\dot{W}_V$	Venturi mass flow
$\dot{W}_{VL}$	Left venturi mass flow
$\dot{W}_{VR}$	Right venturi mass flow
XB	Axial distance from balance center to either N_1 or N_2

XCG	Axial distance between C.G. and balance center
ZCG	Vertical distance between C.G. and balance center
α	Angle of attack
ΔAF	Main balance (axial) disparity parameter
ΔN_1	Actual less computed normal force of forward gauge
ΔN_2	Actual less computed normal force of aft gauge

1 - INTRODUCTION

To contribute to the developing V/STOL air vehicle/non-axisymmetric nozzle data base, the NASA Ames Research Center has sponsored the subject program. A realistic multimission twin-engine V/STOL fighter scale model was tested (June 1979) in the Ames 11 Ft Transonic Wind Tunnel to investigate non-axisymmetric nozzle installed performance and inflight vectoring performance. The Grumman Aerospace Corporation was asked to support this test program because of substantial jet-effects testing experience and, in particular, recent experience with the subject model.

This scale model was previously tested in two other research programs (Ref. 3 and 4), but hardware failures either prevented acquisition of complete aircraft force data or severely limited the test configuration matrix from which worthwhile data could be salvaged. In the subject program, it was possible to obtain complete aircraft force data on all nozzle configurations over a wide range of test conditions.

The overall objective of this program was to acquire complete aircraft longitudinal force data and extensive wing/body surface pressure data on a realistic V/STOL vehicle design in its CTOL mode of operation. These data were used (Ref. 2) to evaluate the aeropropulsion installation effects of different axisymmetric and non-axisymmetric nozzle designs (Fig. 1.1) as well as the effects of thrust vectoring on the lift enhancement and drag characteristics of a non-axisymmetric underwing nacelle installation.

This report discusses the experimental aspects of the static and wind-on testing. Highlights only of the wind tunnel model are presented herein. (A complete discussion of the model appears in Ref. 2.)

Next, a general discussion of jet-effects testing procedures is included. This is followed by a detailed presentation of the flow-through balance and ASME nozzle calibrations. Finally, all major problems encountered during the test are identified and their solutions are explained.

F.S. 50 9

ADEN

W.L. 19.312

NOZZLE METRIC BREAK

ROUND

W.L. 19 312

NOZZLE METRIC BREAK

ALBEN

W.L 19 312

F.S. 50.9
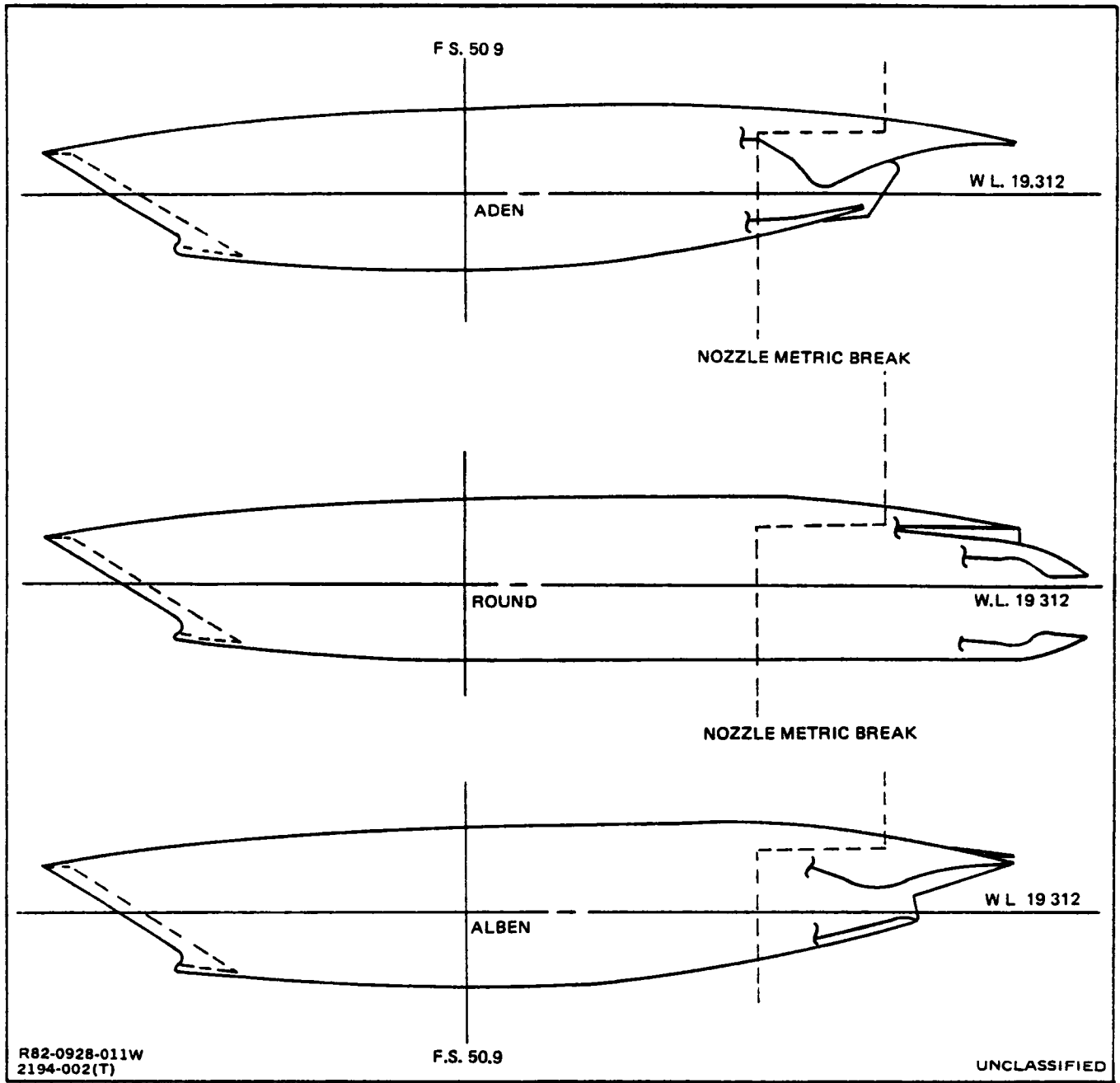
Fig. 1-1 Cruise Nozzle Installation Comparison

2 - WIND TUNNEL MODEL

2.1 MODEL ARRANGEMENT

The model was a 1/8th scale representation of a twin-engine, thrust-vectoring, V/STOL fighter (Fig. 2.1) designed for Navy application. The general assembly and nacelle assembly drawings are presented in Figs. 2-2 and 2-3. A photograph of the model installed in the Ames 11 ft tunnel test section is shown in Fig. 2-4.

Figure 2-5 provides an overview of the model support and air supply systems. As schematically illustrated, the overall model is supported by a bifurcated, twin-boom system which attaches to the vertical tail assemblies. Air supply for powering the model is delivered through the model support system. A representation of the flow path through the model is illustrated in the figure.

A venturi is located in the flow path just upstream of both left and right hand nacelles; this is shown in Fig. 2-6. The venturi tubes are utilized in conjunction with the ASME standard nozzle to determine the left/right tailpipe flow split.

2.2 FORCE BALANCE SYSTEM

The model force balance arrangement is illustrated in Fig. 2-7. With the exception of the vertical tails, the entire model was fully metric to a five component flow-through aircraft main balance (Fig. 2-8). This balance measured total aircraft forces and moments. The main balance metric break was located at the base of the vertical tails. This aircraft force balance was installed near the aircraft c.g. station as shown in Fig. 2-9. A flexible metal bellows arrangement was employed as the method for the airflow to bridge the metric break. This balance was instrumented to provide measuring capability for the three major components of normal force, axial force, and pitching moment. The design limits of these components are ± 5000 lb, ± 800 lb, and ± 25000 in.-lb, respectively.

In addition, a second five-component flow-through balance was employed to measure the forces and moments on the metric section of the left-hand nozzle. This balance attached to the main balance in a "piggy-back" arrangement and was similar to the aircraft force balance in design. The nozzle balance was instrumented to provide ± 200 lb. of normal force, ± 400 lb of axial force and ± 1500 in.-lb of pitching moment.

54 99°

77 875"

F.S 10 625

F S 88 500

A. SIDE VIEW

18 25"

(C.G)
⊕
F.S 56 000

26.50"

45.00"

37°

53 17°

B. TOP VIEW

15 00°

5.00°

R82-0928-012W
2194-001(T)

C. FRONT VIEW

UNCLASSIFIED
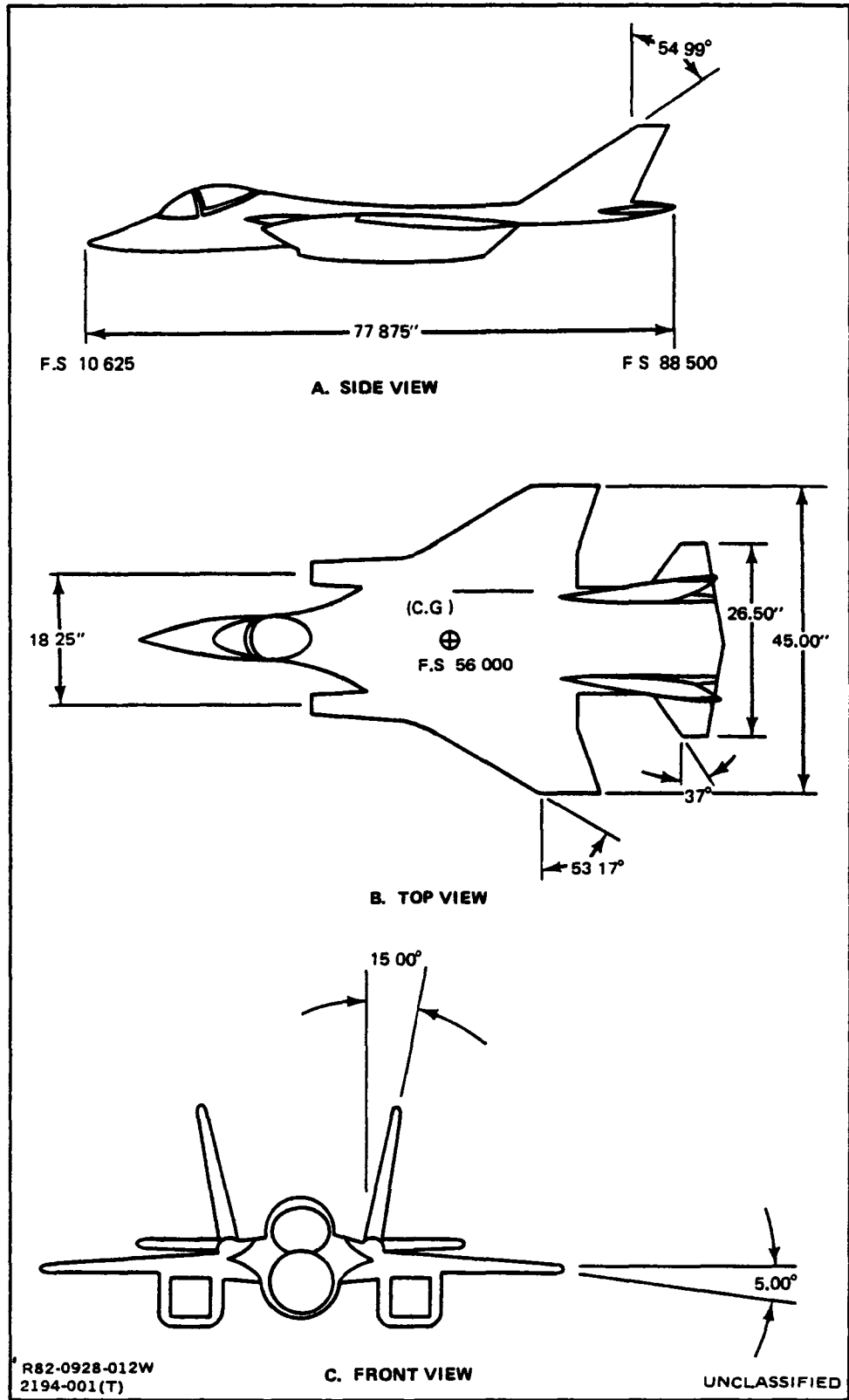
Fig. 2-1 Navy V/STOL High-Speed Model 623-20048

R82-0928-013W
2194-003(T)
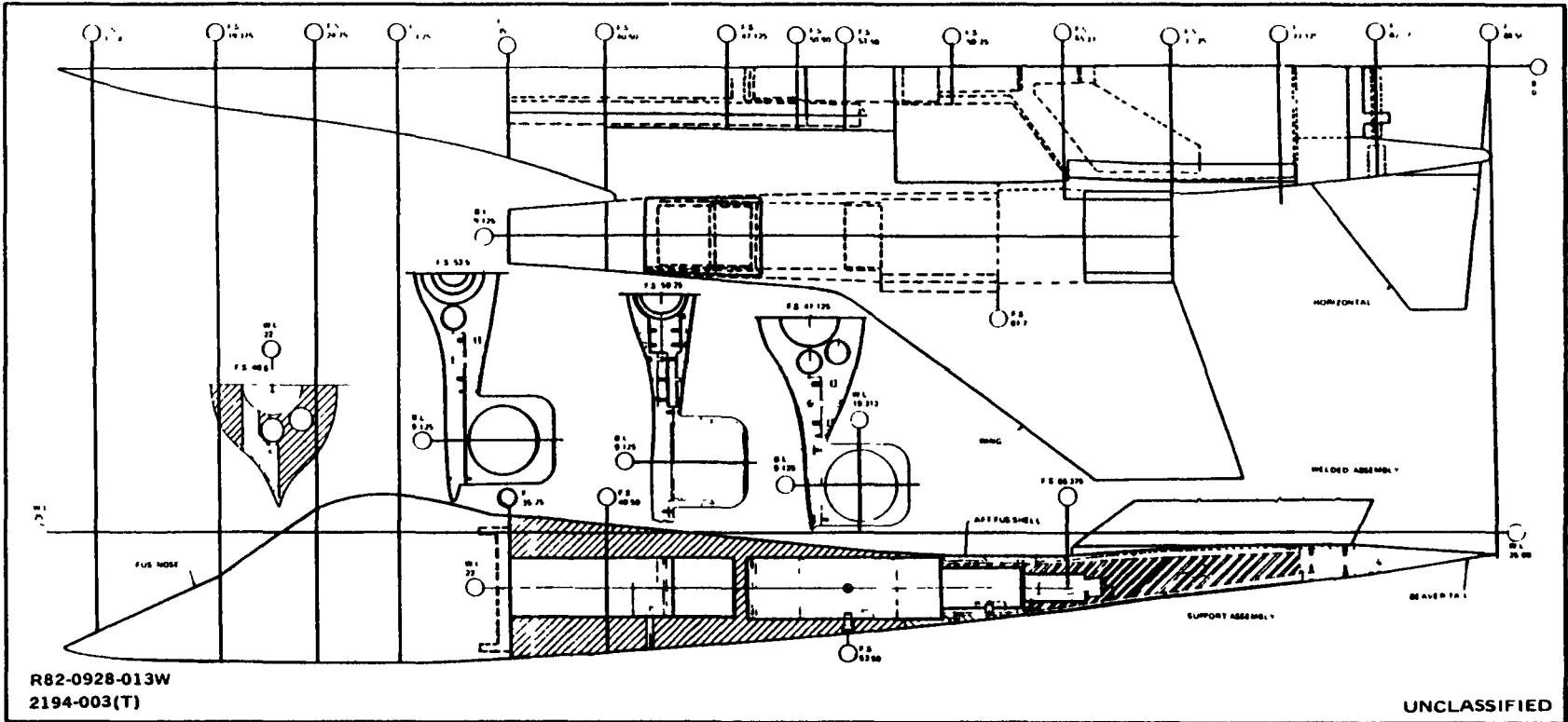
Fig. 2-2 General Assembly Drawing

RH NACELLE

NACELLE

ADAPTER

SECTION AT W L 19.312

S L
9.125

F.S
60.50

F.S
50.80

F.S
61.7

F.S
71.25

W L
29

SECTION AT METRIC BREAK
F.S 61.7

METRIC BREAK

WING

SEAL

CHOKE
PLATES

W L
19.312

NOZZLES

R82-0928-014W
2194-004(T)
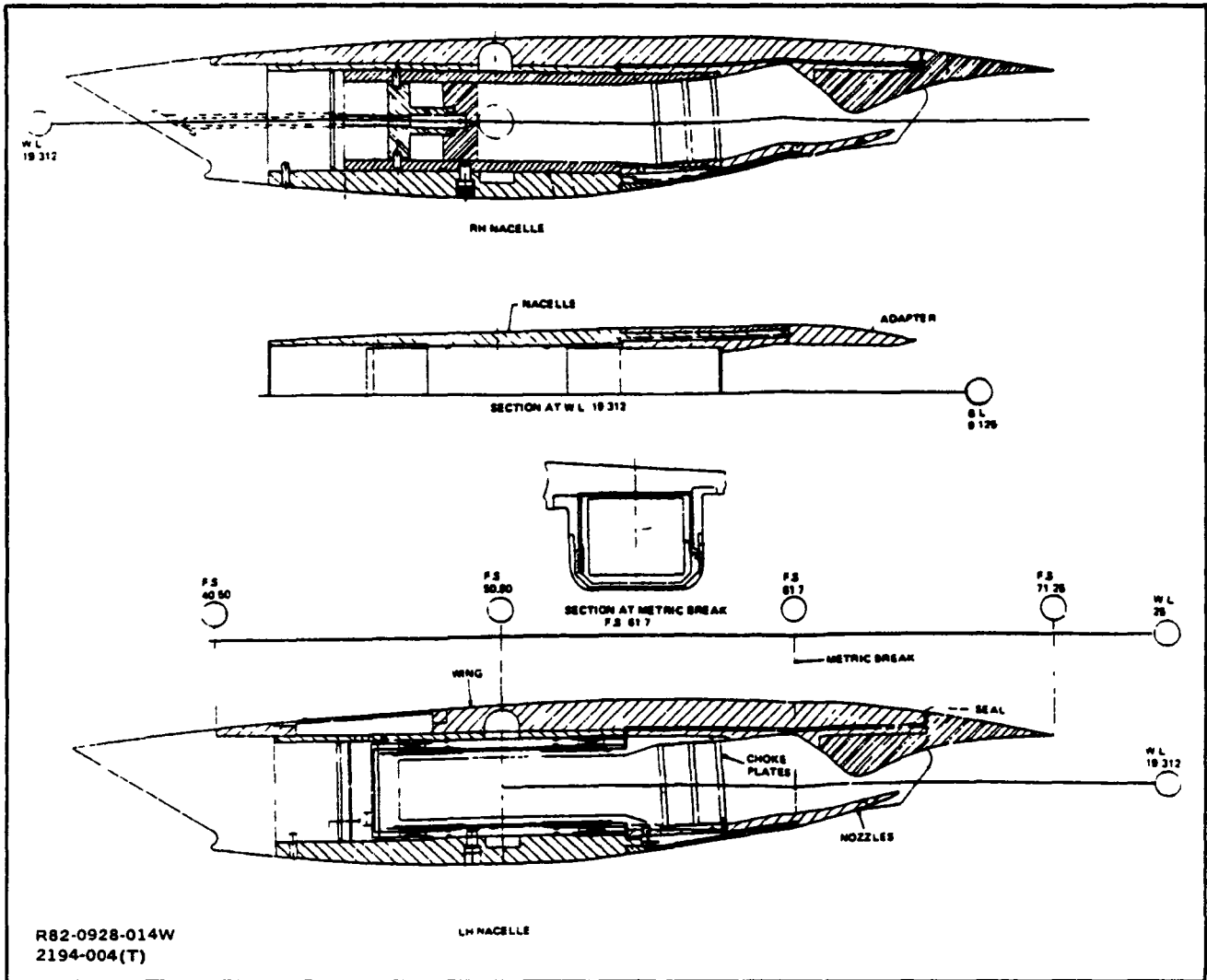
LH NACELLE

Fig. 2-3 Nacelle Assembly Drawing
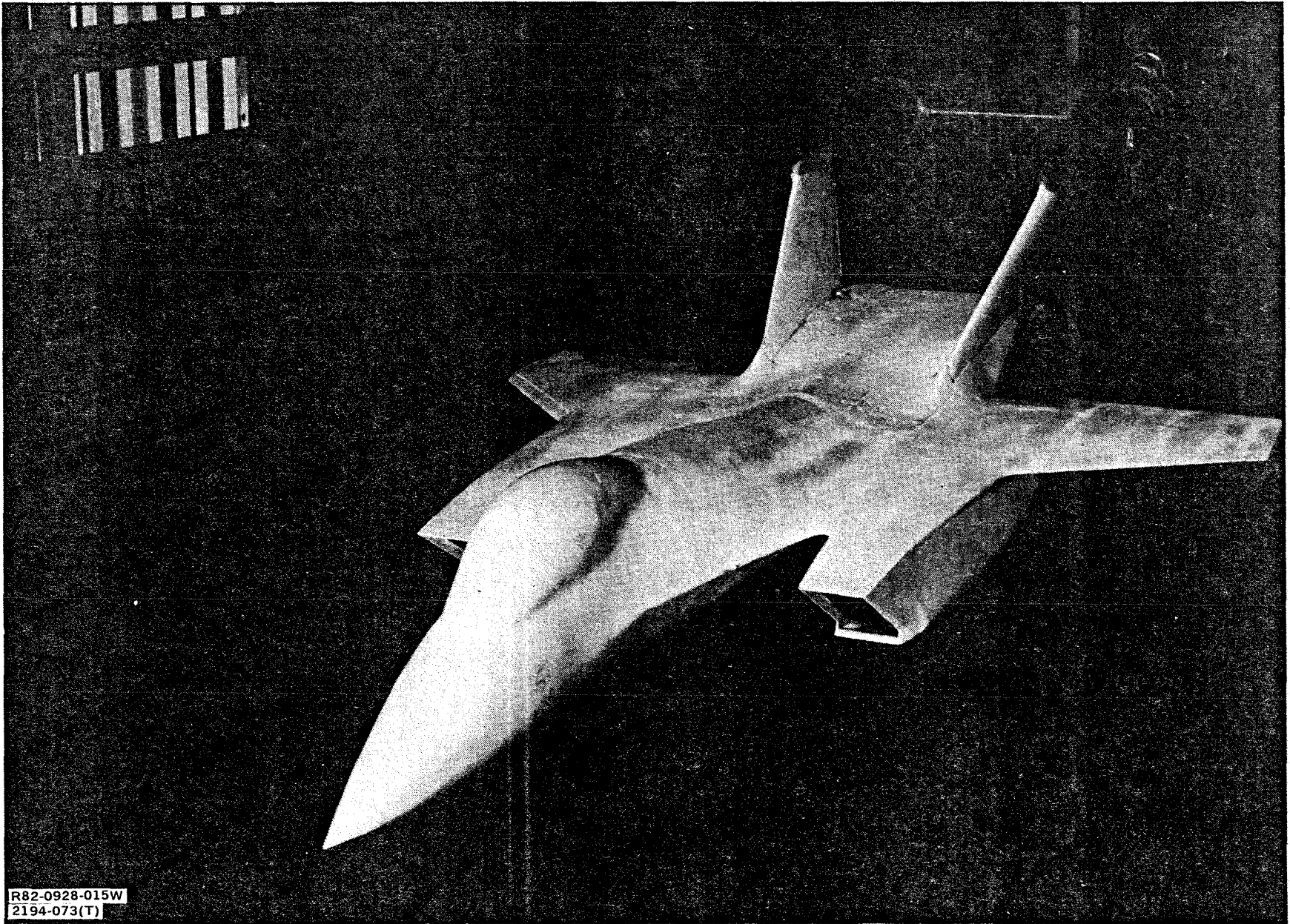
R82-0928-015W
2194-073(T)

Fig. 2-4 Model Installed in NASA/Ames 11-ft Tunnel

NOZZLE AIR SUPPLY

R82-0928-016W
2194-006(T)
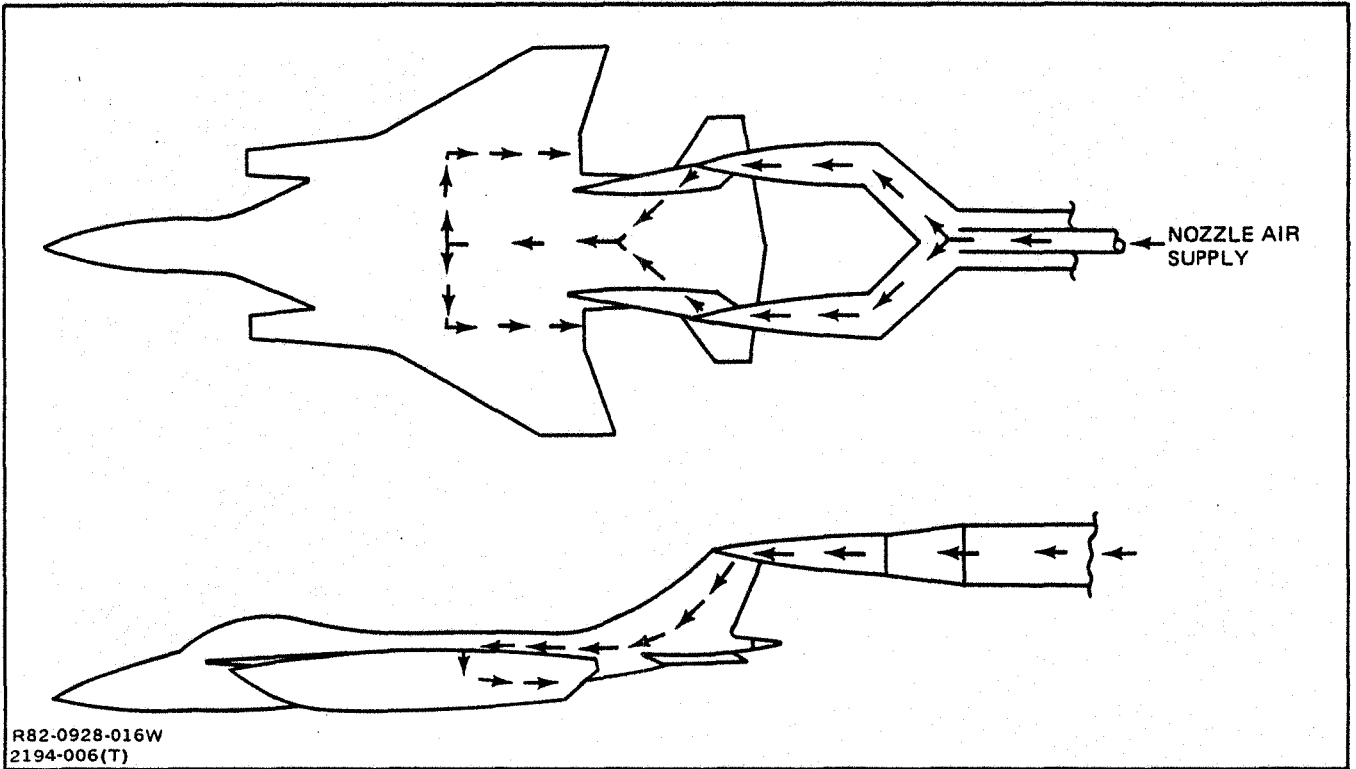
Fig. 2-5 Model Support and Flow Systems

F.S. 50.9

R82-0928-017W
2194-009(T)
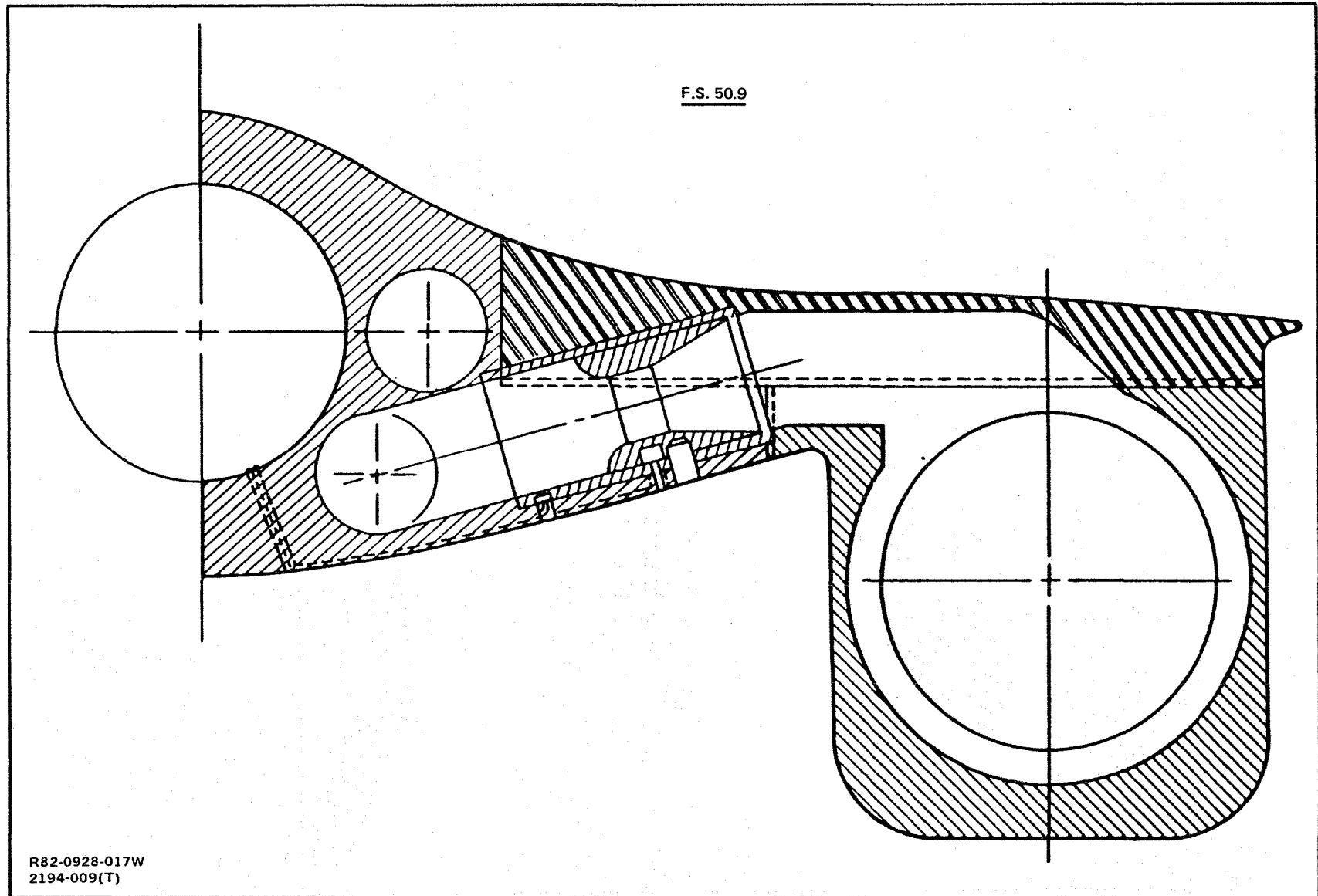
Fig. 2-6 Model Venturi Installation

TOTAL AIRPLANE FORCES

NOZZLE FORCES

NOZZLE BALANCE

SECTION A-A

MAIN BALANCE

R82-0928-018W
2194-005(T)
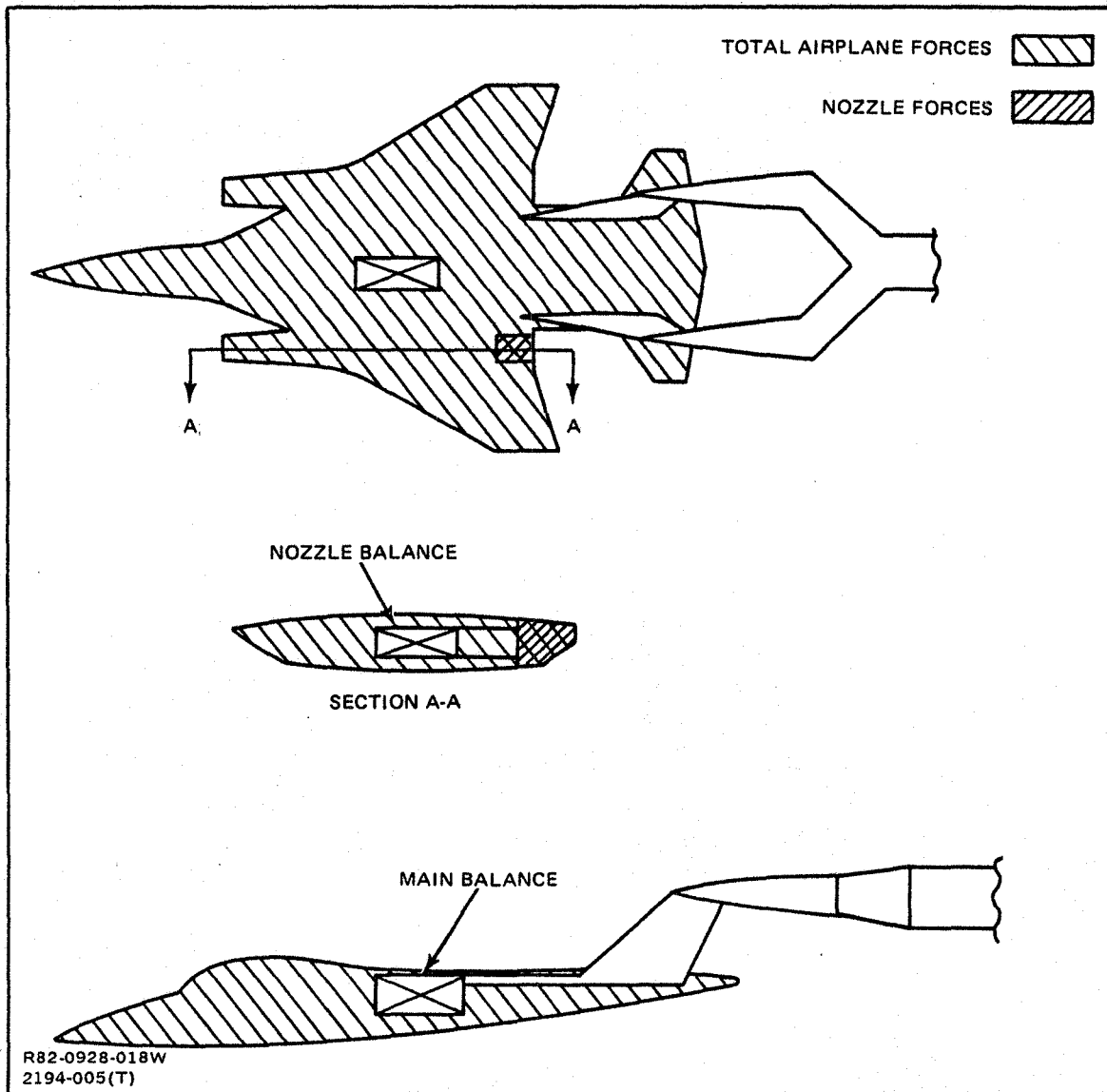
Fig. 2-7 Model Balance Arrangement

R82-0928-019W
2194-074(T)
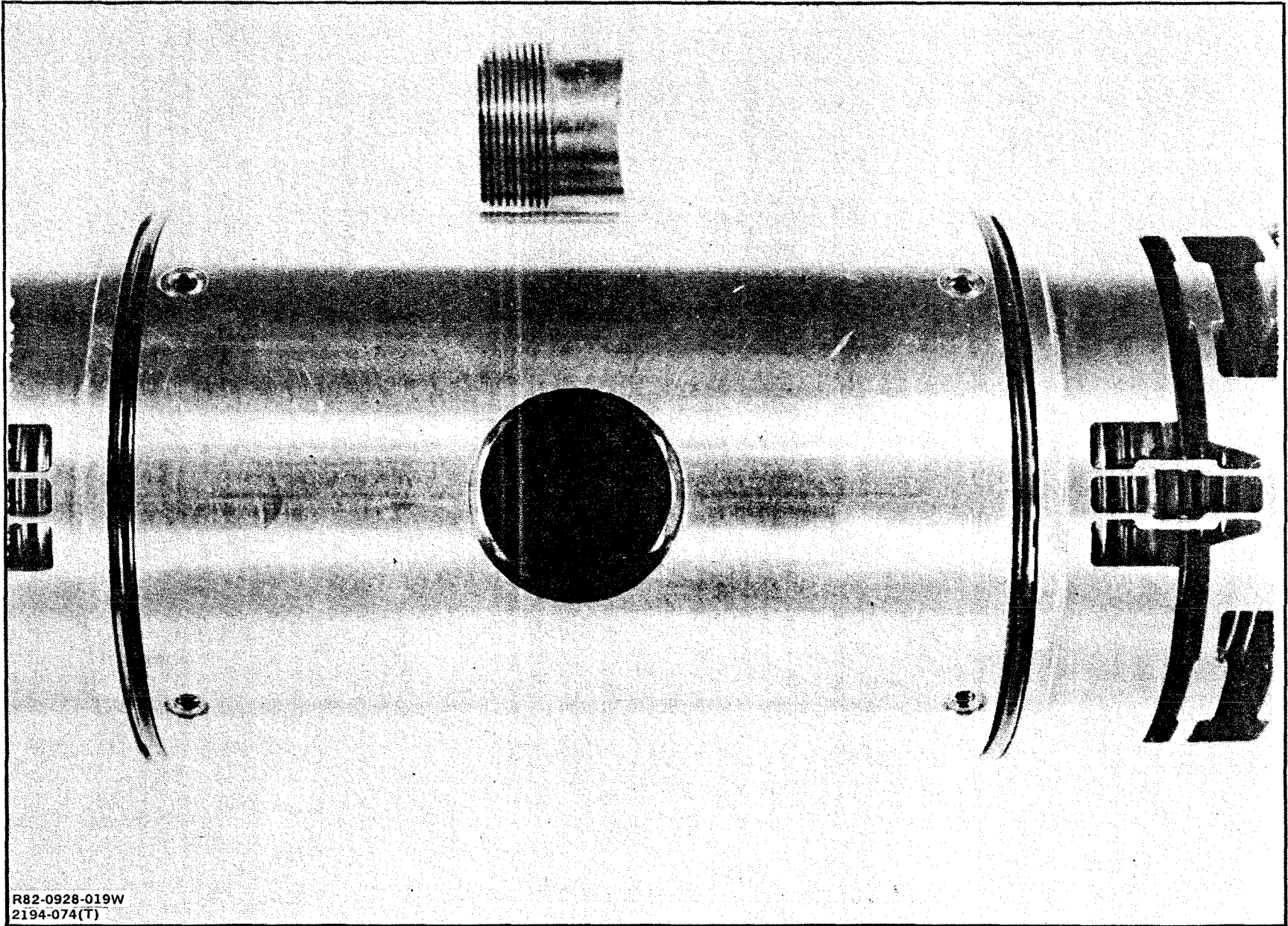
Fig. 2-8 Main Force Balance
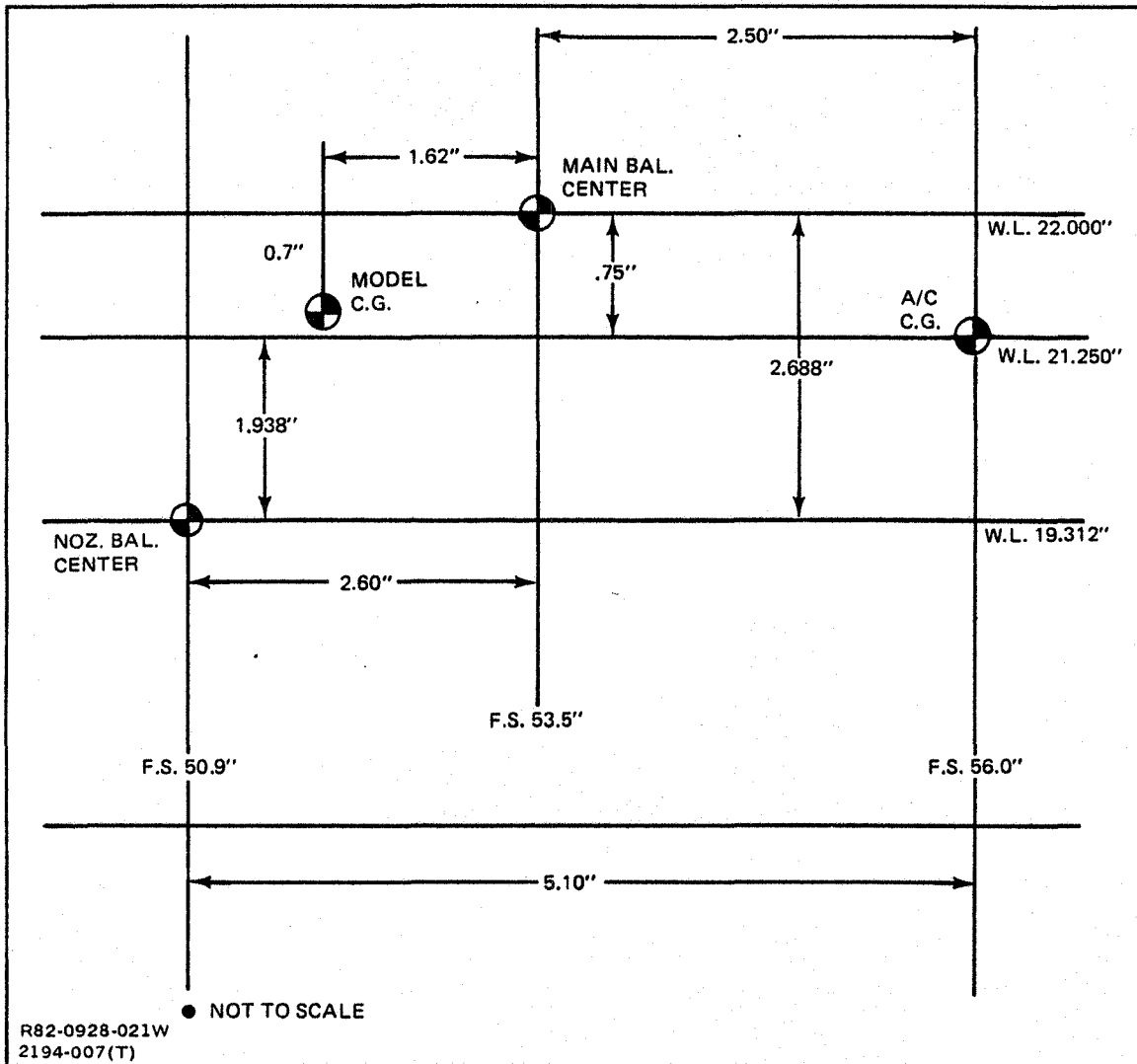
Fig. 2-9 Balance Locations Relative to Aircraft C.G.

For these type of flow-through balances, there are two normal force gauges - - a forward circuit (N_1) and an aft circuit (N_2). There is no pitching moment gauge as exists in "moment-type" balances; instead N_1 and N_2 are used to deduce pitching moment. For this reason, a flow-through balance is much more rigid and deflects much less than a moment-balance.

Note that the axial load ranges of the balances are of the same order of magnitude despite the 400 lb difference in maximum range. With proper calibration, the observed axial force repeatability error of the main balance is not significantly greater than the nacelle balance. This is not true in the normal direction where balance capacities differ by over an order of magnitude. The nozzle balance can be expected to exhibit a much tighter data scatter band than the main balance. If thrust-removed parameters are desired, therein lies the primary reason for employing the additional complexity of the second (nozzle) balance. Static thrust components are required for the determination of the thrust-removed parameters. Under static conditions (wings unloaded) the main balance normal force gauge, which had to be sized for large transonic wing loads, is much oversized for the measurement of the relatively small normal force component of the thrust vector. Typically, the static normal force data measured by the main balance is characterized by large data scatter. (This will be shown in subsection 6.3.)

(It is noted, however, that if great care and time are taken to make the necessary repeat runs to minimize both random and bias errors, then a single balance system may be satisfactory for the measurement of static normal force.)

Another argument for employing the second balance is to determine the wind-on vector angle. However, this requires the additional cost and complexity of the extensive pressure instrumentation to assess tare terms, in both axial and normal directions, on metric surfaces wetted by the external flow. Additionally, friction tare forces must be estimated analytically. Although the wind-on vector angle (if determined with confidence) is an interesting diagnostic, it is not necessary for full-scale aircraft performance to be determined. This is demonstrated in Ref. 4 where the (static) thrust-removed model scale results are combined with real engine data using the static vector angle as the interface.

Yet another common argument for utilizing the second balance is to obtain installed nozzle thrust-minus-drag. Since the location of the nozzle metric break is

arbitrary and generally not outside the nozzle and/or the jet exhaust sphere of influence, this parameter possess little value from the performance point of view (it is merely a function of the metric break location). On the other hand, if the nozzle metric break somehow could be located so that all jet-effects were included on the nozzle balance metric system - then there would be no need for the main balance, and this particular argument for the two-balance system loses validity.

Thus it is concluded again (unless driven by extraordinary objectives), that the primary reason for employing the nozzle balance is to obtain the static normal force component accurately. Furthermore, because the sphere of influence of nozzle variants and jet-effects is not restricted to the nozzle balance metric system, in this program the main balance was used for all drag/lift comparisons (Ref. 1 and 2) to ensure the accounting of all jet-induced phenomena.

For this test program the balance component sign convention is as follows: "+" for drag and lift and "−" for thrust and negative lift.

2.3 ASME CALIBRATION NOZZLE

As explained in Sections 3 and 5, the ASME standard nozzle is to be employed for calibration purposes. An engineering drawing of the ASME nozzle and its mating upstream duct appears in Fig. 2-10. The forward end of the duct attaches to the model nacelle tailpipe just downstream of a series of three flow straightening devices. The duct provides a straight slow path, equivalent to more than five nozzle diameters, that generates a fully-developed turbulent profile at the nozzle entrance. Figure 2-11 shows the ASME nozzle upstream duct installed in the model; note that the nozzle itself is shown removed and replaced by leak-proof plugs employed for pressure checking purposes.

Both left and right hand ASME nozzles were outfitted with cruciform exit rakes. The probe layout is illustrated in Fig. 2-12, and the exit rake installation is shown in Fig. 2-13. The tips of the exit rake probes were specifically located just-inside the exit plane of the ASME nozzle to eliminate any possibility of probe normal shock interference. A fixed upstream monitoring probe in each duct was calibrated against the integrated area-weighted average total pressure of each rake. Once this calibration curve was developed, the rakes were removed during the thrust and mass flow calibrations (Sections 3 and 5).
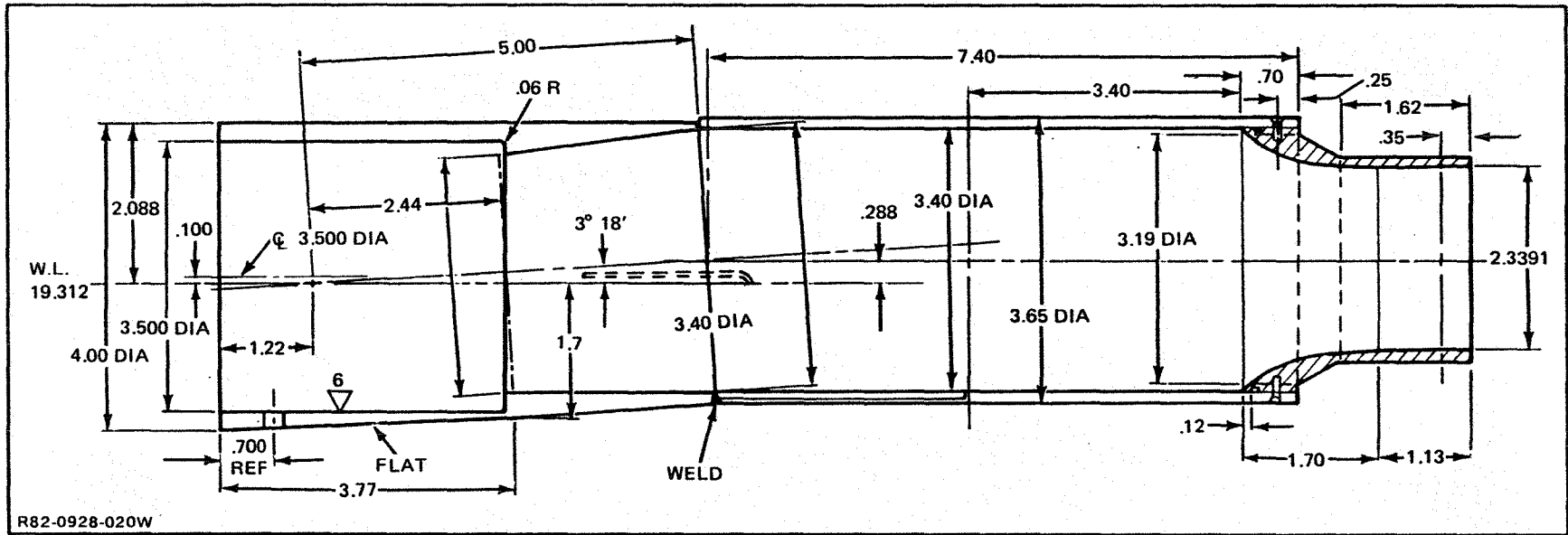
Fig. 2-10 ASME Nozzle Drawing

R82-0928-020W
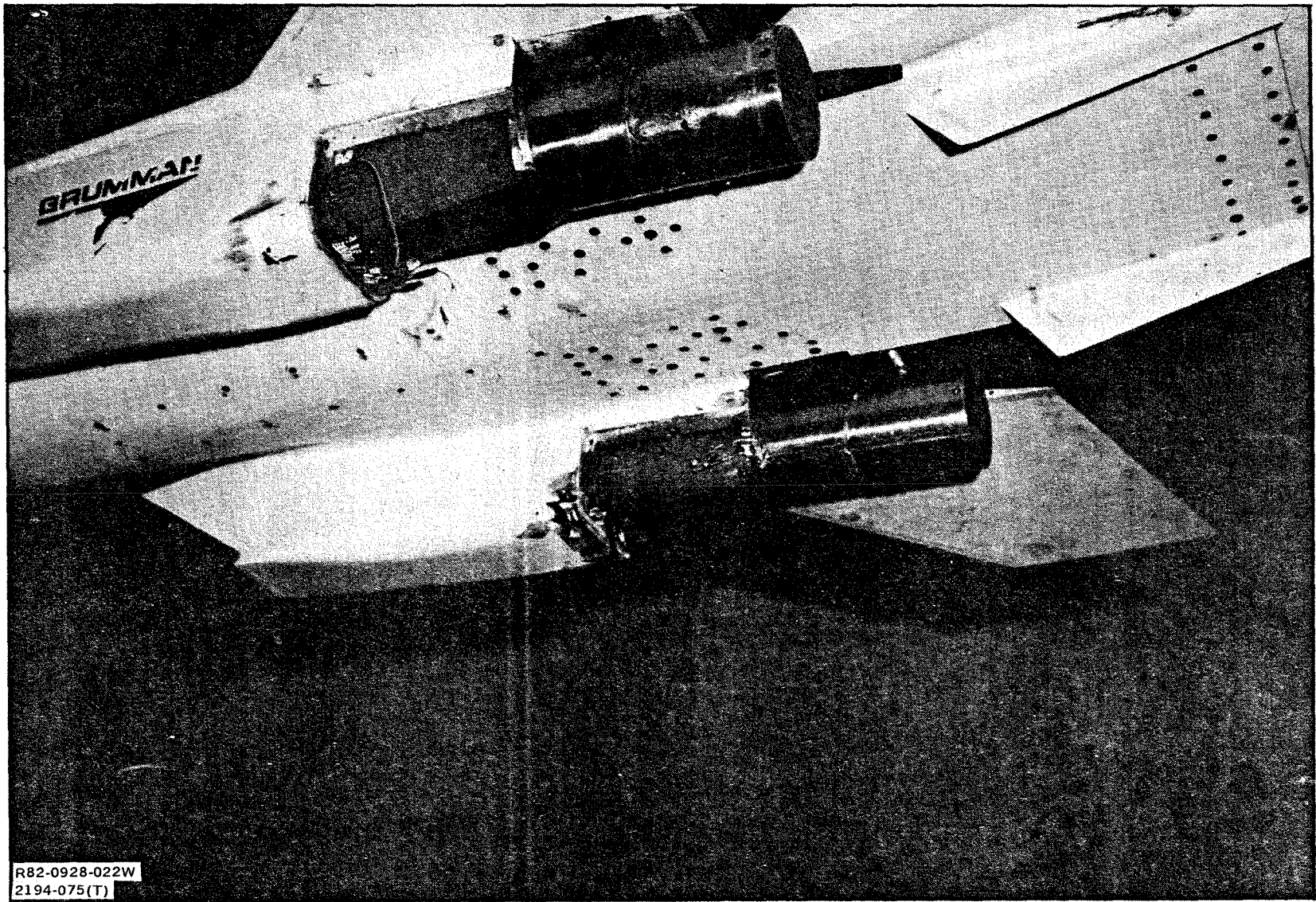
Fig. 2-11 Calibration Tailpipes Installed in Model

R82-0928-022W
2194-075(T)

R82-0928-023W
2194-008(T)

● NOT TO SCALE
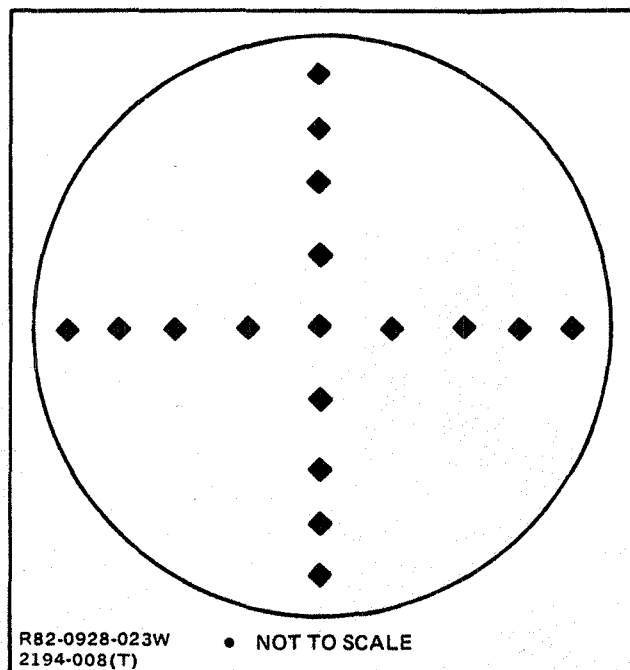
Fig. 2-12 ASME Nozzle Cruciform Exit Rake
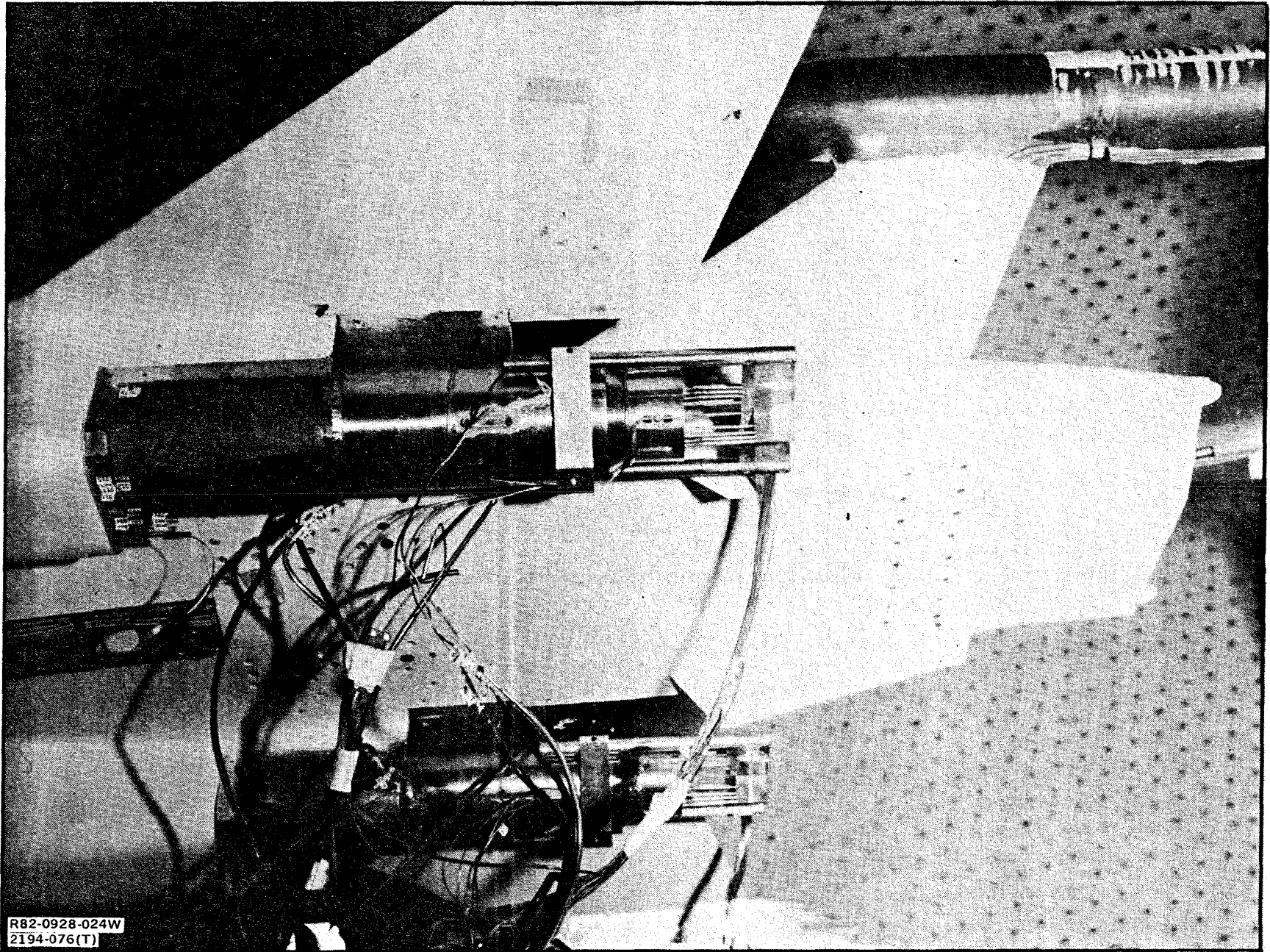
Fig. 2-13 ASME Nozzle Rake Calibration

3 - DISCUSSION OF TEST PROCEDURES

The success of a wind tunnel research program is dependent upon the experimental techniques employed and the effectiveness with which these techniques are implemented. This Section will discuss briefly many of the test procedures that are required for aero/propulsion tests of jet-effects models employing flow-through balances.

Balance Calibration - A bare balance calibration must be conducted to obtain the uninstalled primary and interaction constants. If the balance center is not close to the expected location of the aero/propulsion loads, then the bare balance calibration procedure should include loadings with multiple moment arms. The primary balance constants may or may not be updated after the installed balance calibration (e.g., check loading in the tunnel).

Flow-through balances employ a dual bellows arrangement that creates a tare force under pressure. In general, this tare force is a function of applied load in addition to being a function of pressure level. For example:

Bellows Axial Tare = f (Axial Load, Bellows Pressure).

The above uninstalled calibration and bellows tare determination are to be conducted in the laboratory in advance of the test.

Static Pressure Verification - Before model build-up in the tunnel is complete, a static pressure check, with tailpipes blanked (Fig. 2-11) must be conducted for at least three reasons:

    1. To verify the model pressure vessel leak rate is either zero or within an acceptably low tolerance. This can be done by employing a pressure monitoring gauge and a "soapy solution" that can be applied to all model component joints sensing high pressure.

    2. To conduct an "end-to-end" pressure check of the tailpipe total pressure rake from the individual elements through the Scanivalve to the millivolt readout.

    3. To check the bellows tare correction as an insurance measure.

Data Reduction Check-Point - Prior to the commencement of static and/or wind-on testing, the data reduction computing program should be completely de-bugged and a

check-point should be made using sample input data. This will ensure the data reduction program to be fully functional. Additionally, this will permit data analysis troubleshooting to be undertaken so that decisions, regarding test configurations and test conditions, can be made enabling the most efficient wind tunnel utilization.

Initial Check-Loading - A check-loading or installed calibration must be undertaken to ensure that: mechanical interference (grounding) between metric and non-metric components does not exist at conditions of interest, and balance primary constants either duplicate the uninstalled laboratory (bare balance) calibration or can be adjusted to create new installed balance sensitivities. If laboratory balance calibrations do not simulate the model weight acting at the model center of gravity location, it is likely that a change to the primary sensitivity constants is in order. Further, in conducting the check-loading procedure, the loadings should be located at or near the vector locations of the anticipated aero/propulsion loads for each metric system.

ASME Nozzle Calibration - Utilization of a standard nozzle, such as an ASME nozzle, for which the flow and thrust characteristics are well known, is necessary to: assess the magnitudes of the metric/non-metric cross-over momentum tare forces, and determine the flow-split between left and right hand tailpipes. Several repeat static runs should be made in assessing the momentum tares to eliminate data scatter and provide a sound data base for this balance correction that must be used throughout the entire test for every test configuration. Additionally, flow split ratio is to be used in conjunction with the facility mass flow measurement to calculate left and right hand tailpipe mass flow rates.

Nozzle Throat Area Measurement - Nozzle jet area measurements are required to calculate the nozzle discharge coefficients. Experience has shown that nozzle area varies with each nozzle-build for multiple-pieced nozzle hardware. It is therefore necessary to use actual measured areas after the nozzle is built-up as opposed to either drawing dimensions or areas from previous nozzle builds.

Balance Bias and Static Weight Tares - The bias correction for each metric system is simply the change in the reading of all balance gauges due to the weight of the model. This measurement is made with the balance levelled. The bias is important because the positive and negative load prime constants are generally different for all strain gauges. These constants are determined during the bare balance calibration from a reference level of zero strain. Thus, the proper gauge constant for the calculation of forces and moments must be selected based on the change in strain from this zero reference level. The model weight changes this reference level and, hence, must be

accounted for in the data reduction procedure. A fall out from this bias procedure is that the weight of the model is calculated from the change in reading of the gauges measuring forces in the vertical plane.

The static weight tare is the change in the loading of each balance gauge element with change in model attitude. It is important that this contribution to the balance force and moment readings be removed in the data reduction routine so that purely aerodynamic parameters remain. The tare is calculated from the change in reading of each gauge due to change in model attitude.

Zeros - Immediately prior to each static run or tunnel start up, zeros should be recorded by the data acquisition system. If these zeros are not recorded, data will be referenced to the most recent zero which may not be applicable due to interim electrical drift. Also, immediately after each static run or tunnel shutdown final zeros should be recorded prior to the onset of any possible thermal drift that could affect electrical output.

It is recommended that both initial and final zeros be recorded for every static (Mach = 0) run even if made back-to-back. This will provide the flexibility to select either an initial, final or some average zero during the post-test troubleshooting effort. Similarly, if a tunnel run is temporarily interrupted, a final zero and a new initial zero should be taken for diagnostic and control purposes.

Every balance possesses inherent characteristic natural zeros. These should be documented before and after the test program to assure equivalency thereby enhancing data quality. Lack of agreement could indicate a problem - for example, a gauge that becomes slightly unbonded or disturbed.

In addition to force balance zeros, all other instrumentation requires a zeroing procedure. This is especially true for the angle-of-attack measuring device. Reference angle-of-attack points must be recorded on a scheduled basis that recognizes model handling and human factors.

High Pressure Air Temperature Control - It is highly desirable to maintain constant total temperature for the high pressure air for every run of the entire test. This temperature should be equal to the expected total temperature of the wind tunnel during the planned run. Temperature gradients across the balance will therefore become insignificant.

A constant-temperature operational procedure also allows for employment of the Joule-Thompson throttling equations relating temperature and pressure drops through the entire flow path. Thus, tailpipe total temperature can be calculated very accurately and total temperature instrumentation (which is known to read erratically in a turbulent environment) is not required.

Additionally, the constant-temperature approach provides for direct and convenient correlations between mass flow and flow path pressures because total temperature becomes a constant in the continuity equation

$$\dot{W} = \frac{(\text{Const.})_1 \cdot P_T \cdot A_t}{\sqrt{T_T}} = (\text{Const.})_2 \cdot P_T.$$

Static Calibration Runs - Static runs are made with each different nozzle geometry so that thrust-removed lift, drag and pitching moment can be calculated by removing the static thrust from the wind-on thrust minus drag. This procedure is explained in Ref. 2.

It is recommended to conduct static calibrations either immediately before, immediately after, or both before and after the corresponding wind-on run of the same model-build. Using static calibrations from a prior build of the same geometry possesses the risk of introducing a bias in either the static thrust or wind-on thrust or both.

Generally a static run is the first run made after a configuration change or at the beginning of a new shift. Good experimental practice dictates that a dummy static run be made for several minutes to "shake the model loose" and to "temperature soak" the metric system. By interrupting this run peridically to monitor zeros, the common problem of acquiring "cold-start" data can be avoided or minimized.

It is highly recommended that at least three static runs be conducted at three different levels of tunnel static (back) pressure to improve on data accuracy and confidence for several reasons:

● To verify that back pressure has no effect on thrust coefficients (which is a theoretical fact). If it does, then troubleshooting procedures must be implemented.

● To improve accuracy over the complete nozzle pressure ratio range because larger balance forces are measured at low NPR when the back pressure is high.

R82-0928-010W
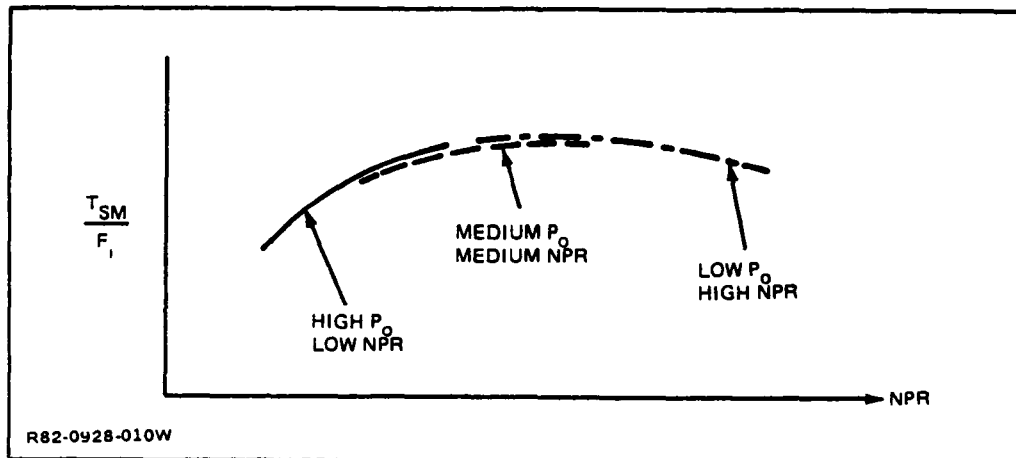
Note that if only one static run were made, it would most probably be at the low P_o to obtain the thrust characteristic over the complete NPR range. This would lead to much greater data scatter at the low NPR's because the balance force readings are low.

- To enhance data confidence by obtaining repeat data points in the "overlap regions".

- To obtain qualitative confirmation that the momentum tares (subsection 5.2) have been assessed properly. Note at the same NPR, in the overlap regions, that two different P_os mean two different mass flow rates and, therefore, two different momentum tare values. Thus, if these tares were not assessed properly, agreement between two runs in the overlap region would theoretically not be possible.

All of the above helps to minimize inaccuracies and ensures that the thrust-removed parameters possess as little uncertainty as possible. Note that uncertainties in either static thrust or wind-on thrust minus drag contribute equally to errors in the thrust removed parameters. Since cost considerations generally do not allow repeat runs of the latter, at least inexpensive repeats of the former should be conducted to optimize the thrust-removed parameter accuracy/cost trade.

Wind-off/Jet-off α-Sweep - Prior to the start of the wind-on test phase an α-sweep should be conducted with both internal and tunnel air off. At such a condition all the net aero-propulsion forces should be zero (within balance accuracy) at each angle-of-attack. This run provides verification that: biases, weight tares, primary
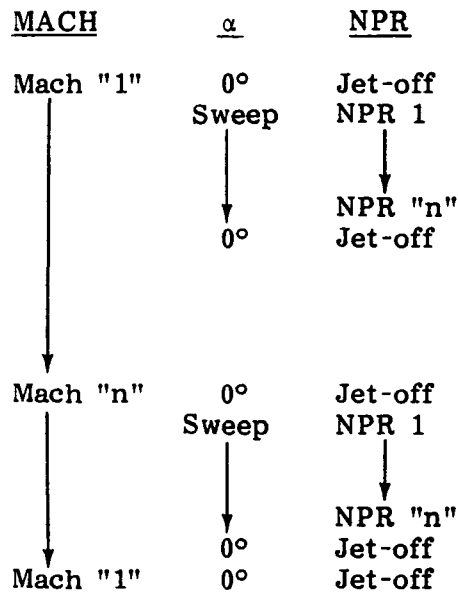
balance constants, and interaction constants have all been assessed correctly and are being handled properly by the facility data reduction routine.

Wind-on Test Operation - The wind-on test runs should be conducted in accordance with a specific schedule because the flow through balances may be characterized by a degree of hysterisis; this will be discussed in subsection 4.1. As explained in Ref. 2, the most important objective of this test program is to compare one nozzle installation against another. Any bias error due to hysterisis could upset this nozzle-to-nozzle comparison if consistency of loading direction is not maintained. It is therefore highly recommended that the variation of angle-of-attack and nozzle pressure ratio always be conducted in the same direction - preferably from low to high load levels.

Scanivalve Check - On tunnel pump-down to the desired static pressure required for a given Mach number, the pressure readings on the Scanivalve ports should be monitored. If the output printout format is organized properly all ports can be checked, at a glance, to see if they read the tunnel static pressure. Ports that reflect a plugged line are easily identified. Leaks are not identified in this way since all pressures, tubes, and the Scanivalves are in the same pressure environment. However, leaks are not generally as troublesome as plugs. Plugs can be noted in the test log book to be later taken into account during post test data analysis. Additionally, this Scani-check allows for the identification of plugged tailpipe total pressure probe readings so that adjustments to the area-weighted integration scheme can be made on-the-spot in the data reduction program (as a constant update) prior to the wind-on run.

Air-off and Jet-off Data Points - Diagnostic data points are useful for monitoring balance behavior and trouble-shooting purposes in general. First, an air-off data point (both jet and tunnel air off) should be acquired just prior to the start of either a static run or a tunnel blow and immediately afterwards. These air-off points can be viewed as the diagnostic equivalent to initial and final zeros. The recording of air-off points is necessary because the official zero points do not appear on the same physical print-out output as the data. and therefore are not conveniently available.

Second, the acquisition of jet-off data points, in addition to the normal jet-off α-sweeps taken as part of the standard test condition matrix, are very useful as repeat data diagnostics to be used for trouble-shooting. These additional jet-off points should be acquired for $\alpha = 0^{\circ}$ at the beginning and end of each Mach sequence as illustrated below.

```
MACH            α         NPR

Mach "1"       0°        Jet-off
               Sweep     NPR 1



                         NPR "n"
               0°        Jet-off




Mach "n"       0°        Jet-off
               Sweep     NPR 1



                         NPR "n"
               0°        Jet-off
Mach "1"       0°        Jet-off
```

Note that this jet-off procedure ensures that each Mach sequence is flanked by repeat jet-off points that represent a time difference on the order of one hour. Additionally, note that at the end of all the desired test Mach conditions the very first Mach number is repeated for a final jet-off repeat data point that represents a time difference of many hours. Analysis of these jet-off data is invaluable in assessing data quality and confidence.

Check Load Verification - In addition to the initial check-loading discussed above in Section 3, it is good experimental practice to conduct additional check-loadings in the middle of the test and in particular at the completion of the test program. Thus the health of the flow-through balances will be monitored and data confidence will be enhanced. In the event that these check-loadings do not duplicate the initial check-loading, corrective action can be implemented while the model is still in the test-mode before teardown.

Data Reduction Hand Calculation - A hand calculation of all the facility-developed and contractor-developed data reduction equations should be undertaken very early in the test program. In particular, the many steps involved in calculating the final net aero/ propulsion forces from the actual individual balance gauge readings must be verified. These eight steps are illustrated below (for the main balance normal force gauges, N1 and N2) - the first five are components of the facility standard data reduction code while the last three are generally incorporated in the contractor's computational data reduction program.

1. EUBAL.N1, N2 represents the actual load on the balance gauge and includes the bias weight. It is expressed in engineering units.

2. EXINT.N1, N2 represents the adjustments for interactions of the individual gauges on each other. It also includes the bias weights.

3. EXBIAS.N1, N2 removes the bias interactions from EXINT.N1, N2 as shown below:

$$EXBIAS.N1, N2 = EXINT.N1, N2 - BIAS.EXINT.N1, N2$$

   Note that the removal of the bias occurs after the bias has gone through the interaction equations.

4. EXRESOLVED.N represents the summation of the two normal force gauges:

$$EXRESOLVED.N = EXBIAS.N1 + EXBIAS.N2$$

5. EXTARE.N takes EXRESOLVED.N and removes the static weight tare increment relative to $\alpha = 0°$. EXTARE.N represents the net aero/propulsion force prior to the three model tare force corrections (6) - (8).

6. NFB is the normal force after the bellows pressure tare force (BNF) has been removed:

$$NFB = EXTARE.N - BNF.$$

7. NFBC is the normal force after both the bellows tare and cavity tare (CNF) have been removed:

$$NFBC = NFB - CNF.$$

   The cavity tare results from the unbalanced pressure/area force at the metric/non-metric interface.

8. NFBCM is the resultant normal force after the momentum tare (MNF) correction has been made in addition to the removal of the bellows and cavity tares:

$$NFBCM = NFBC + MNF.$$

   It represents the net aero/propulsive force that is to be used to calculate the aerodynamic coefficients.

Data Troubleshooting Tasks - As early as possible during the test operation, checks
on the data should be made to isolate any problem(s). Examples of data trouble-
shooting tasks are noted below:

- The Static (Mach=0) thrust coefficients determined from the main and nozzle
  balances should show agreement, within balance accuracy:

$$\frac{T_{SM}}{F_{iM}} = \frac{T_{SN}}{F_{iN}}$$

  This comparison should show better correlation in the axial direction as op-
  posed to the normal direction because of the relative balance gauge capacities.
  This is discussed in Ref. 2.

- The mass flow rate as determined by the facility flow meter can be checked
  by utilizing the model-mounted venturi tubes.

- Flow path pressure correlations using bellows, venturi and tailpipe rake
  pressures should be made as a function of pressure level or mass flow.
  Additionally, correlations between left and right tailpipe pressures and
  temperature are useful.

- Main balance and nozzle balance internal cavity pressure studies should be
  made as angle-of-attack varies to analyze the cavity pressure/area tare
  correction. This should be the same for every configuration since changes
  to the nozzle geometry do not influence the vertical tail metric/non-metric
  interface.

- Left and right hand wing external pressure comparisons can be made to check
  symmetry and model alignment.

- Detailed comparisons of wing upper and lower surface pressure distributions
  are to be used to substantiate the force data trends between different
  configurations.

- Initial and final air-off points (or zeros) and repeat jet-off data (discussed
  earlier in this section) should be studied to monitor balance behavior.

- Axial and normal force can be plotted versus angle of attack to check for
  grounding by observing distinct breaks in the characteristics.

- Comparisons between the two fundamental methods of determining thrust-removed parameters - P_o-Method and F_i-Method - add much to the understanding of data accuracy. This is discussed in Ref. 2.

- Where possible, data checks should be made using either previous data obtained on the same model or predicted values.

4 - BALANCE CALIBRATION

The calibration of the flow-through balances was undertaken by NASA Ames. First a laboratory bare (uninstalled) balance calibration was conducted with and without exercising bellows pressure. Second, these calibrations were checked with the balance installed in the model in the tunnel. This section presents highlights of the flow-through balance calibration results in terms of primary and interaction constants, and bellows tare corrections.

4.1 BALANCE CONSTANTS

The laboratory bare balance calibration data, aimed at the determination of primary constants, is illustrated for the aft normal gauge (N_2) in Fig. 4-1. The difference between the actual and computed load is plotted against applied load. The first observation is the large hysterisis effect that represents 4-5% of fullscale. This problem was alleviated to some extent by exercising the balance as much as possible, in a single direction only, as recommended in Section 3.
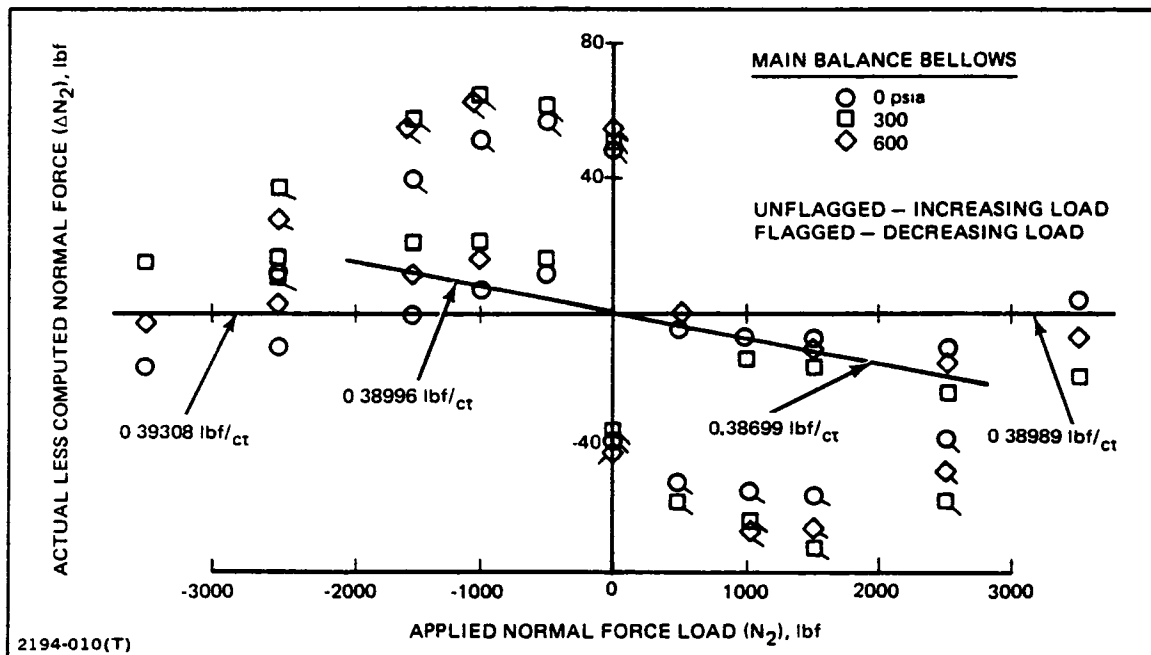

Fig. 4-1 Laboratory Calibration of Uninstalled Main Balance

Second, the faired curve represents the first-pass at updating the 1978 primary constant. The 1979 constants are calculated from the slope(S) of the faired curve as follows:

$$K^{\pm}_{1979} = (1 + S) \cdot K^{\pm}_{1978},$$

where the superscripts refer to plus or minus applied load. Note that the faired curve reflects the increasing load data in the region of interest (-1000 lbf to +2500 lbf) and therefore is appropriate for the determination of the primary constants.

Figure 4-2 provides an example of check-loading in the tunnel with the balance installed in the model. This is shown for the forward normal gauge (N_1), under positive loading, which exhibits a large disparity between the computed reading and the applied load. This may be due to the effect of model weight that was not simulated during the laboratory bare balance calibration. An adjustment to the uninstalled primary constant is made by using the slope(S) of the faired curve of Fig. 4-2.

$$K_{INSTL} = \frac{K_{UNINSTL}}{(1 + S)}.$$

By employing the updated installed constant the adjusted check-loading characteristic exhibits far less disparity as shown in Fig. 4-3.
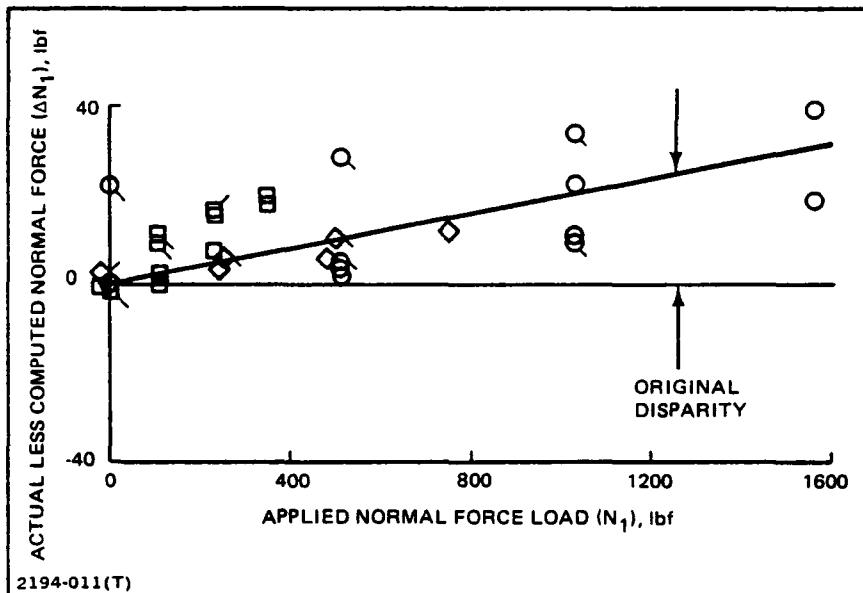

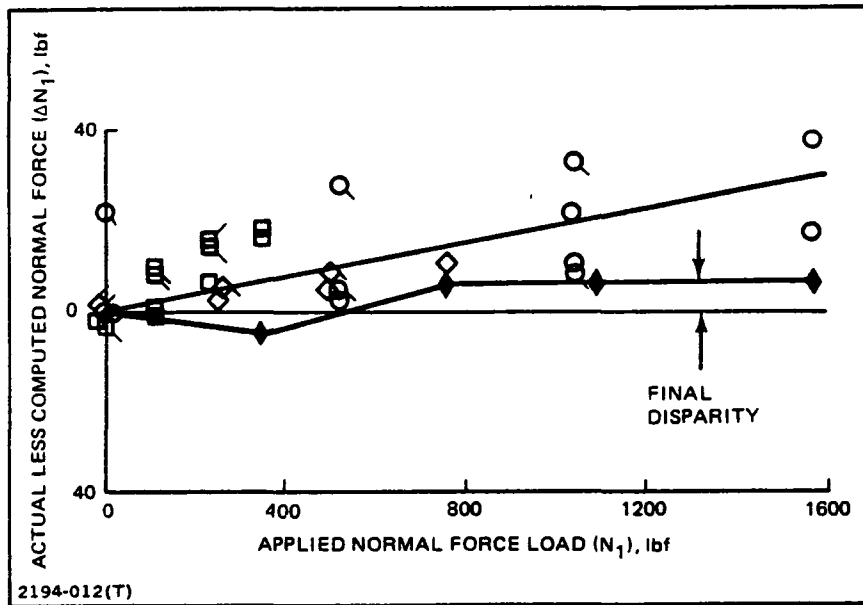Fig. 4-2 Installed Main Balance Check Loading

4-2

Fig. 4-3 Effect of Main Balance Constant Adjustment

Of the six main balance primary constants (axial and two normal in both ± directions) that had to be checked in the tunnel only two required adjustment: K^{+}_{N1}, K^{+}_{N2}. For the nozzle balance, no adjustment was required probably due to its very small weight bias as opposed to the main balance.

Loads on any particular gauge in general create electrical output on the other gauges. These are called balance gauge component interactions. Restricting the discussion to only the gauges of interest (axial and two normal) for this test, the adjustments for interactions are given by:

- $\text{EXINT.A}_x = \text{EUBAL.A}_x - \dfrac{dA_x}{dN_1} \cdot \text{EUBAL.N}_1 - \dfrac{dA_x}{dN_2} \cdot \text{EUBAL.N}_2$

- $\text{EXINT.N}_1 = \text{EUBAL.N}_1 - \dfrac{dN_1}{dA_x} \cdot \text{EUBAL.A}_x - \dfrac{dN_1}{dN_2} \cdot \text{EUBAL.N}_2$

- $\text{EXINT.N}_2 = \text{EUBAL.N}_2 - \dfrac{dN_2}{dA_x} \cdot \text{EUBAL.A}_x - \dfrac{dN_2}{dN_1} \cdot \text{EUBAL.N}_1$

It was recognized that the traditional procedure of taking the interaction data and applying least-squares fits indiscriminantly could be improved upon for three reasons: a boundary condition of zero interaction at zero load could be imposed, hysterisis effects could be taken into account, and data outside the region of interest

could be ignored. Accordingly, the interaction data was plotted and hand faired using engineering judgment.

The interactions resulting from axial applied loads appear in Fig. 4-4. Note that no interaction was considered to exist on N_2; however, interactions (on the order of 1%) do exist on N_1 for both plus and minus loadings.
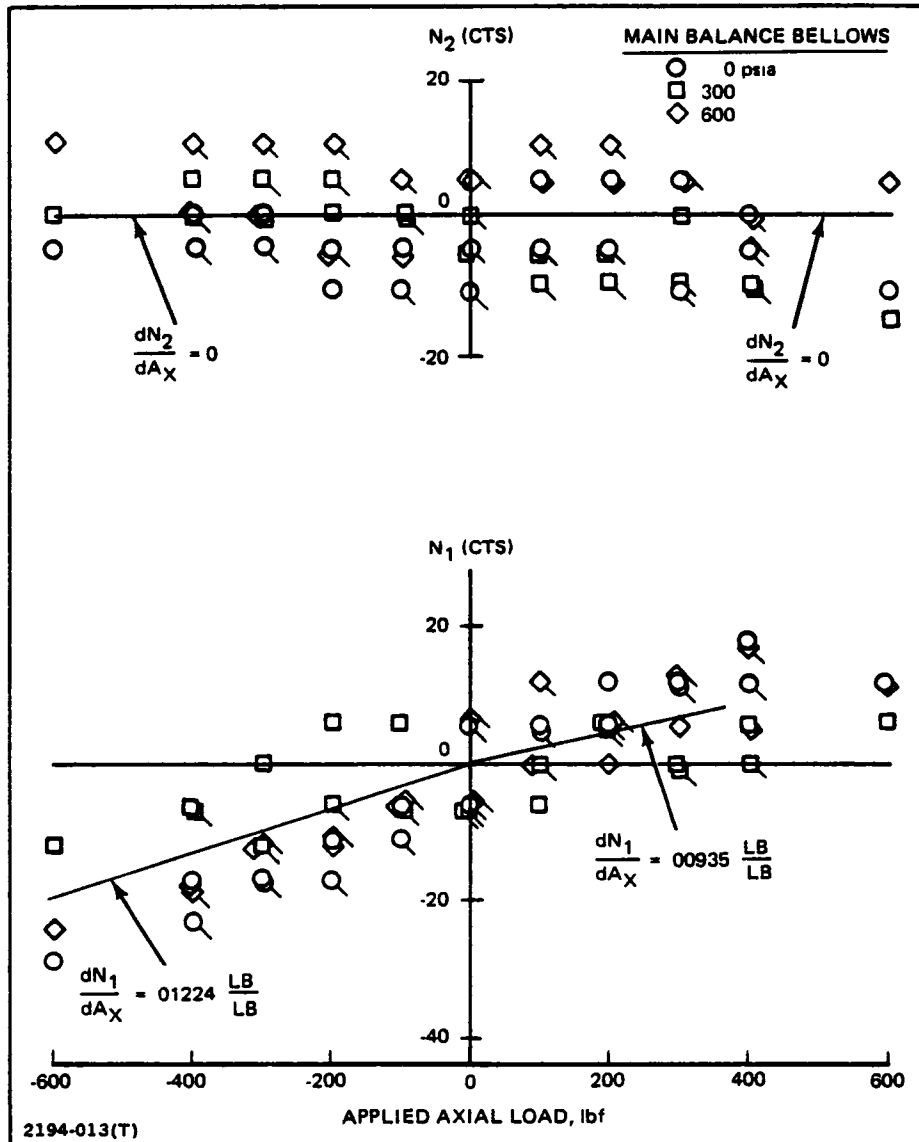

Fig. 4-4 Interactions Caused by Main Balance Axial Load

The interactions caused by the forward normal gauge are shown in Fig. 4-5. For the axial gauge, in the plus direction, the effect is small (1/10%), while, for the minus direction, a 1.4% interaction exists. The interaction on the aft normal gauge provides a good example of how the hysterisis effect was taken into account. Here the interactions are rather large exceeding 2% in the minus direction, while approaching 4% in the plus direction. These large interactions are a result of a stiff bellows assembly in the main balance. Ideally it is desirable to keep interactions below the 1% level, nevertheless, these magnitudes are acceptable if assessed and handled properly.
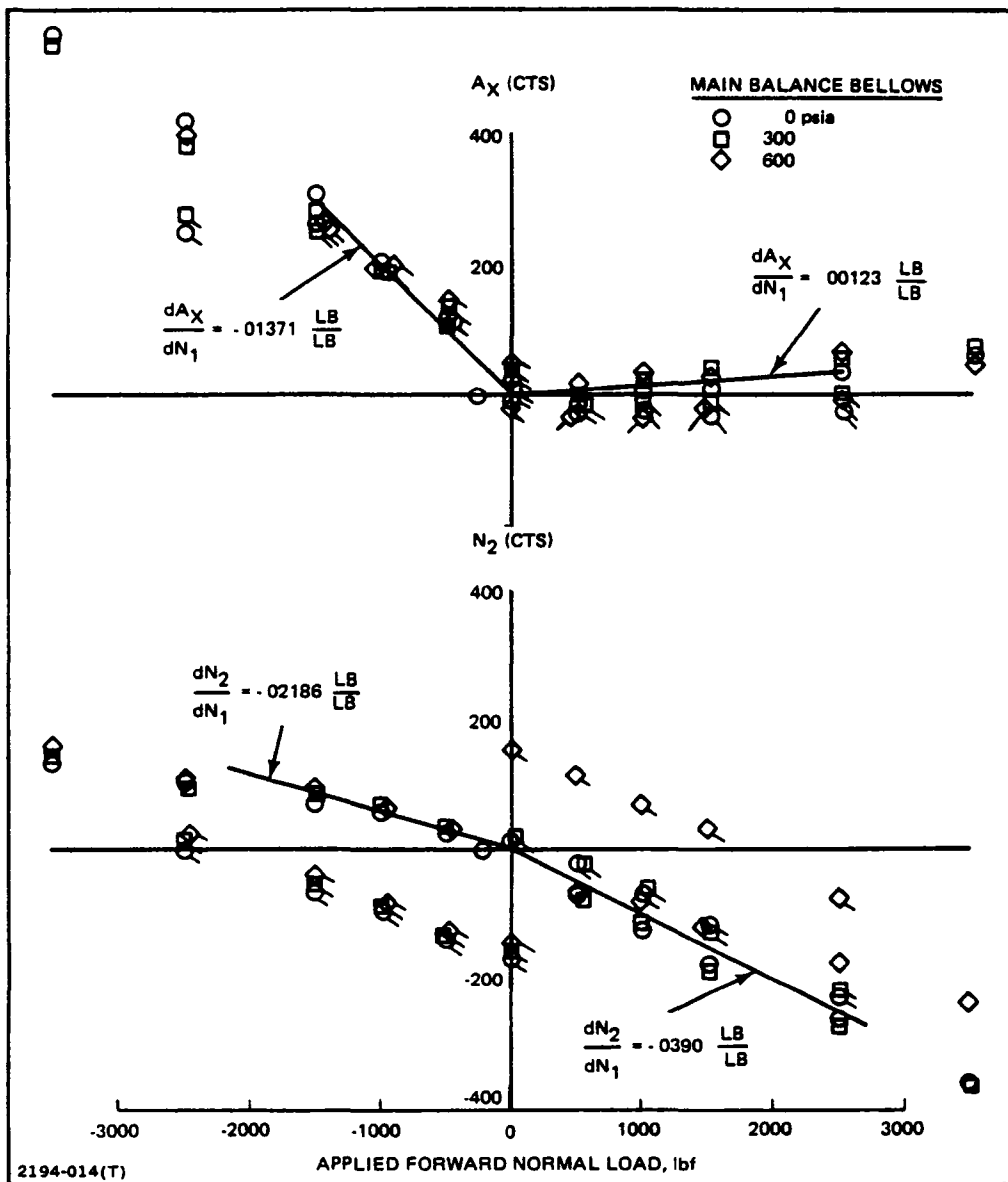

Fig. 4-5 Interactions Caused by Main Balance Forward Normal Load

The interactions resulting from aft normal gauge loadings are presented in Fig. 4-6. The effect in the axial direction is small, but on the forward normal gauge a significant 3% interaction is observed.

As recommended in Section 3, a wind-off/jet-off α-sweep was conducted which showed that the aero/propulsion forces were computed as zero. This indicated that the balance primary and interaction constants had been properly assessed.
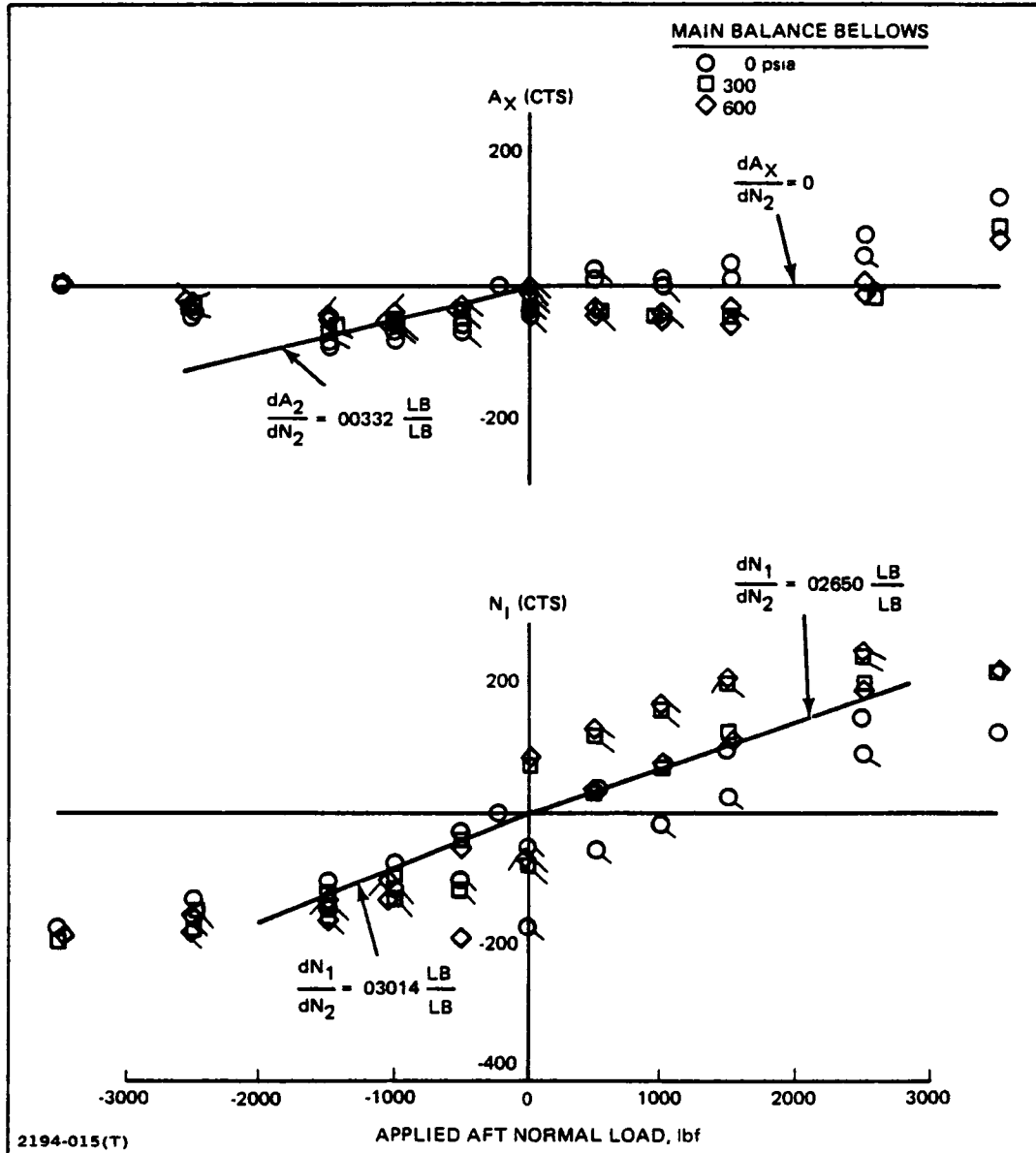

Fig. 4-6 Interactions Caused by Main Balance Aft Normal Load

4.2 BELLOWS TARE CORRECTION

Both main and nozzle flow-through balances have a dual bellows system. A portion of the convolutions of the forward and aft bellows can be observed in Fig. 2-8. In theory, any stress in the former should be cancelled by an equal and opposite stress in the latter. However in practice, due to material and fabrication differences, this is not exactly true and a bellows pressure tare must be assessed. As explained in Section 3, the bellows pressure tare is, in general, a function of load level in addition to pressure. In utilizing the bellows tare characteristics presented in this subsection, it was recognized that the particular load level to be used was not the net force but instead the gross force (that includes model weight). Thus, the appropriate gross forces would be:

- $EXINT.A_x$ for Axial

- $(EXINT.N_1 + EXINT.N_2)$ for Normal

Figure 4-7 presents the main balance axial bellows tare which is seen to be a function of both pressure and axial load level. This tare is at all times positive, which according to the sign convention defined in subsection 2.2, indicates a drag force. Thus, thrust would be too low in magnitude if no correction was made. Accordingly, the adjustment must be:

$$AFB = EXTARE.A_x - BAF$$

For example (at $\alpha = 0°$), if the uncorrected thrust magnitude was -100 lbf and the bellows tare was 10 lbf (in the drag direction) then the corrected thrust magnitude would be -110 lbf.:

$$AFB = EXTARE.A_x - BAF$$

$$-110 = (-100) - (+10).$$

Also observe that the size of the bellows tare is on the order of 4% of full scale at the high pressure levels - this is considered a sizable correction, but one that can be satisfactorily handled.

Figures 4-8 and 4-9 present the corresponding main balance bellows tares for normal force and pitching moment. The faired curves represent the characteristics used in the data reduction program. Linear interpolation techniques were employed
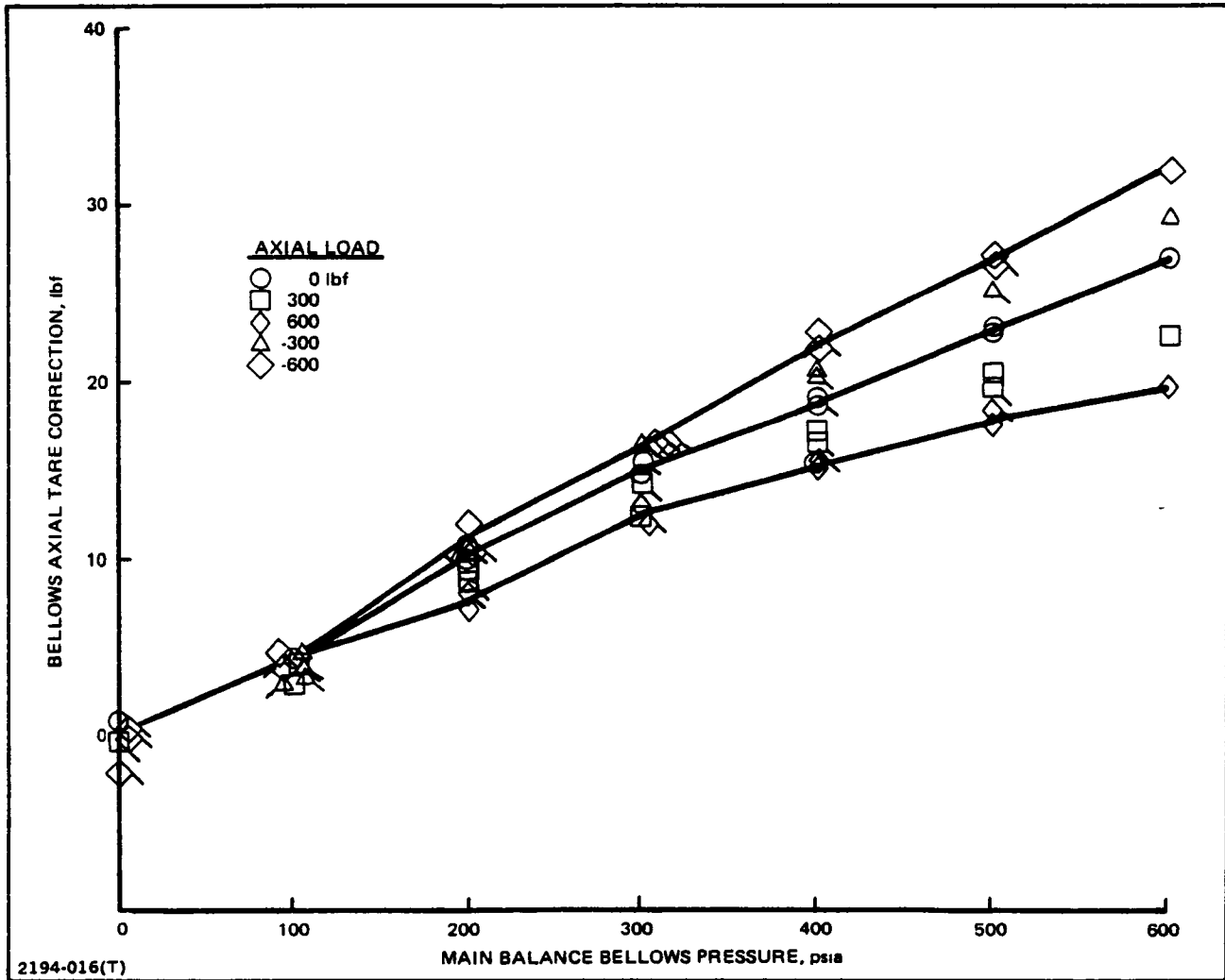
Fig. 4-7 Main Balance Bellows Axial Tare

between applied load levels. Note that these tare corrections can be either positive or negative. If the uncorrected normal force was +1000 lbf and the bellows tare was +10 lbf, the corrected normal force would be 990 lbf as shown below:

$$NFB = EXTARE.N - BNF$$
$$990 = (+1000) - (+10).$$

On the other hand, if the uncorrected normal force was -1000 lbf and the bellows tare was -10 lbf, the corrected normal force would be -990 lbf as shown below:

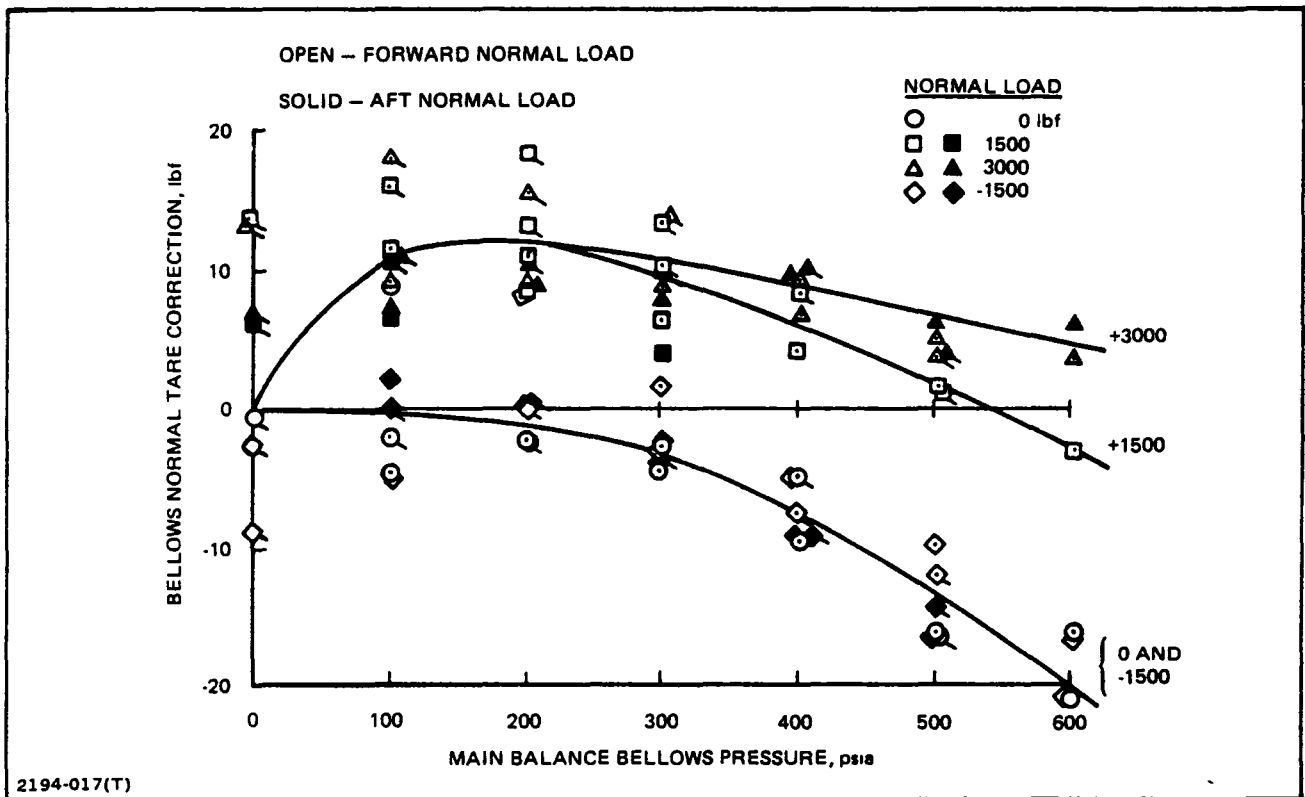$$NFB = EXTARE.N - BNF$$
$$-990 = (-1000) - (-10).$$

4-8

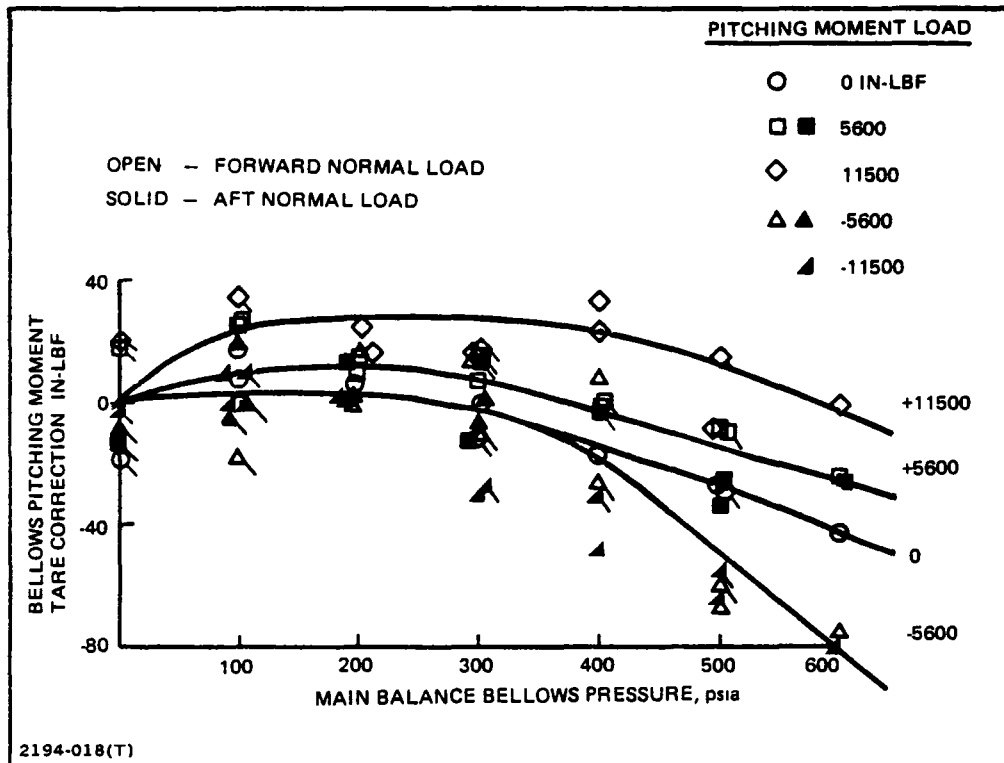**Fig. 4-8 Main Balance Bellows Normal Tare**

Fig. 4-9 Main Balance Bellows Pitching Moment Tare

4-9

The nozzle balance <u>axial</u> bellows tare is also a function of load level as well as pressure as shown in Fig. 4-10. As opposed to the main balance, this tare is much smaller in magnitude and is in the thrust direction. Here, thrust would be too high if no correction were made, and the correction would be in the direction to reduce thrust. The same reasoning used above with the main balance of course applies here.

It is noted that these flow-through balances can be calibrated backwards (+ and - axial reversed). There is nothing incorrect with the reversed procedure; however, it becomes extremely important to be aware of the polarity employed during calibration. Generally the personnel involved in balance calibrations do not become involved in the test -- a situation which sets the scene for potential sign convention confusion. Such a situation developed during the subject test, and the only solution was to follow-up, check, and re-check. This was ultimately done successfully.

Prior assessment (at AEDC, 1977) of the nozzle balance bellows tare in the normal direction and for pitching moments indicated that these tare components were only a function of pressure and not load level (within acceptable tolerance). This is shown in Fig. 4-11 for the bellows normal tare component plotted against venturi pressure. Figures 4-12 and 4-13 present the NASA Ames normal and pitching moment bellows tares for the nozzle balance plotted against nozzle balance bellows pressure (98% of venturi pressure). Observe that the Ames and AEDC bellows normal tare are in excellent agreement - within one pound which represents 1/2% of full scale.

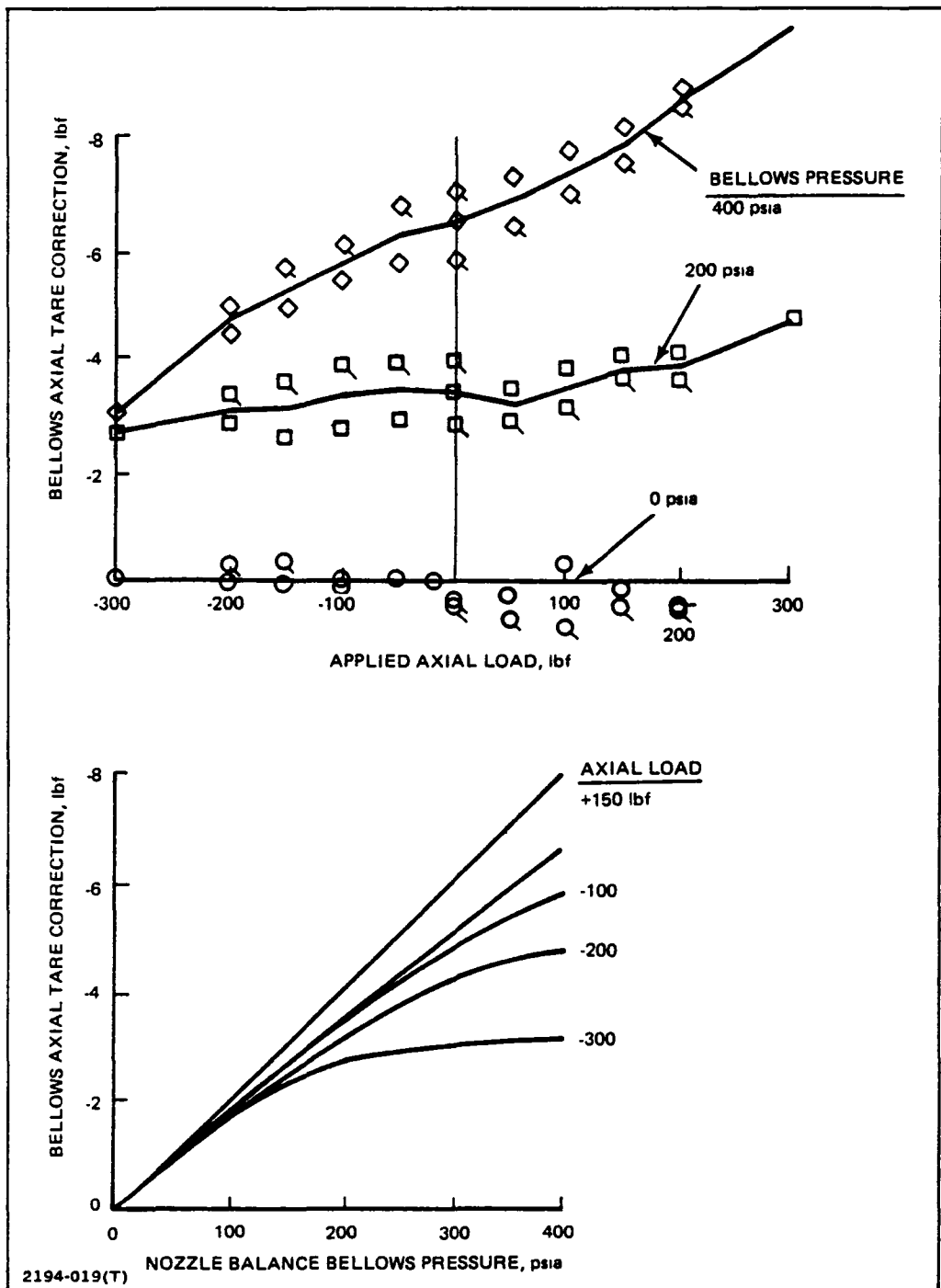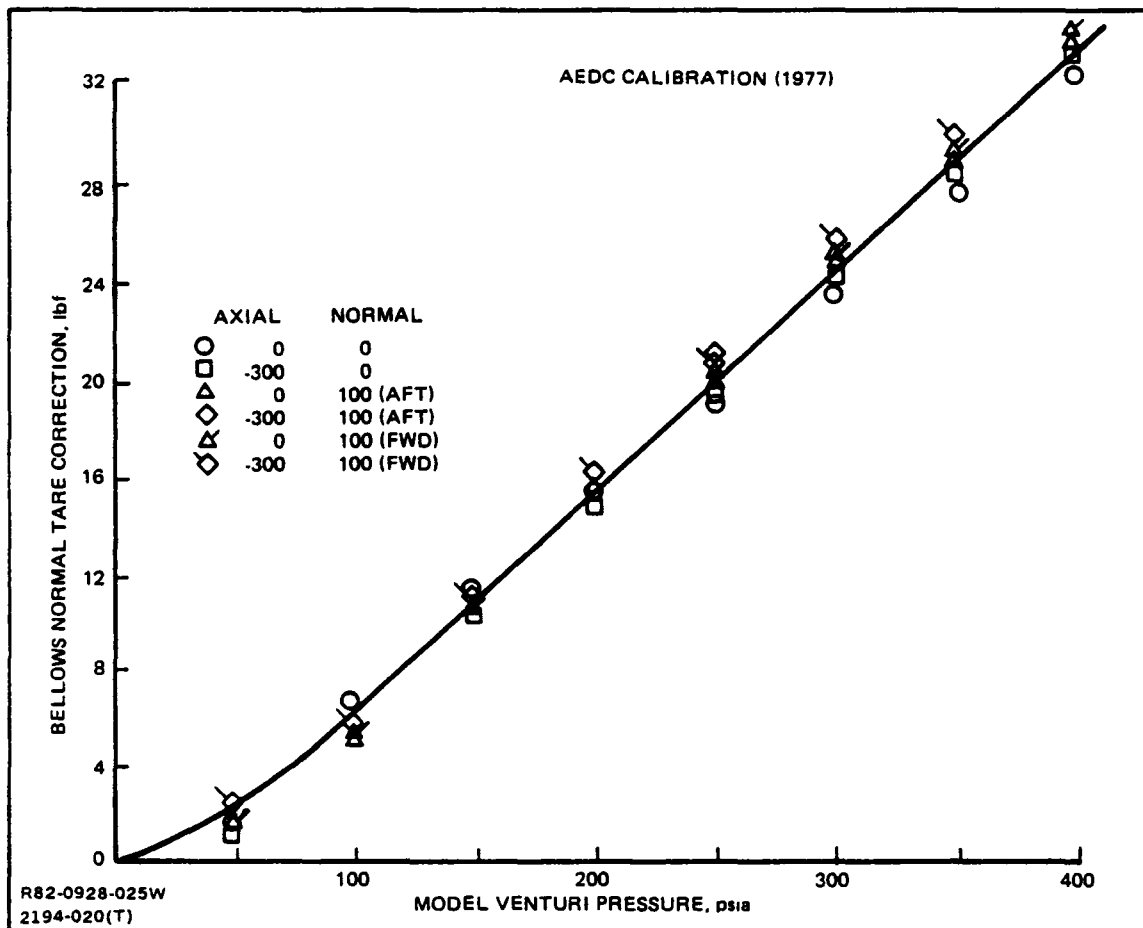Fig. 4-10 Nozzle Balance Bellows Axial Tare

2194-019(T)

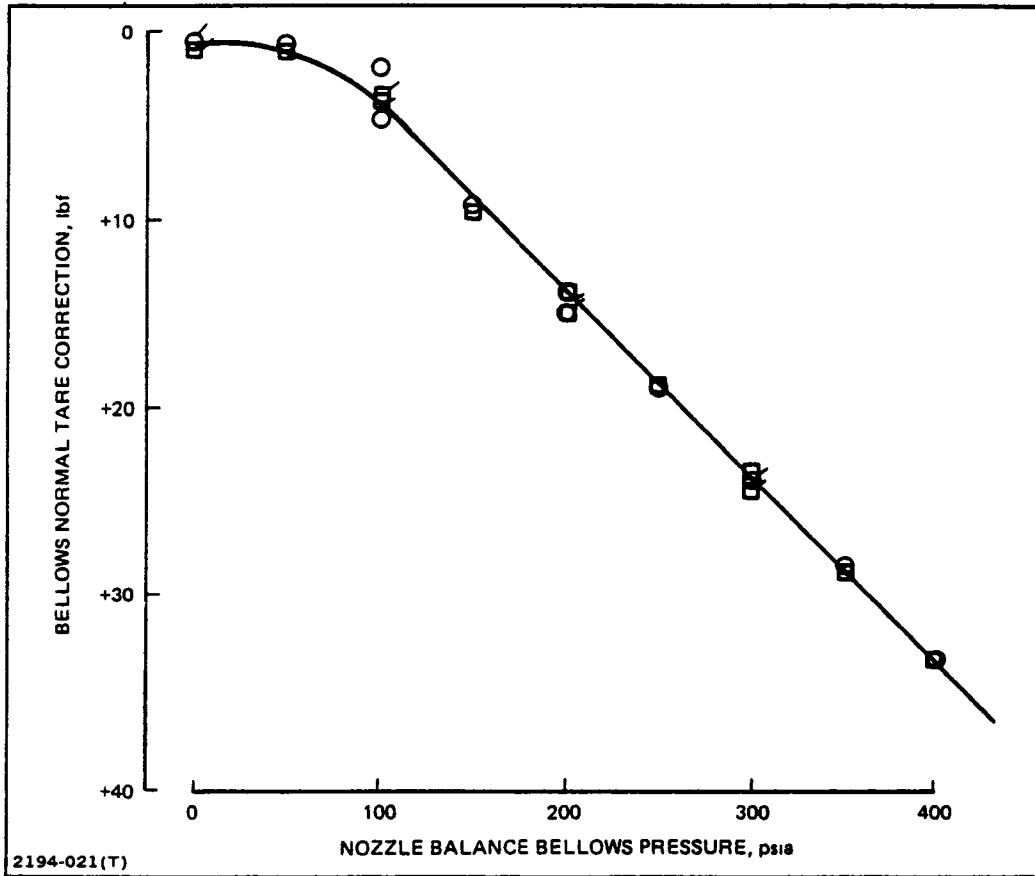Fig. 4-11 Independence of Nacelle Balance Bellows Normal Tare to Applied Load
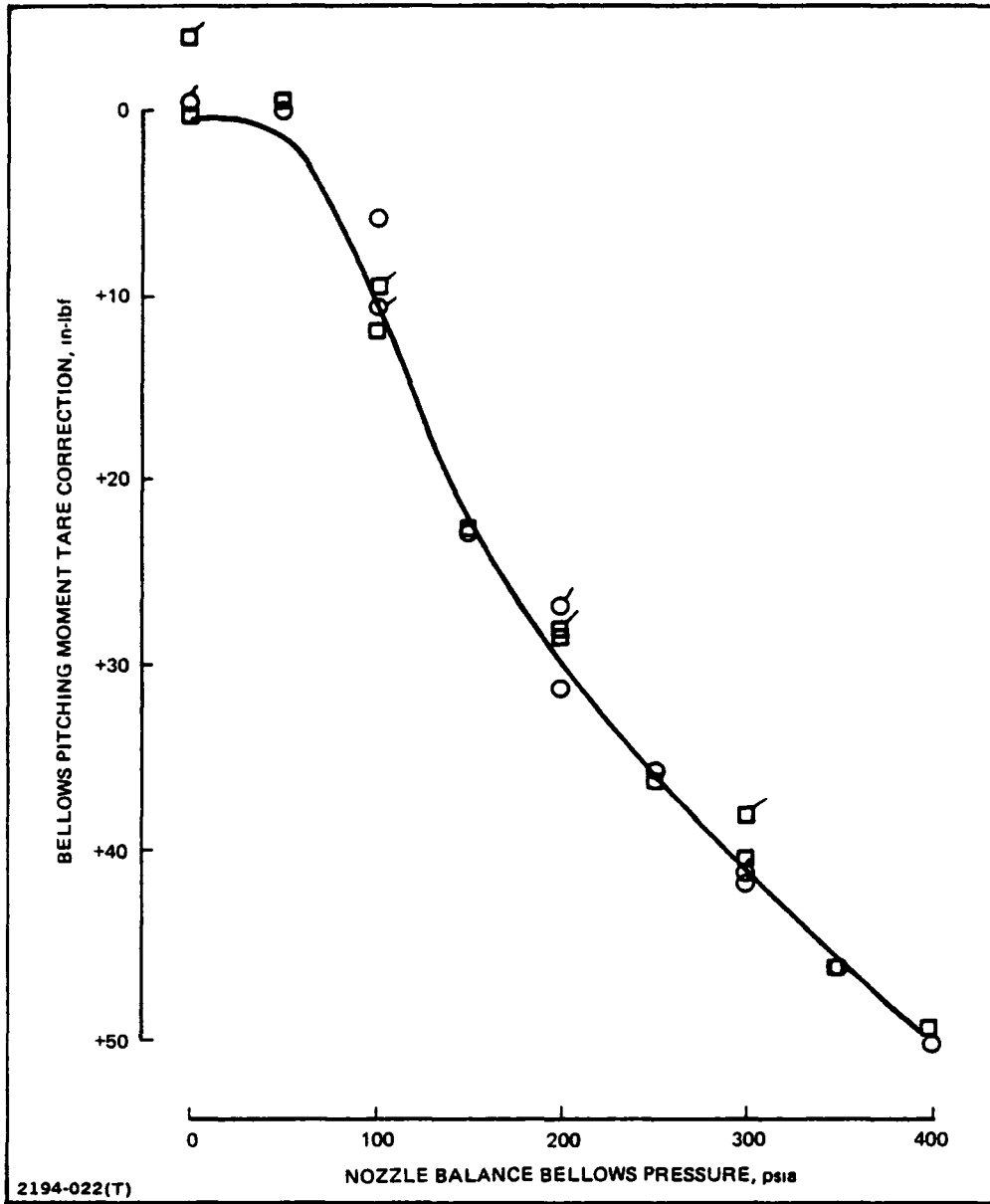
Fig. 4-12 Nozzle Balance Bellows Normal Tare

2194-021(T)

Fig. 4-13 Nozzle Balance Bellows Pitching Moment Tare

2194-022(T)

5 - ASME NOZZLE CALIBRATION RESULTS

By utilizing an ASME nozzle (or any standard nozzle), the mass flow rate and the thrust can be easily determined from tailpipe pressure and temperature measurements. Knowledge of the mass flow and thrust is utilized for calibration purposes as discussed in the following two subsections.

5.1 MASS FLOW CALIBRATION

The objective of the flow calibration was two-fold: flow calibrate the model mounted venturi tubes (Fig. 2-6) as an alternate to the facility flow measurement, and determine the flow split ratio between left and right hand tail pipes.

In this test program, total pressure and total temperature were the two measurements sufficient to determine mass flow. It is noted that static pressure and total temperature are also sufficient measurements; however, this latter procedure mandates low duct Mach numbers (at the pressure measurement station) and also requires an iterative calculation procedure because the ratio of specific heats (taking into account real gas effects) is a function of total pressure.

The steps employed in the determination of the ASME nozzle mass flow rate are as follows:

1. Measure total temperature using thermocouples in both tailpipes. Left and right temperatures must either agree within accuracy or must be "forced" to agree or else unnecessary error will be introduced.

2. Measure left and right tailpipe total pressure using an exit rake calibration of an upstream monitoring probe. Recall that Fig. 2-12 showed the multi-probe cruciform exit rake. Figure 5-1 verifies an accurate measurement because all profiles are relatively "flat" across the exit diameter. The integration of these exit rake profiles for many pressure levels plotted versus the monitoring probe is shown in Figs. 5-2 and 5-3. The calibrations are straight lines with slopes that are close to unity (1.006 and 0.995) as expected. Also note that the repeatability is excellent.

3. Calculate Reynolds number from (1) and (2) above.
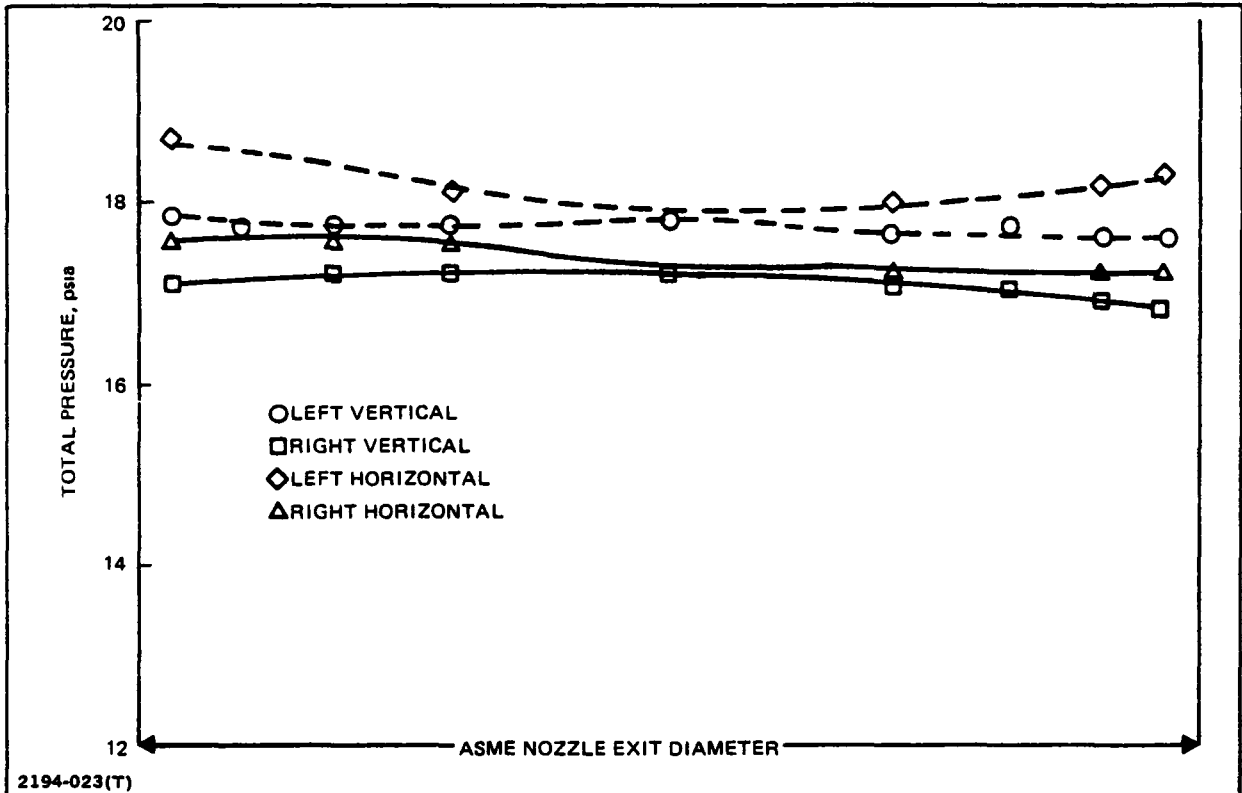
Fig. 5-1 ASME Nozzle Exit Total Pressure Profiles

4. For the ASME nozzle, the discharge coefficient, which is a measure of the displacement thickness and hence Reynolds number, can now be calculated:

$$C_{DIS} = (1 - 0.184 \; Re^{-0.2})$$

5. The ASME nozzle mass flow is then calculated from the continuity equation including the small correction for real gas effects as follows:

$$\dot{W}_{ASME} = \frac{.5318 P_T \cdot A_{geom} \cdot C_{DIS} \cdot f(P_T)}{\sqrt{T_T}}$$

where: $f(P_T) = (1 + 1.7077 \times 10^{-4} P_T - 2.7042 \times 10^{-7} P_T \cdot T_T)$
      if NPR < 1.893

and $f(P_T) = 1.0$
      if NPR ≥ 1.893 .

Fig. 5-2 ASME Nozzle Left Duct Calibration

2194-024(T)
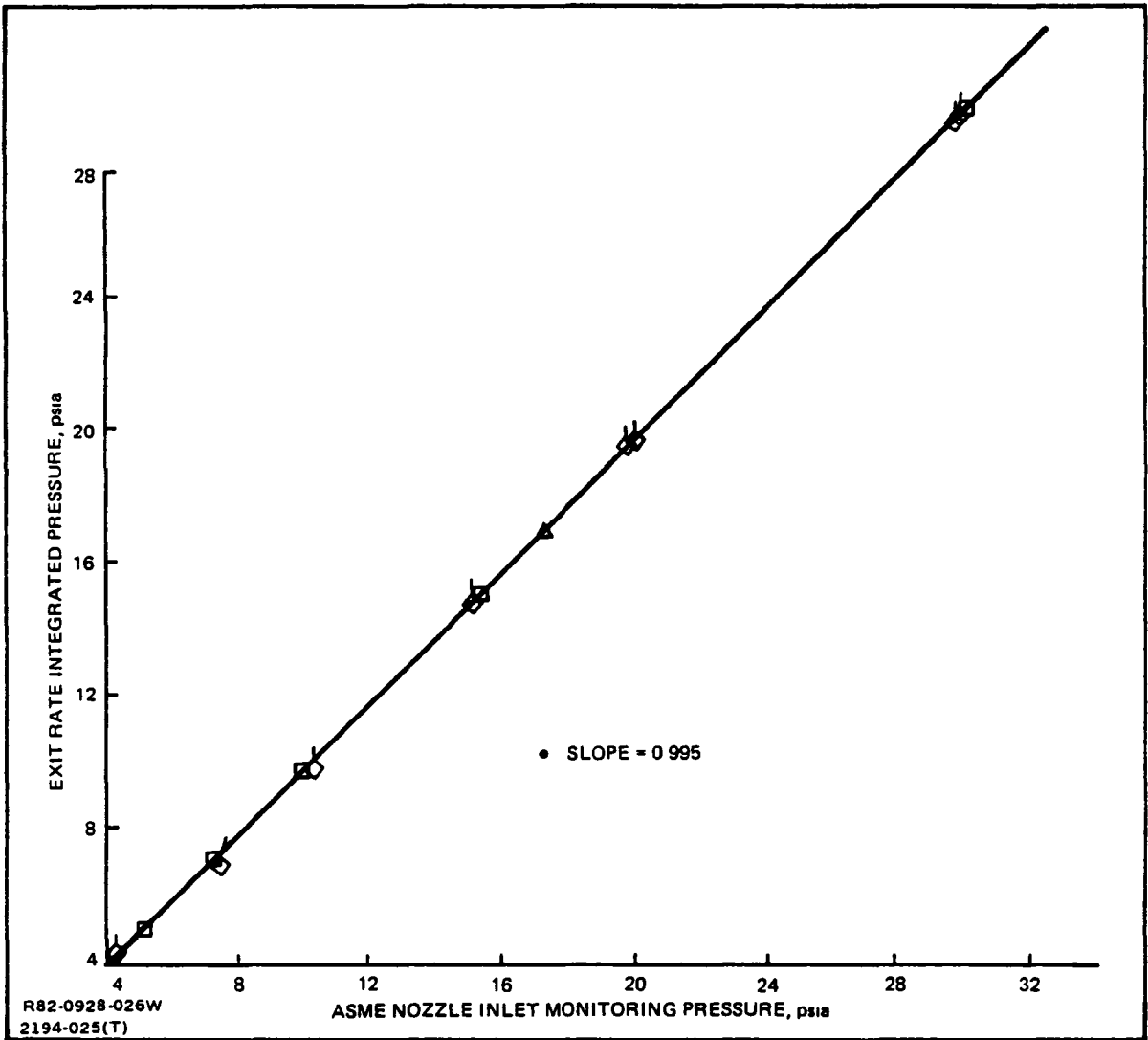
Fig. 5-3 ASME Nozzle Right Duct Calibration

R82-0928-026W
2194-025(T)

During the ASME nozzle test runs, the upstream flow path pressures are to be monitored as diagnostics. At three critical points, upstream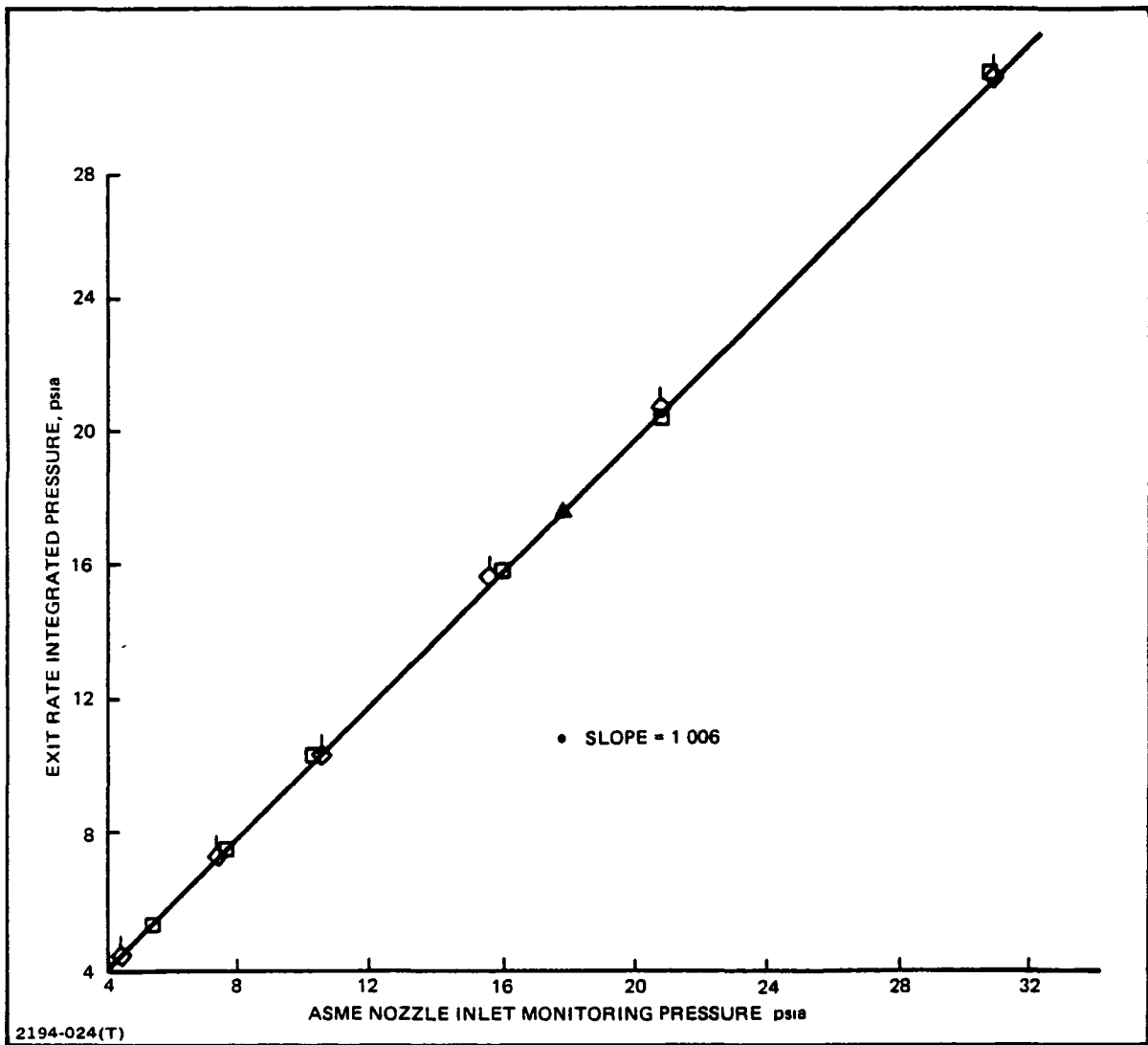 of the tailpipe, pressures are measured: nozzle balance bellows, model venturi tubes, and main balance bellows. A unique relationship exists between these upstream pressures (for constant total temperature) as shown in Fig. 5-4. Observe that there is a large drop in total pressure between the main balance and the venturi, with only a small additional drop from the venturi to the nozzle balance (as would be expected from Fig. 2-6). The venturi pressure measurement instrumentation had to function properly, as shown in the figure, in order to calibrate the model venturi tubes.
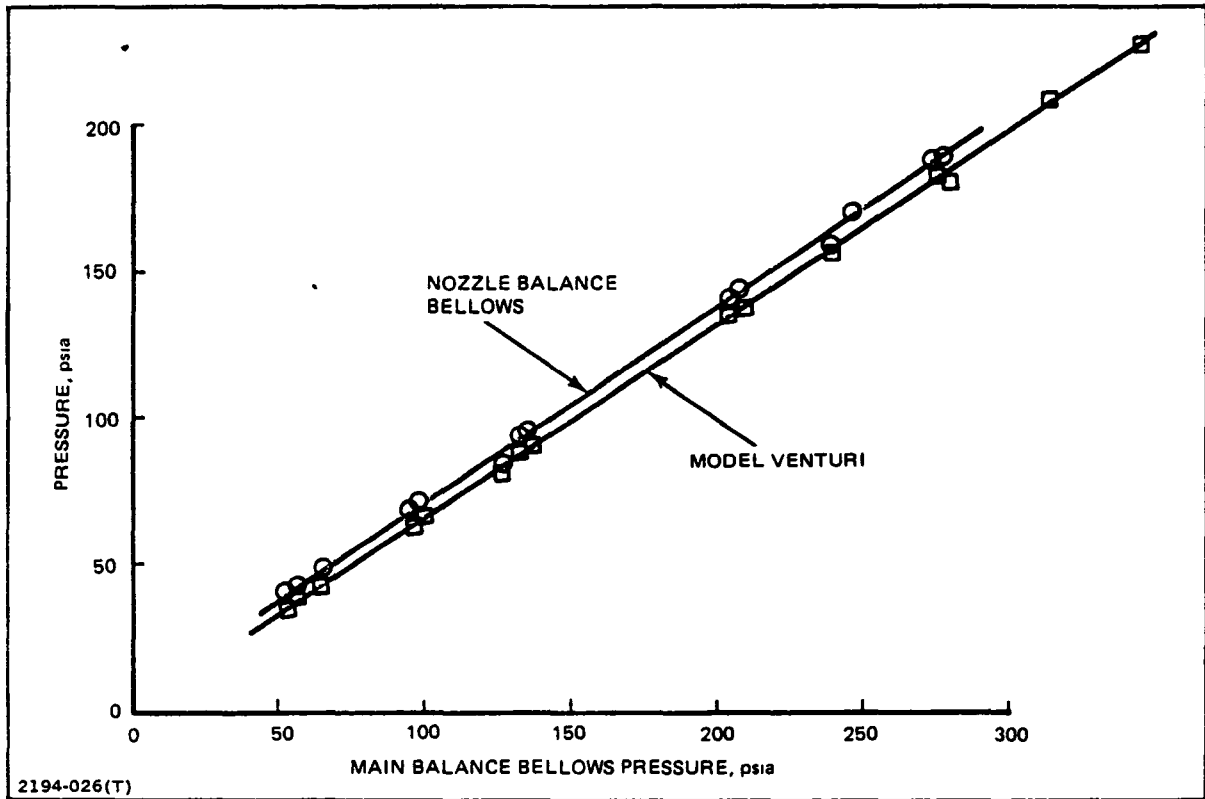
Fig. 5-4 Model Flow Path Pressure Characteristics

Both left and right venturi tubes were calibrated using the venturi-flow-parameter defined as follows:

$$VFP = (\dot{W}_{ASME}) \cdot \left(\frac{\sqrt{T_{TV}}}{P_{TV}} \right).$$

5-5

The parameter is sometimes considered as a "lumped-discharge-coefficient" because for choked flow it is the one-dimensional discharge coefficient times a constant $(.5318 \times A_t)$. It has the typical convergent nozzle discharge coefficient shape at low pressures and at high pressures is characterized by a gently rising trend (due to slight Reynolds increases as pressure increases) as shown in Figs. 5-5 and 5-6. Note the repeatability for several test runs is excellent.

R82-0928-027W
2194-030(T)

Fig. 5-5 Model Left Venturi Mass Flow Calibration

R82-0928-028W
2194-031(T)
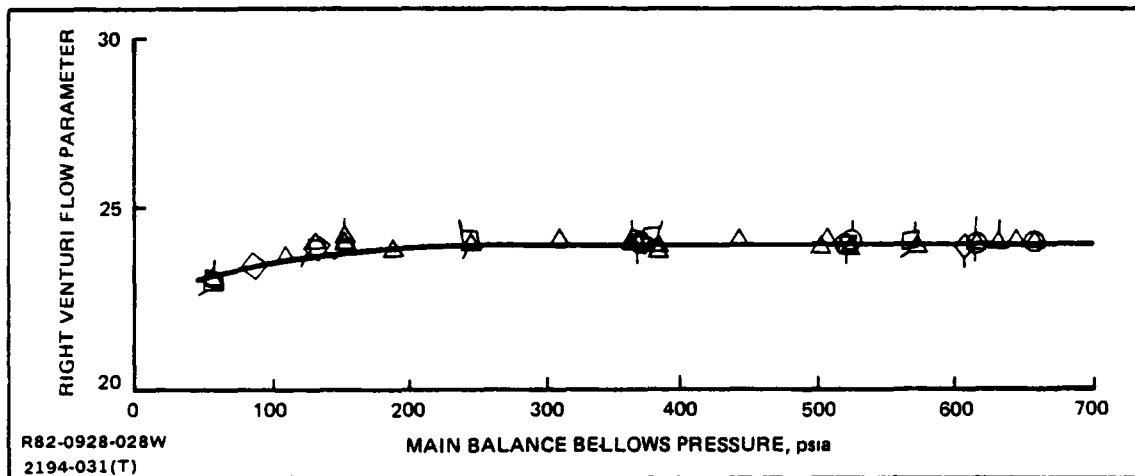
Fig. 5-6 Model Right Venturi Mass Flow Calibration

Using the calibration curves of Figs. 5-5 and 5-6, the model mass flow, as determined by the model venturi tubes, can be obtained for any combination of venturi total pressure and temperature:

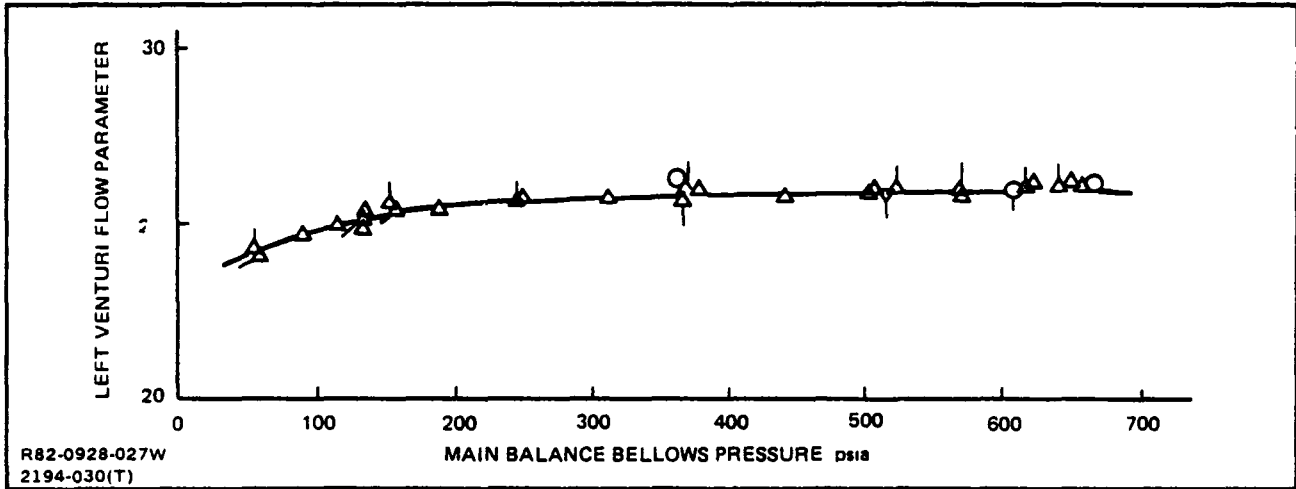$$\dot{W}_V = (VFP) \cdot \left(\frac{P_{TV}}{\sqrt{T_{TV}}} \right) \cdot$$

This was done for left and right hand venturi tubes and then summed to obtain total model mass flow.

Once left and right tailpipe mass flows are known (from either the ASME nozzle test runs or any later run using the venturi calibrations), the flow split is easily determined as shown in Fig. 5-7. In the region of interest the left to right flow split ratio is a constant (within measurement repeatability) equal to 1.056. This translates into 51.36% and 48.64% for left and right tailpipes respectively. This flow split is different every time the model is assembled and no explanation is given for the small left to right mass flow difference. The important thing is to be able to assess the difference so it can be included in the data reduction equations.
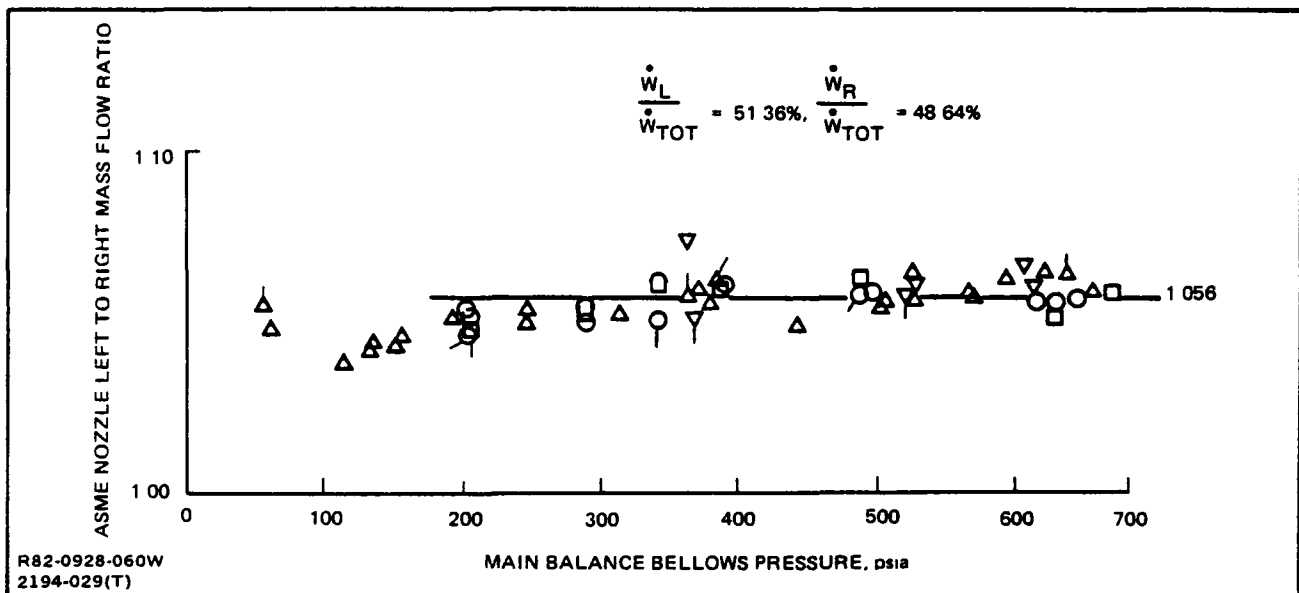
Fig. 5-7 Model Left to Right Duct Mass Flow Split

It is interesting to compare the total model mass flow rates determined by the ASME/venturi calibration relative to the independently calibrated facility flow meter. This is presented in Fig. 5-8 where the average ratio between the two methods is about 99%. The facility flow meter predicts a flow rate about 1% lower than the ASME nozzle; this is not a large difference and merely reflects instrumentation bias error.
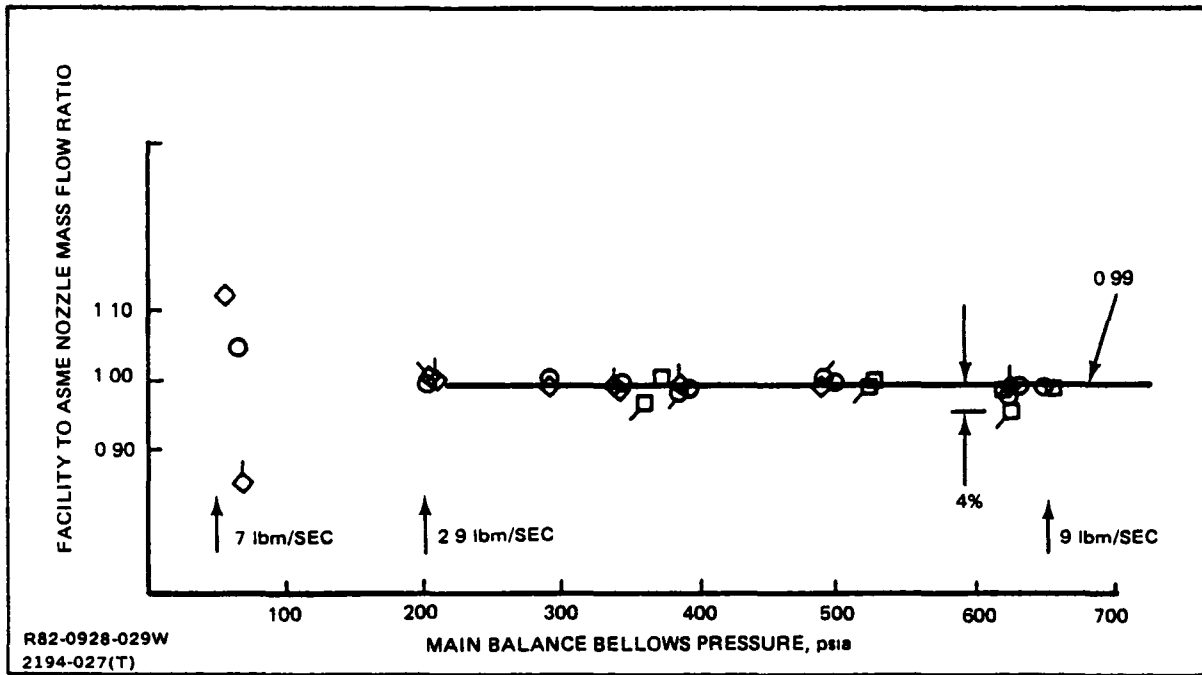
Fig. 5-8 Facility to ASME Nozzle Mass Flow Comparison

The official method of obtaining left and right as well as total model mass flow rates was to be selected. Three choices existed:

1. Use the model venturi calibrations
2. Use the facility measured flow rate in conjunction with the flow split ratio (determined with the ASME nozzle).
3. Use a hybrid method combining 1. and 2. above.

Methods 1. and 2. preserve the correct flow split ratio, but the absolute values are about 1% different as shown in Fig. 5.8. Method 3. also preserves the correct flow split ratio but uses a total mass flow based on the average of methods 1. and 2. Method 3. provided a compromise "minimum-error" approach and was selected.

If "r" is defined as the left to right flow split ratio, then the left and right tail-pipe flow rates become:

$$\dot{W}_L = 1/2\,\dot{W}_{VL} + \left(\frac{r/2}{1+r}\right) \cdot \dot{W}_{facility}$$

$$\dot{W}_R = 1/2\,\dot{W}_{VR} + \left(\frac{1/2}{1+r}\right) \cdot \dot{W}_{facility}.$$

Now $\dot{W}_L$ is used to calculate the ideal thrust for the nozzle balance, while the sum of $\dot{W}_L$ and $\dot{W}_R$ is used for the main balance.

5.2 FORCE BALANCE TARE CORRECTIONS

By knowing the total pressure (P_T), total temperature (T_T), and static pressure (P_O), the thrust coefficient (non-dimensionalized with ideal thrust) of the ASME nozzle can be determined from the following equation:

$$\left(\frac{T}{F_i}\right)_{ASME} = \frac{(CFS) - (P_T/P_O)^{-1}}{(C_{DIS})\,(CFI)}$$

where:

$$CFS = \left(P/P_T\right)\left[1 + 1.4\,C_{DIS}\left(1 - \frac{1}{1.6855} + \frac{C_{DIS}}{1.6855}\right)M^2\right]$$

$$C_{DIS} = 1 - 0.184\,(R_e)^{-0.2}$$

$$R_e = \frac{const.\,(P_T)\,(M)\,(TR)^{1.5}\left[(TR) \cdot T_T\,198.6\right]}{(T_T)^2}$$

$$TR = \left[1 + \frac{M^2}{5}\right]^{-1}$$

$$CFI = const.\left[1 - (P_T/P_O)^{-0.2857}\right]\,1/2$$

$$M = 1.0 \text{ for } (P_T/P_O) \geq 1.893$$

$$M = \left\{5\left(\left[P_T/P_O\right)^{0.2857} - 1\right]\right\}^{1/2} \text{ for } (P_T/P_O) < 1.893$$

This performance characteristic and the discharge coefficient, both obtained from this test program, are presented in Fig. 5-9. It is noted that this thrust, non-dimensionalized with the appropriate ideal thrust, is what should be measured on the main and

nozzle balance <u>axial</u> force gauges if no tares existed within the system. Correspon-
dingly, since the ASME is aligned in the axial direction, the force balance normal gauge
outputs should be identically equal to zero. Additionally, measured pitching moment
should be exactly equal to the thrust (axial) multiplied by the ASME nozzle offset
distance.
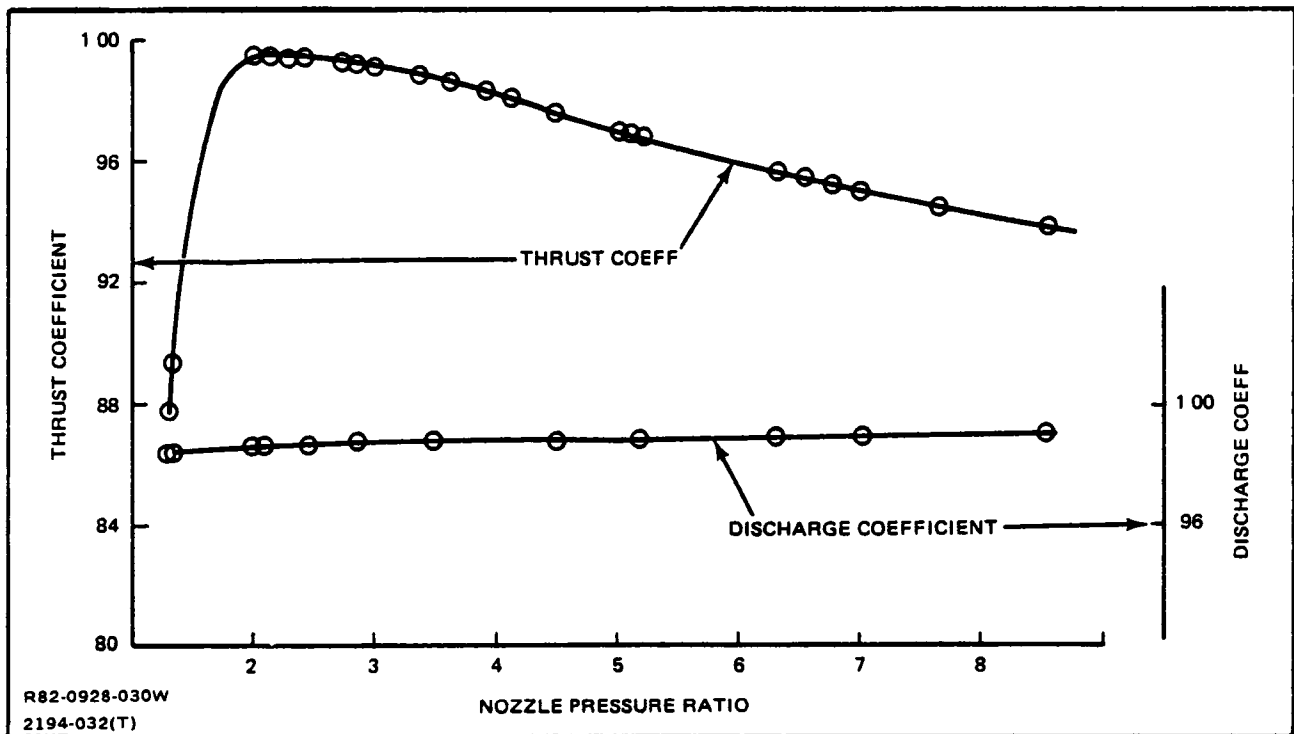
Fig. 5-9 ASME Nozzle Performance Characteristics

In general it is expected that force balance system possess momentum tares occur-
ing at the point at which the incoming momentum crosses over the metric/non-metric
interface. The difference between the actual force balance gauge readings and the
known ASME nozzle forces and moments is equal to the momentum tare. The three mo-
mentum tare components for each balance system are presented in Fig. 5-10 through 5-15.

In particular, note the main balance axial tare of Fig. 5-10. Although ±2 1/2 lbf
scatter (within balance accuracy) is observed, a definite tare force does exist. Also
note that the momentum tare is independent of ambient pressure as verified by the
three repeat runs at each of three back pressure levels (400, 1000, 1900, psf).

5-10
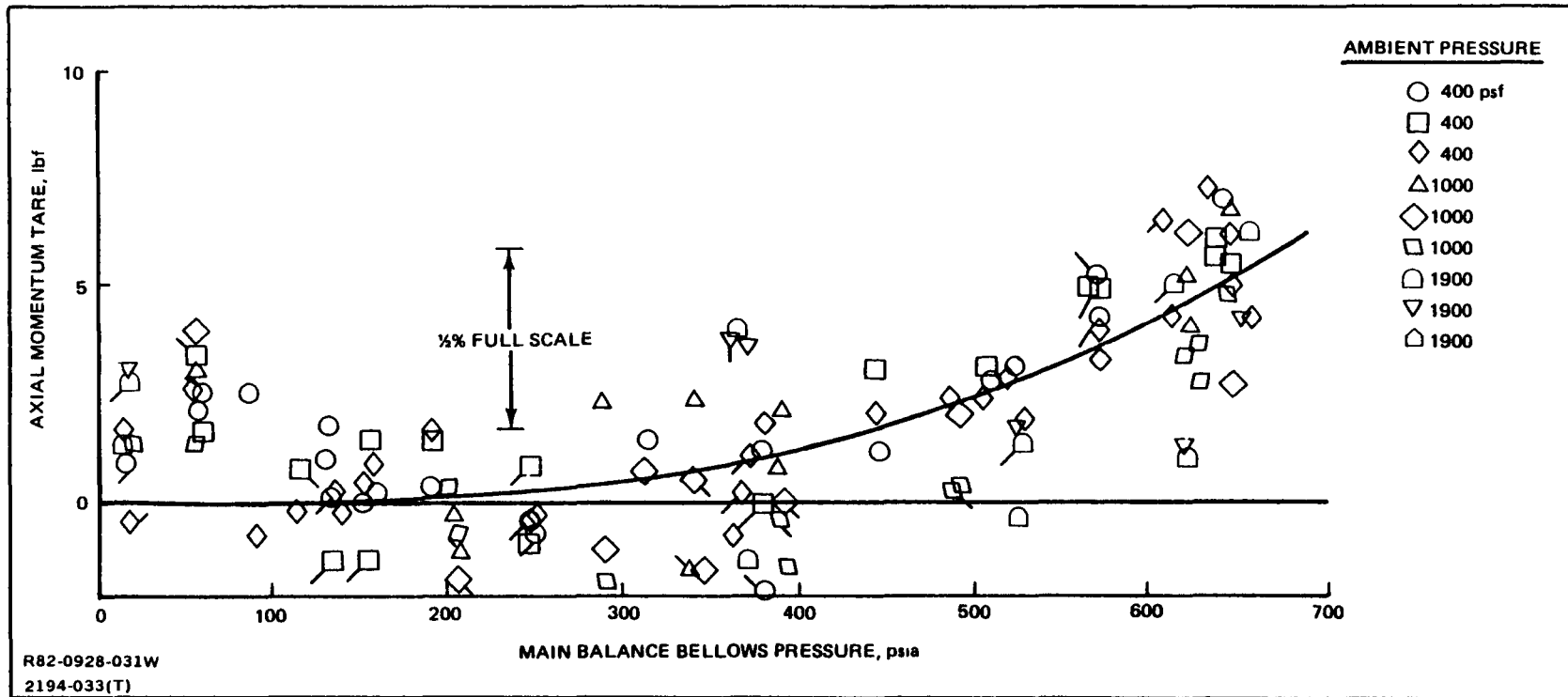
Fig. 5-10 Main Balance Axial Momentum Tare Calibration

R82-0928-031W
2194-033(T)

As expected the momentum tare fairs into zero at low pressure levels. However, the data trend at 50 psia and below is considered non-real and is ignored. This also appears for the nozzle balance axial momentum tare; and, such a coincidence if it were real, would be highly unlikely. Furthermore, the intrinsic nature of bellows is such that this apparent reversal in the data at low pressure cannot be explained. It is concluded that this data bias at low pressures is caused by slight inaccuracies in the measured mass flow at these low flow rates introducing error in ideal thrust which in turn affects the momentum tare calculation. Consequently, engineering judgment was used to continue the data fairing asymptotically to zero as pressure was decreased.

The importance of conducting several momentum tare assessment test runs is noted by observing Figs. 5-10 through 5-12. These tares are used for every test nozzle configuration, and they should be assessed and implemented with as little error as possible. Thus, many repeat runs were conducted.

Fig. 5-11 Main Balance Normal Momentum Tare Calibration

Fig. 5-12 Main Balance Pitching Moment Momentum Tare Calibration
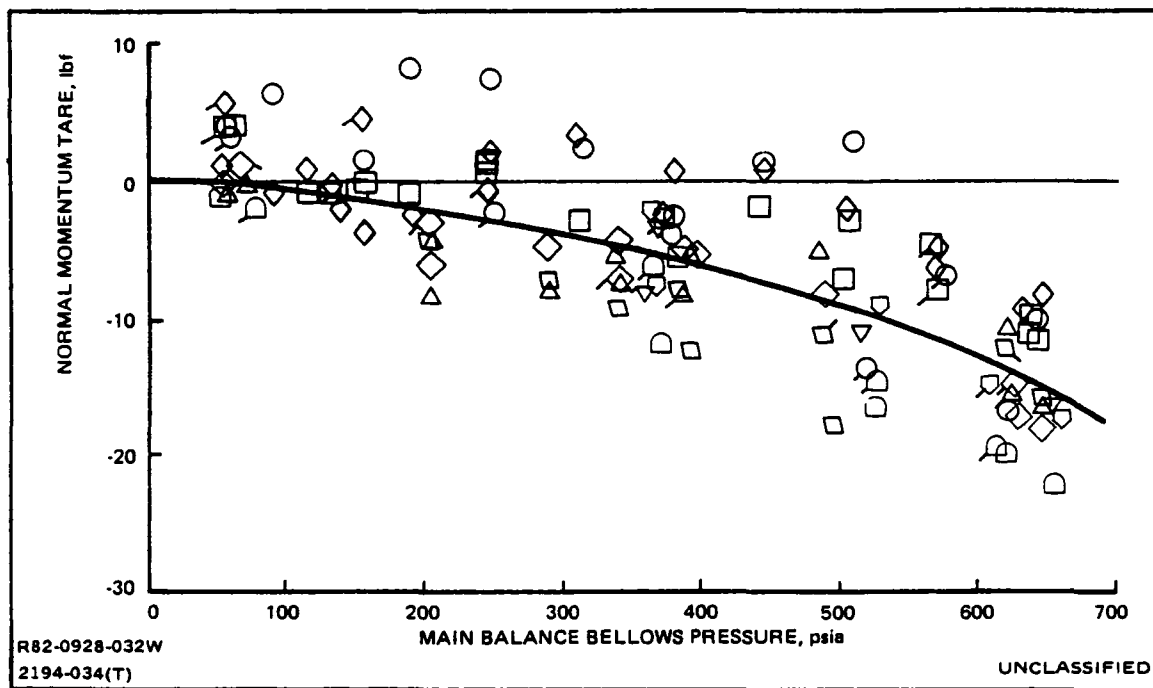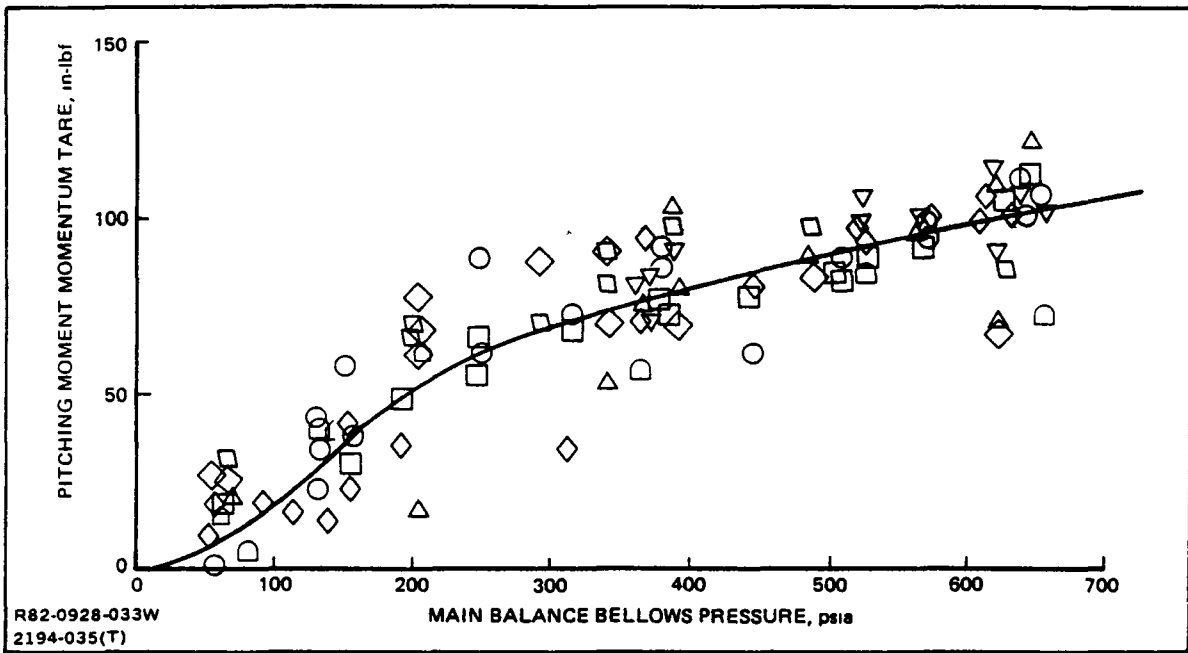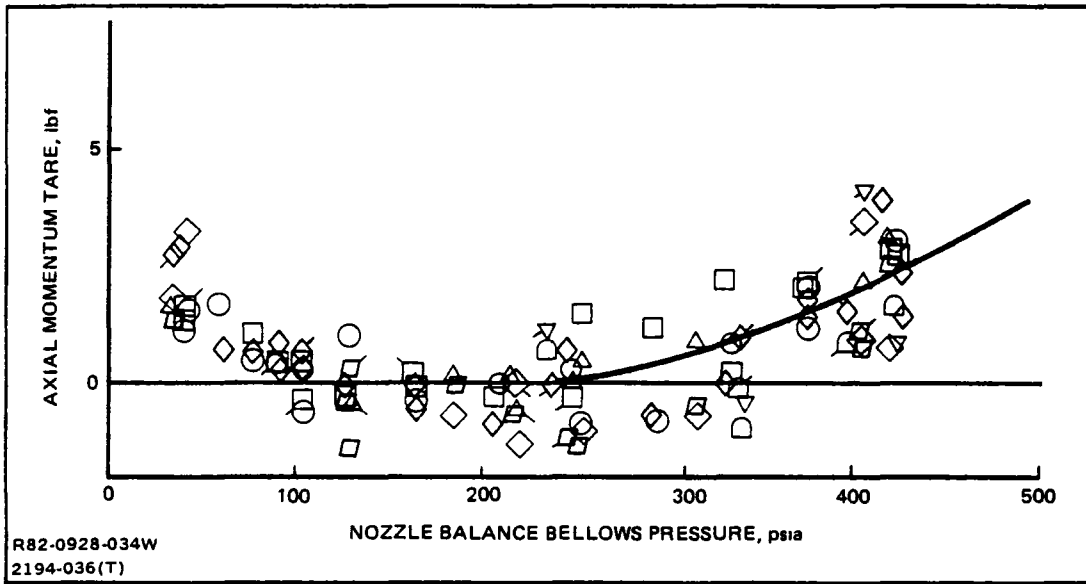

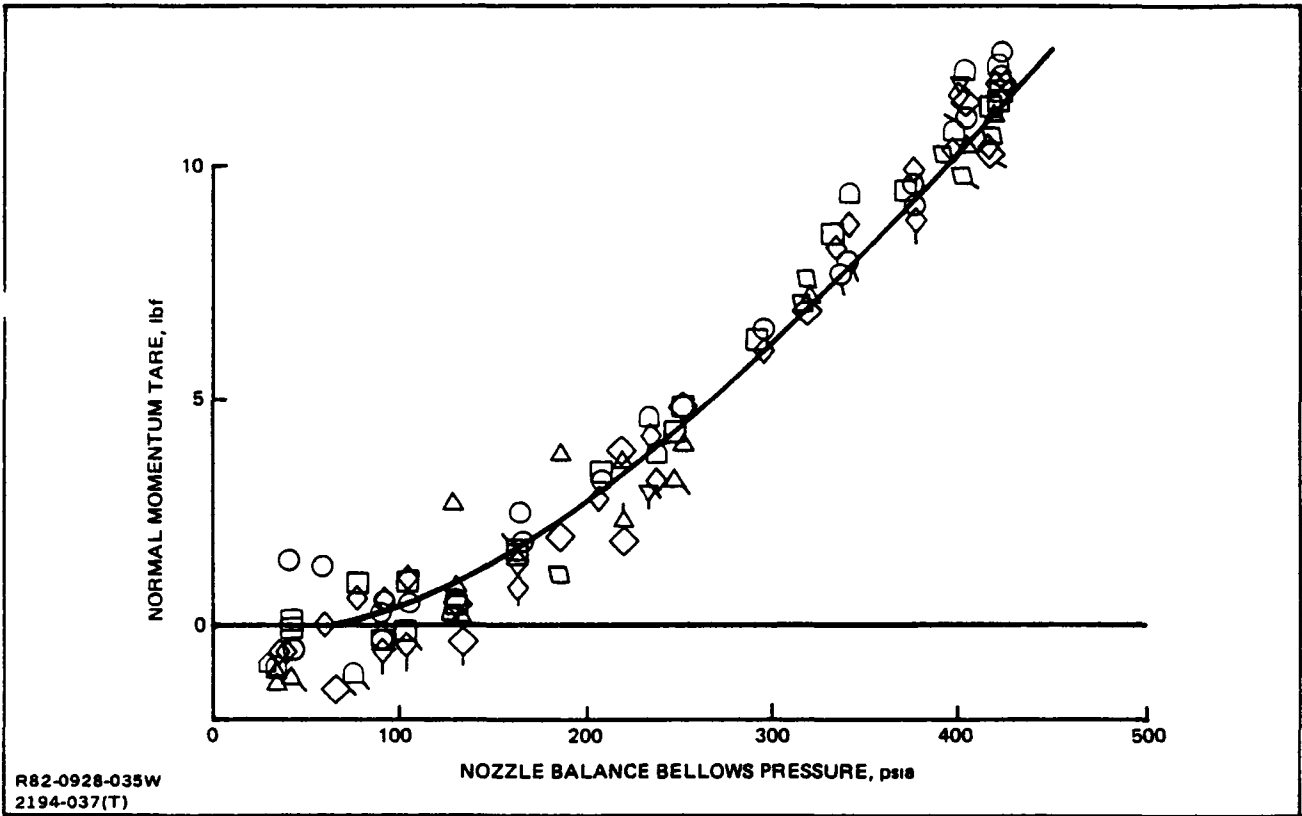Fig. 5-13 Nozzle Balance Axial Momentum Tare Calibration

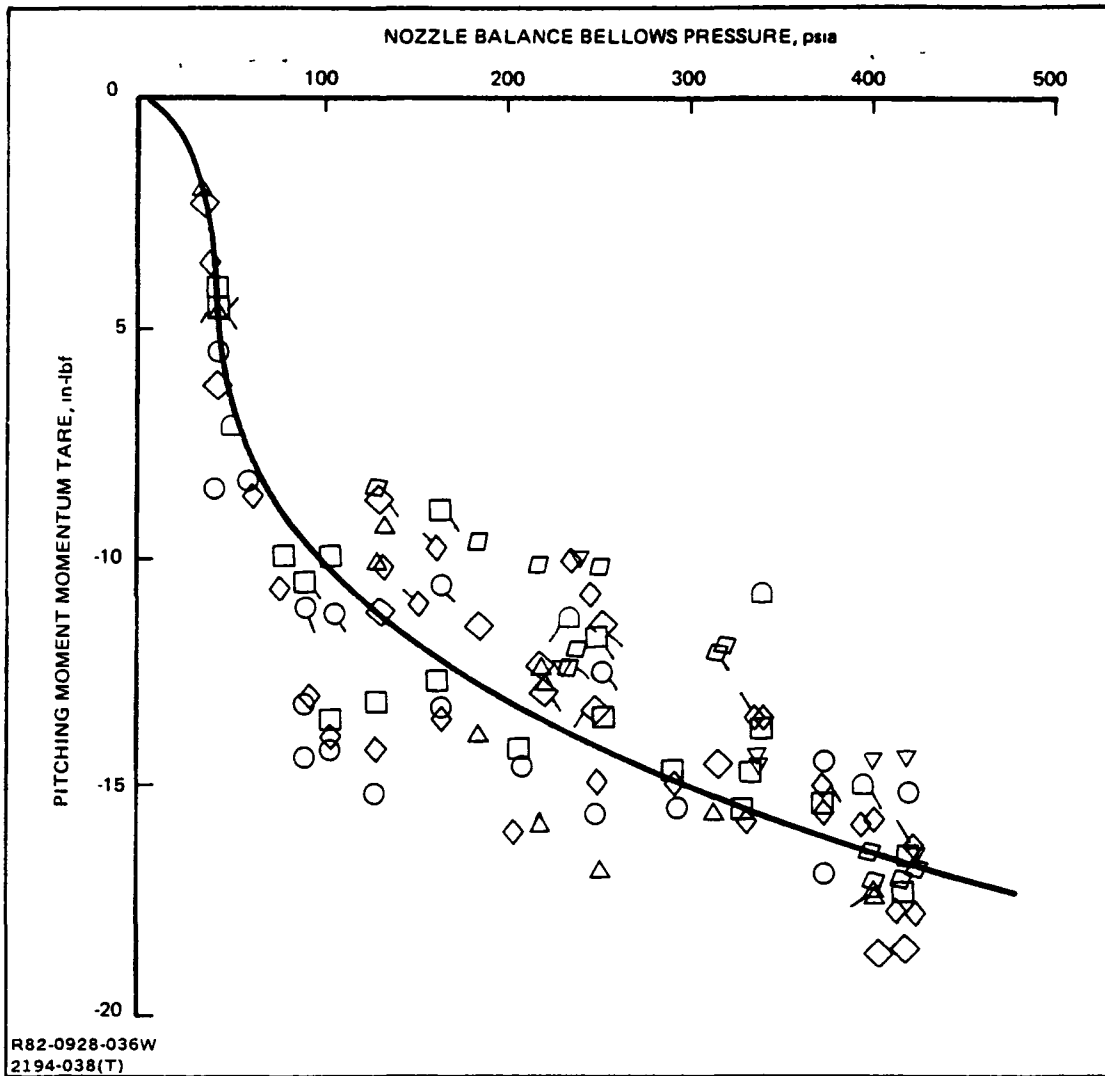Fig. 5-14 Nozzle Balance Normal Momentum Tare Calibration

R82-0928-035W
2194-037(T)

Fig. 5-15 Nozzle Balance Pitching Moment Momentum Tare Calibration

R82-0928-036W
2194-038(T)

6 - TEST PROBLEMS AND SOLUTIONS

Throughout the test program various experimental problems were encountered. These problems varied from minor to major and their solutions varied from exact to approximate. The technical problems and their respective solutions that are considered worthy of note are discussed in this section.

6.1 NOZZLE RAKE SCANIVALVE FAILURE

Difficulty was encountered operating the high pressure (50 psi) scanivalve that was used to measure the tailpipe rake total pressures. The rotor was constantly separating from the stator thereby creating interport leakage and invalidating the individual port pressure measurements. Operating high pressure scanivalves, in general, requires a greater level of expertise than operating the more common low pressure (0-15 psi) valves. Attempts at generating a variable back-up pressure schedule for the valve as a function of tailpipe total pressure failed. The lack of availability of scanivalve support personnel complicated the situation because valuable time was eroding from an already compressed test window.

Because of the uncertainty regarding the development of a timely "operational-fix" for the scanivalve, an alternative approach was devised. The scanivalve was dispensed with and instead the 19 probes on each tailpipe rake were manifolded together and read-out on a single 50 psi transducer. Note that this procedure now produced the arithmetic average instead of the area-weighted average.

However, the assumption that these two averages agreed was checked by using previously acquired tailpipe pressure data (AEDC 1977) from the same model and computing the average total pressure both ways. It was recognized that this should be done for both the ADEN CRUISE (non A/B) and ADEN COMBAT (max A/B) nozzles because tailpipe duct Mach numbers are very low with the former and much higher with the latter. It was to be expected that the high duct Mach number situation should be characterized by larger distortion thereby making it less likely for the linear average to equal the area-weighted average. The data checks showed that the CRUISE 0° nozzle agreement was typically within ± 1/4% of the absolute pressure value. On the

other hand, for the COMBAT 0° nozzle the average of the left and right tailpipes was about 1 1/2% high. Nevertheless, this was considered acceptable and substantiated the decision to manifold the rake probes and dispense with the high pressure scanivalve.

After actual test runs were made with the manifold scheme, additional verification was obtained by comparing the AMES arithmetic-average total pressure with the AEDC area-weighted average total pressure. This is shown in Figs. 6-1 and 6-2 for the right and left ADEN CRUISE 0° nozzles. The AMES data falls right on the AEDC fairing and the agreement is considered excellent (the break in the curve of Fig. 6-2 will be addressed as a separate problem in subsection 6.2.)

For the large jet area ADEN COMBAT 0° nozzles, the corresponding comparison is presented in Figs. 6-3 and 6-4. As predicted the agreement is not perfect, although acceptable, on the right side; but, on the left side the agreement is excellent. Combining both left and right duct data, the total discrepancy between the two methods is between 1 - 2 %.

It is further noted that if the "static-pressure-method" as opposed to the "ideal-thrust-method" (Ref. 2) is employed for the calculation of thrust-removed parameters (e.g. lift and drag), then any impact of nozzle total pressure uncertainty is greatly minimized. The only minor impact on drag, for example, would be the drag increment between an NPR of 5.0 versus 5.1 which reflects a 2% error in total pressure. The data of Ref. 1 show this to be negligible with respect to the overall balance accuracy.
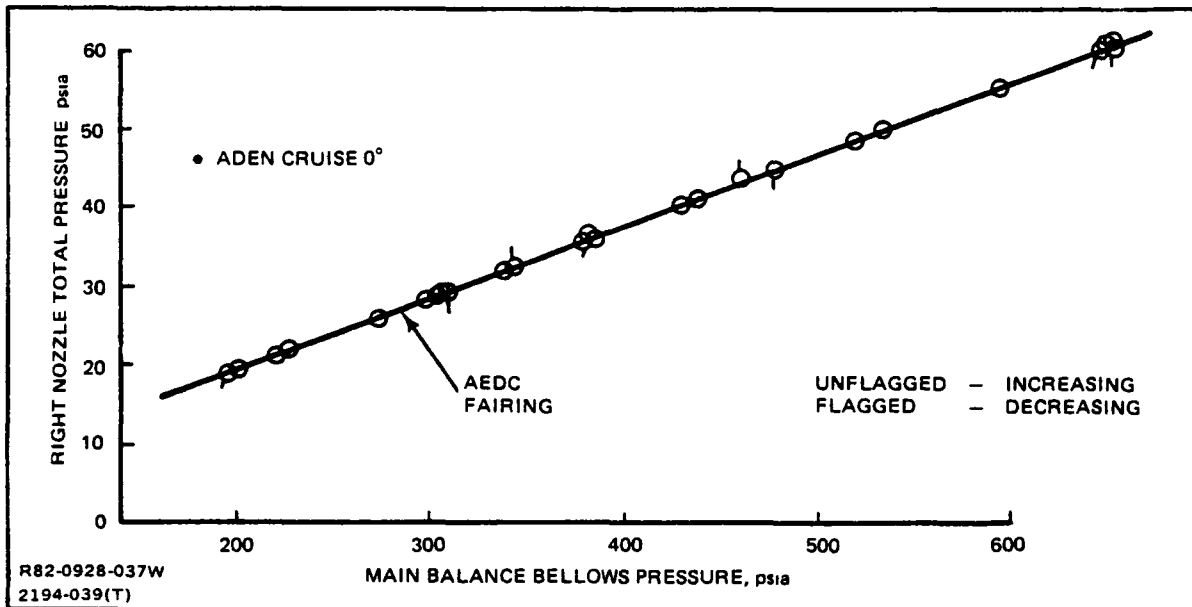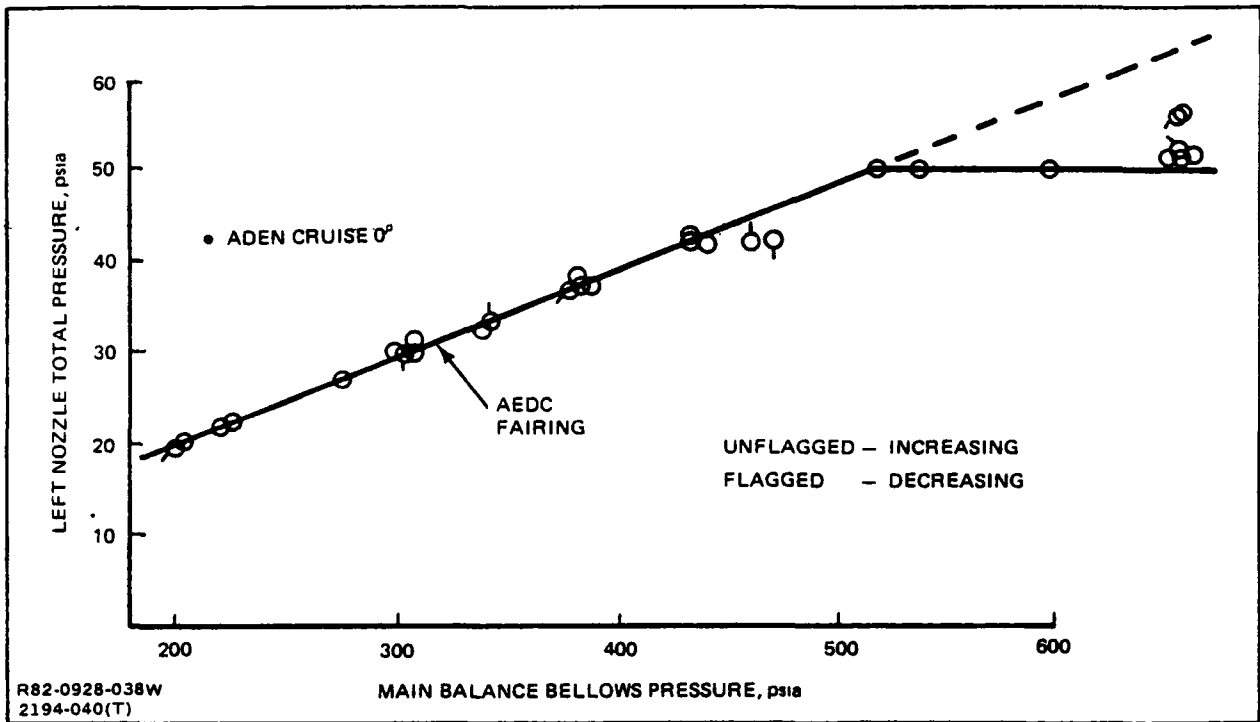

Fig. 6-1 Right Nozzle Total Pressure Correlation

Fig. 6-2 Left Nozzle Total Pressure Correlation
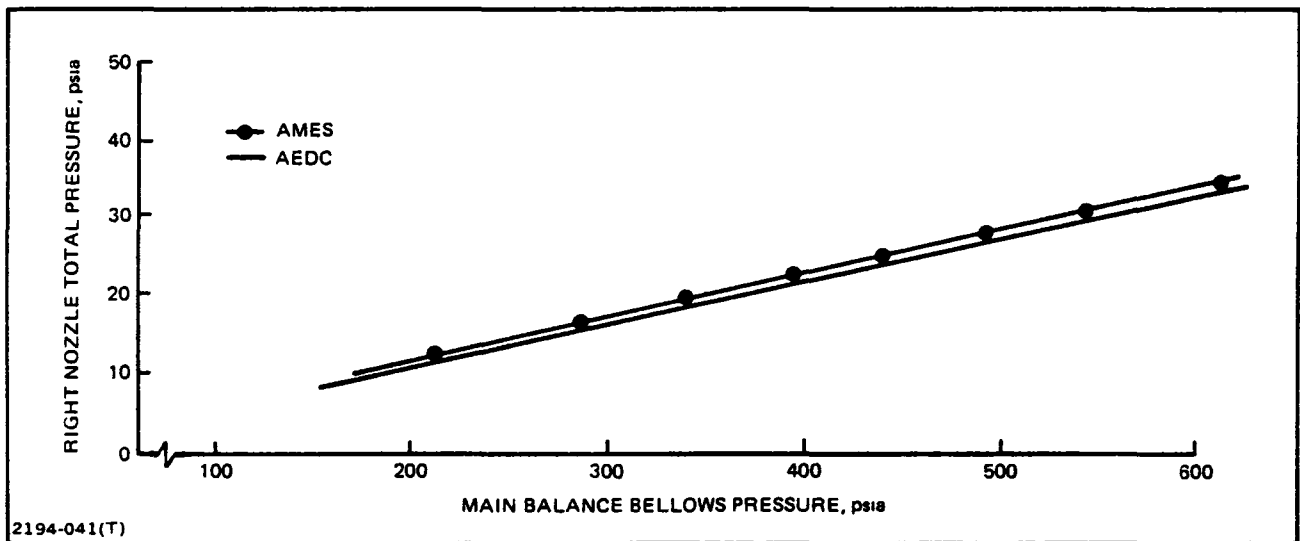
Fig. 6-3 Right Nozzle Total Pressure Comparison
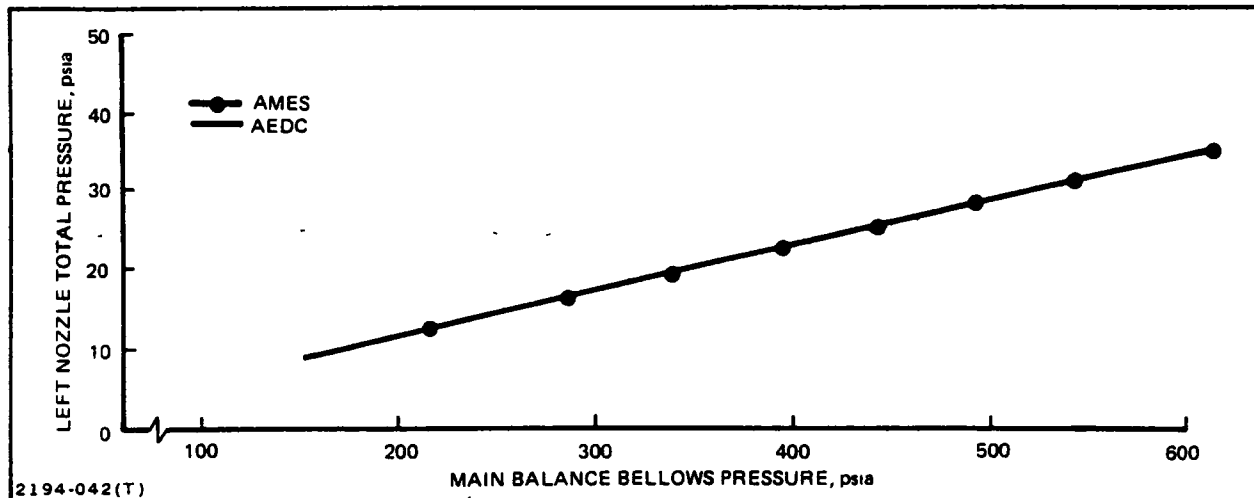
Fig. 6-4 Left Nozzle Total Pressure Comparison

6.2 NOZZLE RAKE TRANSDUCER RANGE LIMITATION

As discussed in subsection 6.1, individual 50 psid capacity transducers were used in lieu of the malfunctioning scanivalve. Generally, tranducers have at least a 20-25% "override". It was anticipated that this would be the case for this test; however, although the left duct transducer exhibited an override, the right one did not as shown in Fig. 6-2. Thus, the rake total pressure data at the high pressure levels was in error.

The solution to this problem is straightforward. The data reduction program was modified to ignore all measured values of left duct total pressure (P_{TL}) above 400 psia, and instead use the following expression:

$$P_{TL} = .0975 \times PMB$$

which represents the equation of the extrapolated line shown dashed in Fig. 6-2. Although the break in the curve of Fig. 6-2 only occurred at a bellows pressure (increasing) level of over 500 psia, the 400 psia "cut-off" was selected for conservatism because a hysterisis effect was observed when the malfunctioning transducer was operating at high pressures. This can be observed by noting the flagged symbols at a bellows pressure of approximately 460 psia.

6.3 GROUNDING - NOZZLE BALANCE

Potential for grounding the nozzle balance metric system was suspected where the non-metric nacelle lower cover plate was in close proximity with the metric tailpipe.

6-4

In the clearance gap between these two hardware pieces, many plastic pressure tubes were routed towards the scanivalve. After the ADEN COMBAT 0° configuration was tested, a zero shift was observed by the technicians. Using soft clay inside the lower cover plate, diagnostic fitting was conducted to investigate the possibility of mechanical interference by the plastic pressure tubes. It was concluded that grounding was a distinct possibility, but its severity was still open to question.

Prior to the running of the next configuration, ADEN COMBAT 0° ALT, the plastic pressure tube routing was rearranged so grounding could not occur. Note that the COMBAT 0° nozzle possesses the identical geometry as the previous COMBAT 0° ALT nozzle (Ref. 2). Therefore, by comparing the static thrust coefficients of the latter with the "suspect data" from the former, insight into the grounding severity should be forthcoming.

Surprisingly, the data of Fig. 6-5 show little difference between these two nozzle configurations. It is possible that the grounding, which was suggested by the zero shift and diagnostic fitting check, was only apparent at jet-off conditions. At jet on conditions, the mechanical vibration caused by the high pressure air can relieve a minor grounding situation. This, of course, would be fortuitous, but evidently appears to be the case.
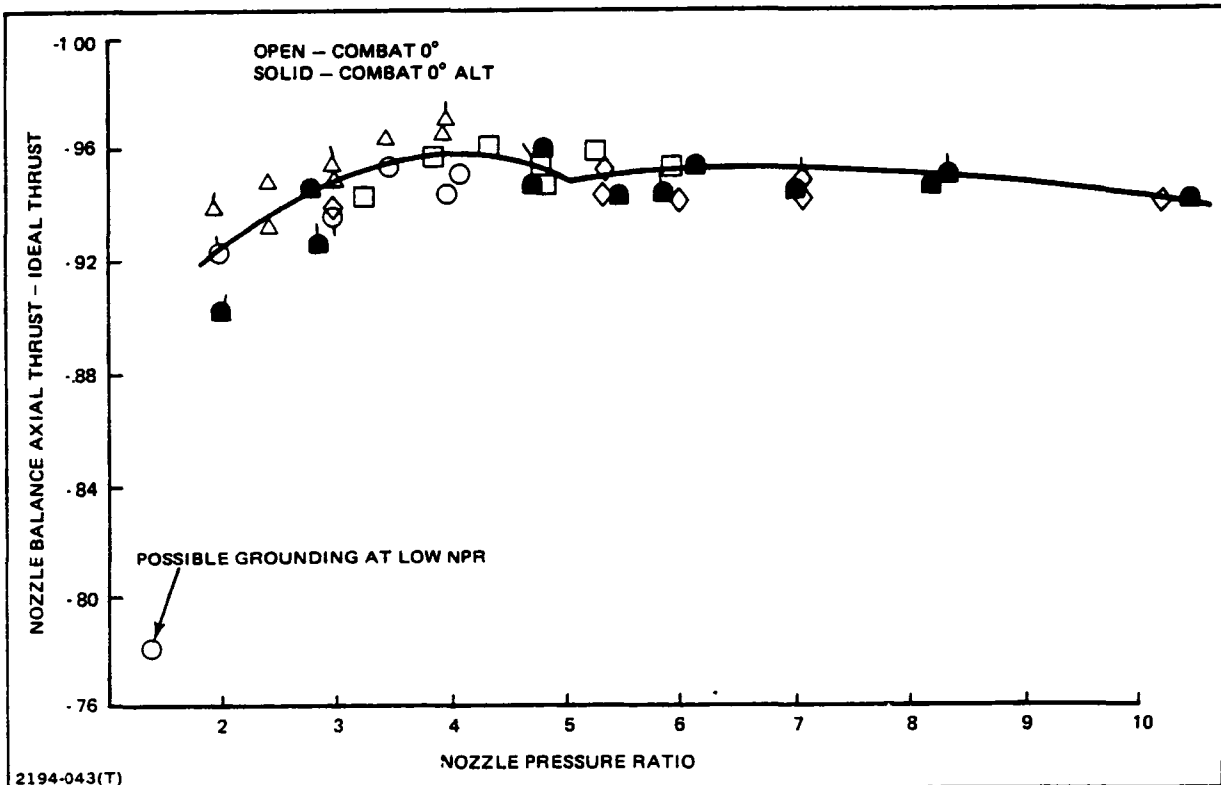
Fig. 6-5 Possible Effects of Grounding on Nozzle Balance Thrust

Nevertheless, because the possibility of nozzle balance grounding always existed during the test, a study was conducted after the completion of the test program to check out the extent of grounding, if any, for the entire configuration matrix. It was recognized that the AMES nozzle balance data could be compared with both a previous test at AEDC (Ref. 4) using the same nozzles and General Electric Co. predications based on empirical results. It can be hypothesized that if grounding were prevalent in the AMES data, then the thrust of this test program would be consistently lower than either the AEDC thrust data or the GE predictions.

The results of this nozzle balance study are presented in Figs. 6-6 and 6-7 for two typical nozzle pressure ratios (NPR). Observe that the AMES data is always slightly higher or within 1% of either the AEDC or GE levels. Since differences of 1% of ideal thrust are considered small, especially between different test programs, it is concluded that the AMES nozzle balance data were not characterized by any significant grounding after all.
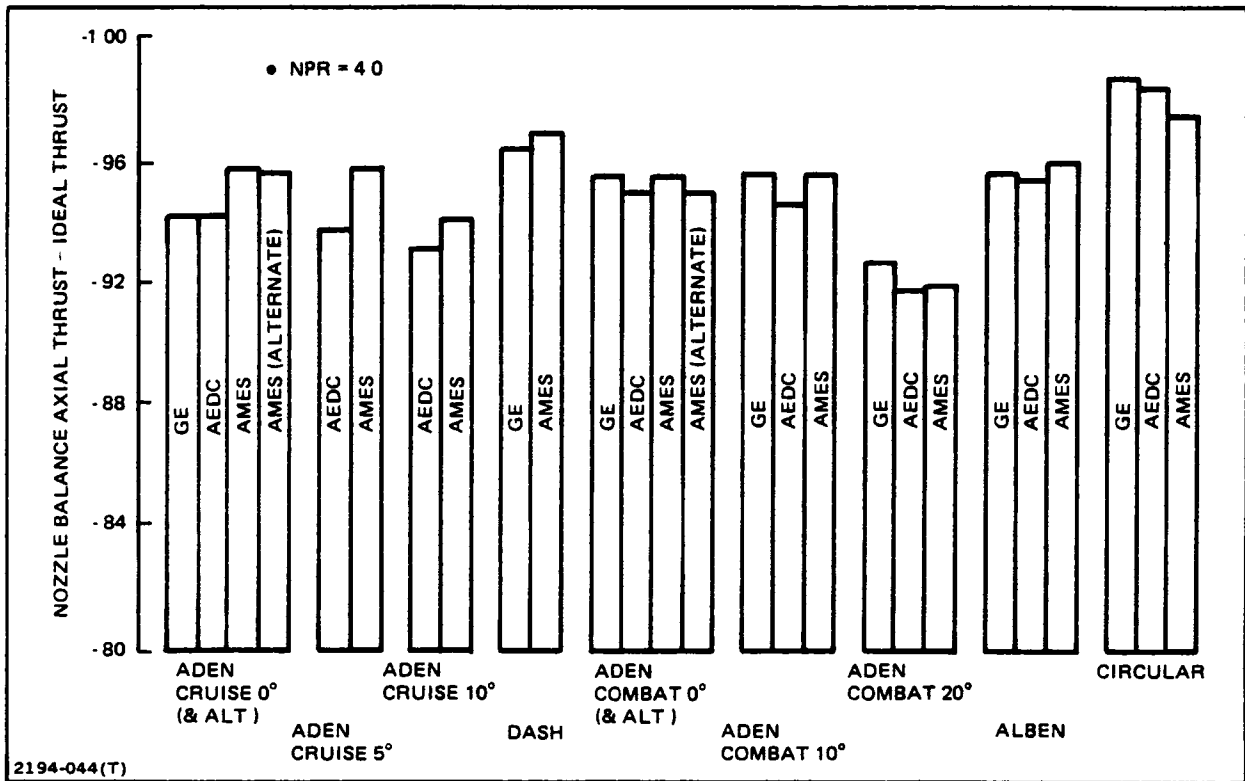
Fig. 6-6 Nozzle Balance Thrust Comparison at NPR = 4.0
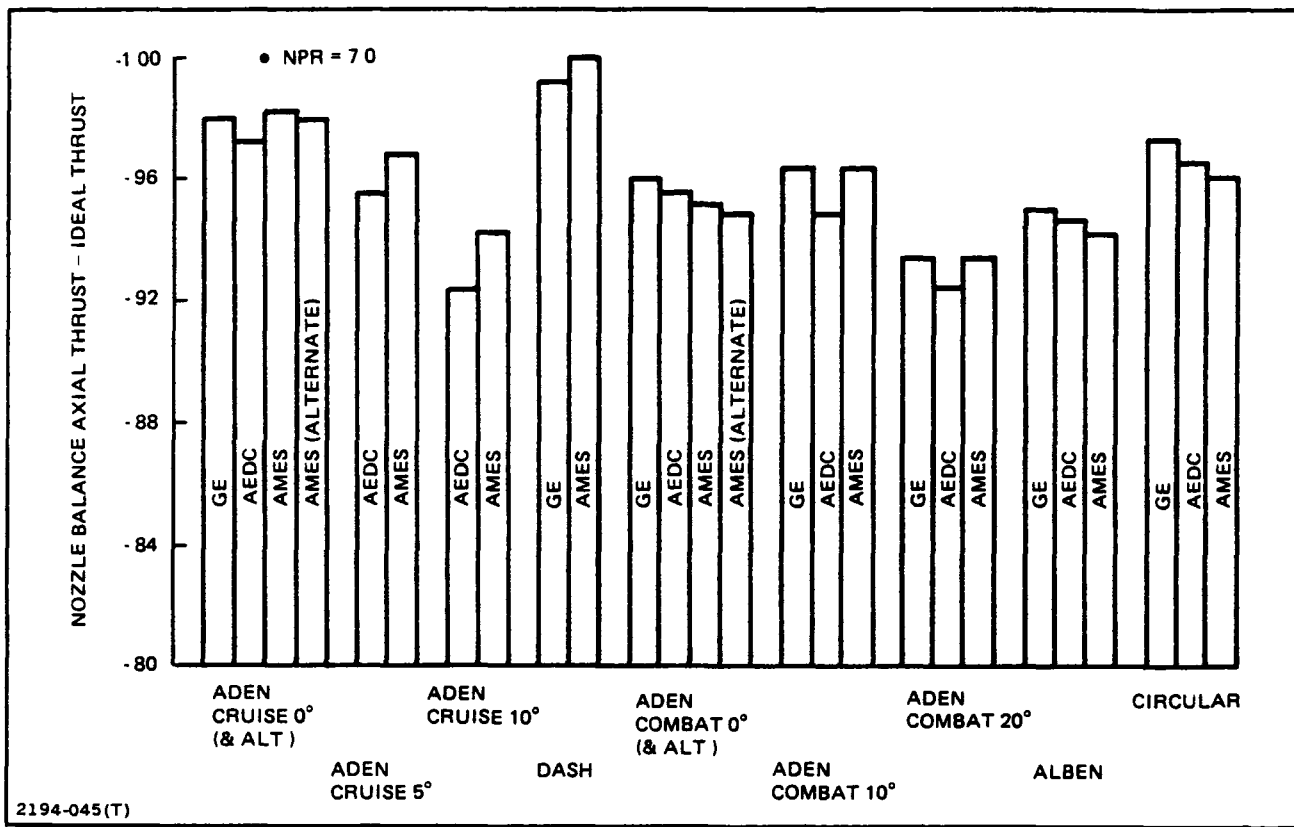
Fig. 6-7 Nozzle Balance Thrust Comparison at NPR = 7.0

6.4 GROUNDING - MAIN BALANCE

Post test data analysis surfaced a main balance grounding problem that was not apparent during the test runs. The model grounding alarm systems evidently were not sufficiently extensive to include all potential grounding situations. Many times, the a priori identification of all possible areas of mechanical interference and the wiring of these areas are very difficult tasks during model installation - especially under the pressure of a short occupancy time period. Nevertheless, it is highly desirable.

The effect of the metric/non-metric grounding as angle-of-attack is increased was very noticeable in the axial force coefficient as shown in Fig 6-8. Note the clear cut break in the axial force characteristic at the higher attitudes. Furthermore, grounding occurs at all nozzle pressure ratios as well as jet-off.

An in depth study was undertaken to determine if this main balance grounding phenomenom was intermittent or regular. A computer plot code was developed to plot the axial force coefficient versus angle-of-attack for every test configuration at every Mach/NPR combination. The idea was to inspect each of the plots in order to identify

all grounded data points. A sample computer plot appears in Fig. 6-9. From this plot it is easily concluded that the inception of grounding occurred between about 8 1/2 and 10 degrees.

Fig. 6-8 Effect of Grounding on Axial Force

Fig. 6-9 Computerized Diagnostic Grounding Study

2194-047(T)

By studying all the grounding-screening plots in perspective it became clear that the mechanical interference was dynamic pressure depende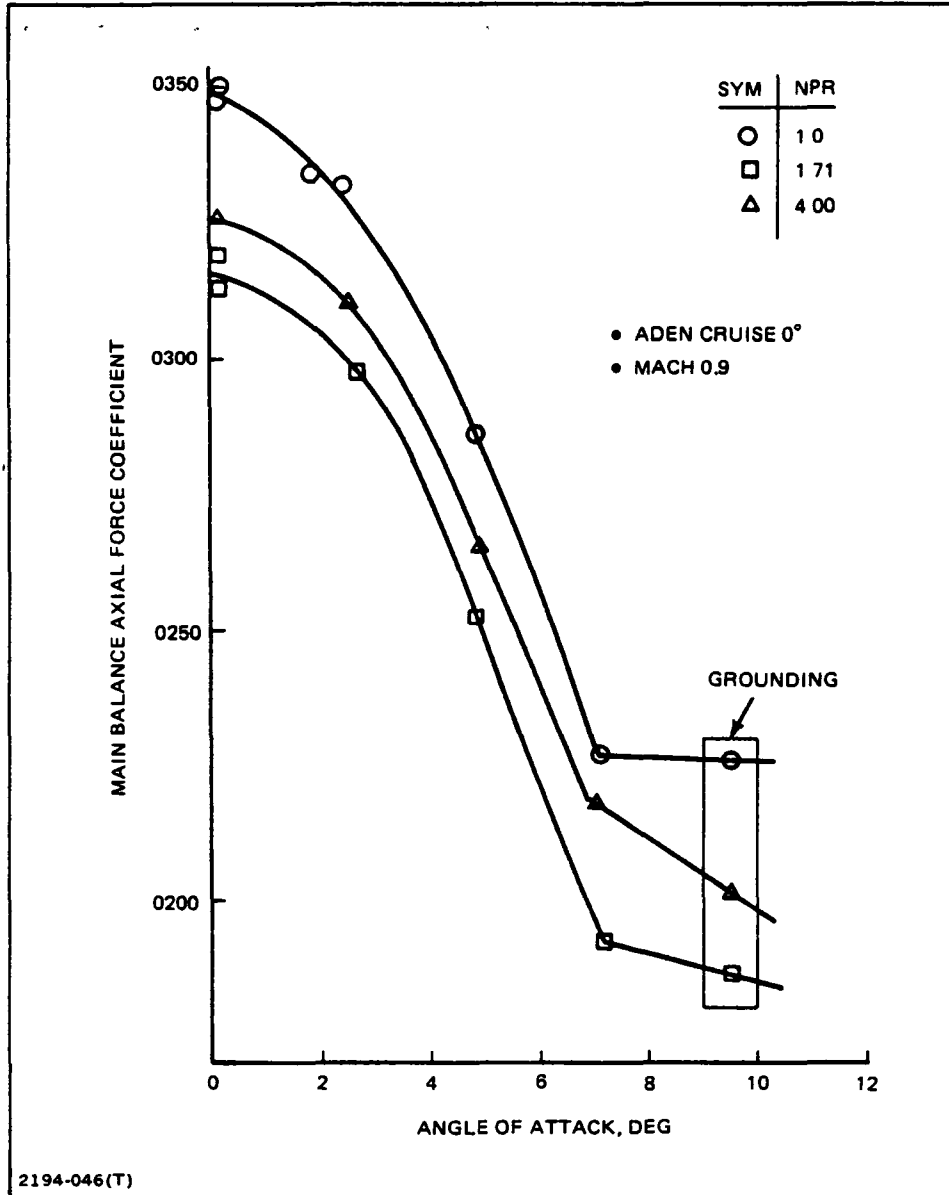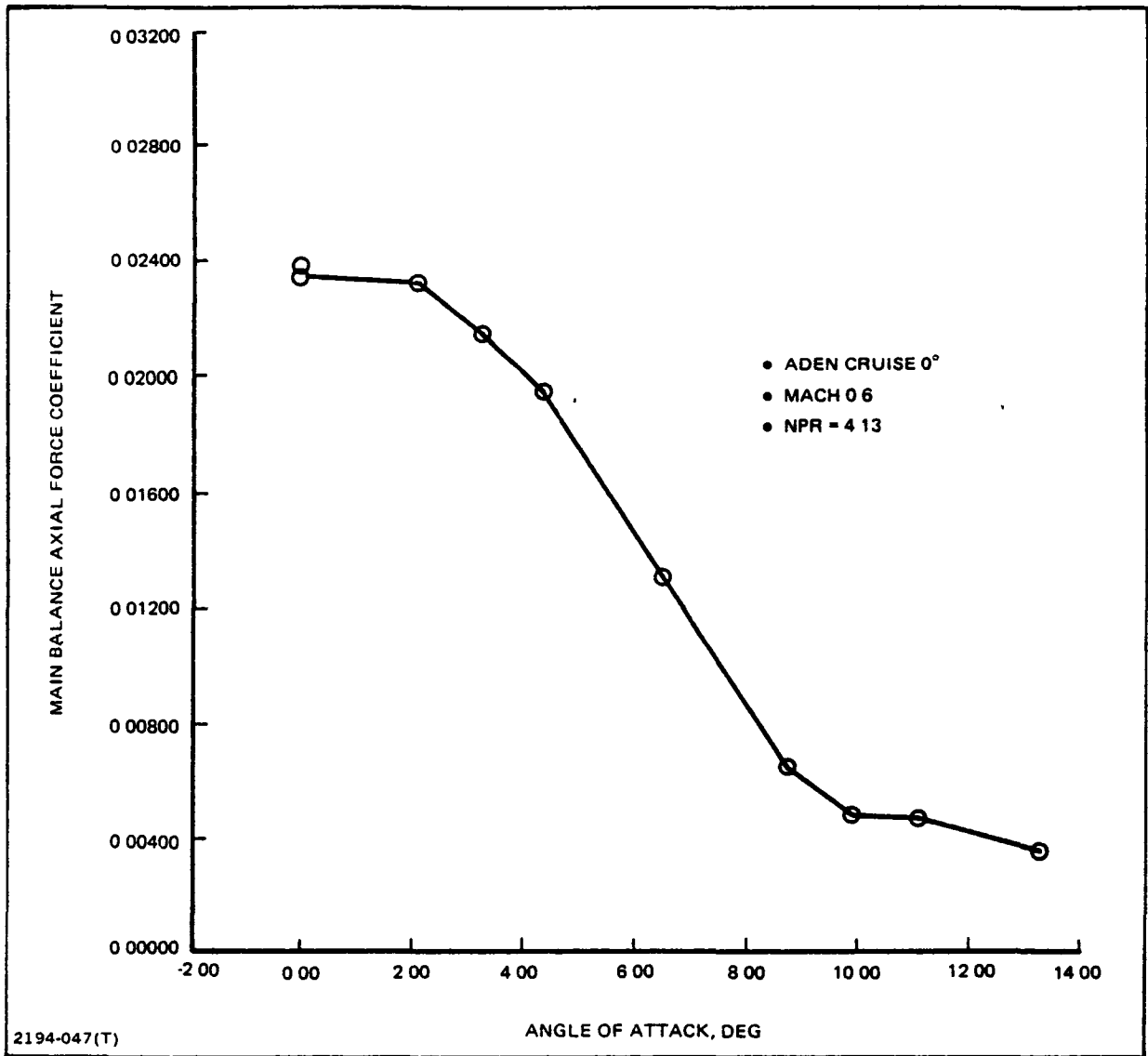nt. The α at which grounding first occurred decreased as dynamic pressure increased. The result of this study is summarized in the following table (which is also discussed in Ref. 1):

Mach No.	Limit α (Deg)
0 4	9-1/2
0 6	8
0 8	7
0 9	6-1/2
0.95	6-1/2
1 2	~5
1 4 (1.35)	~5
R82-0928-059W	

All data points that were identified as grounded were voided from the test data matrix. Fortunately, un-grounded data existed over a sufficient α- regime so that the major objectives of the test program were not seriously compromised.

6.5 BALANCE ZERO SELECTION

Recall the discussion of Section 3 that recommended a dummy static run to "shake the model loose" and "temperature-soak" the metric system. The intent is to eliminate or minimize the "cold-start" problem. During a significant portion of the subject test program, this recommendation was not implemented due to human factors considerations. Therefore, discrepancies occurred between the initial and final zero as reflected by the sample air-off points (see Section 3 for discussion of air-off data) below:

Run no.	Main balance				Nozzle balance			
	Axial, lbf		Normal, lbf		Axial, lbf		Normal, lbf	
	Init	Fin	Init	Fin	Init	Fin	Init	Fin
43	+0.8	-2.7	+1.2	-14 9	-0.4	-1 7	-0 3	+0.2
44	-2 7	-3.3	-13 3	-15.7	-1 1	-1 7	+0 2	+0.6
45	-3.5	-4 1	-14 8	-21 0	-1.1	-1.4	+0 7	+0 3
R82-0928-001W								

For example, between the beginning and end of run 43, the main balance axial force shifted by 3.5 lbf. (0.8 + 2.7), while the main balance normal force shifted by 16.1 lbf (1.2– –14.9). As a percent of full scale, these shifts represent about 1/2% and 1/3% respectively. Although not huge numbers, these errors should not go uncorrected.

Based on studies, similar to the above, it was decided to reduce the complete test data matrix on the basis of final zeros instead of initial zeros.

A prime example of the solution to the initial/final zero problem is highlighted in Figs. 6-10 and 5-11. First, Fig. 6-10 presents the normal momentum tare for runs 19, 20 and 21 and shows a level difference compared to the other six runs. Note that these three runs were conducted in a batch and all were reduced with a very severe "cold-start" zero. Second, Fig. 5-11 shows that the utilization of a final zero methodology virtually collapses the data so that all nine runs now agree within normal data repeatability.
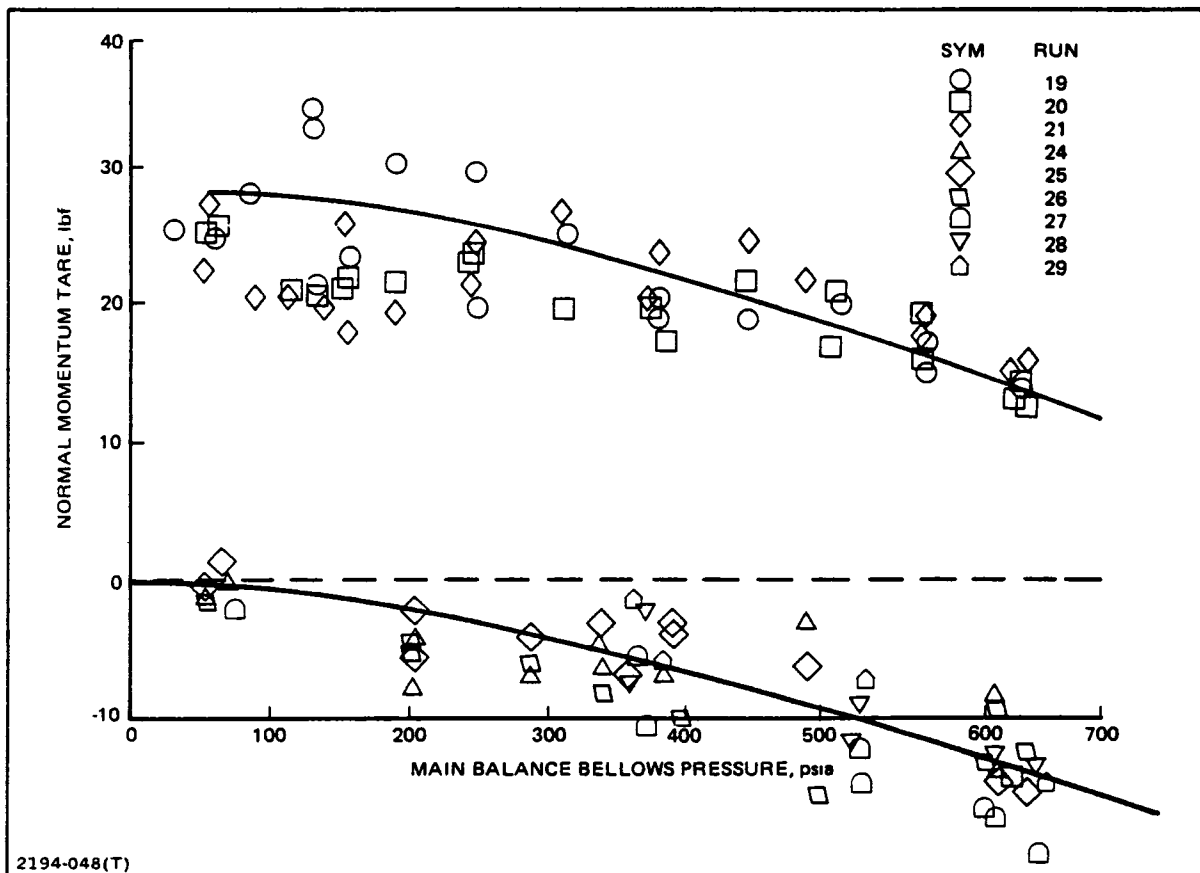

Fig. 6-10 Impact of Zero Shift on Main Force Balance Data

6.6 MODEL WEIGHT BIAS CORRECTIONS

Before discussing the bias problem encountered during this test and its solution, a brief discussion of the bias weight is appropriate.

Recall that Section 3 presented all the steps required to calculate the net aero/ propulsive forces from the actual gauge readings. At wind-off/jet-off conditions, with zero angle-of-attack (balance level), EUBAL.N1 and EUBAL.N2 are the bias weights which represent the distribution of the model dead weight to the forward normal (N_1) and aft normal (N_2) gauges. The sum of EUBAL.N1 and EUBAL.N2 is not equal to the model weight, because of inter-gauge interactions, although it is close (within 1%). The model weight, on the other hand, is equal to the sum of the two normal force gauges after interactions are computed:

$$\text{MODEL WEIGHT} = \text{EXINT. N}_1 + \text{EXINT.N}_2. \quad (M = o, \ \alpha = 0°; \ \text{for this model})$$

The reason the bias correction is obtained is so that it can be removed, along with the static incremental weight tares, to obtain the net aero/propulsive forces.

Note that the bias weights (as well as the static incremental weight tares) should be determined for each configuration that either possesses a different weight or weight distribution.

The bias weights were not available for any of the test nozzle configurations for both main balance and nozzle balance. The solution to the problem was four-fold:

1. Utilize an existing static weight tare run to calculate the model weight using the axial gauge (more accurate than using normal gauges):

$$W = \frac{-AF}{\sin \alpha}$$

2. From the same static weight tare run the c.g. location (XCG;ZCG) can be determined by writing two moment equations (at two different angles-of-attack) of the following form:

$$(N_1 - N_2).(XB) = (W \cos \alpha).(XCG) - (W \sin \alpha).(ZCG).$$

3. Incremental weights and c.g. locations for other test nozzle configurations were obtained by weighing and balancing the various nozzle configurations.

4. Calculate the bias weight for each configuration for each balance system and input them into the facility data reduction program for each configuration.

The last step requires elaboration as explained below. In order to back-calculate the biases, the following two ground rules were employed:

1. $EXINT.A_x = 0$

2. $EXINT.N_1 + EXINT.N_2 = W$

This merely means that for the balance level, no component of model weight should appear in the axial direction (after interactions) and that all of the model weight is distributed over the two normal force gauges.

Since XCG is known (from above), the exact distribution of the model weight is therefore known:

- $EXINT.N_1 = \dfrac{W}{2}\left(1 - \dfrac{XCG}{XB}\right)$
- $EXINT.N_2 = \dfrac{W}{2}\left(1 + \dfrac{XCG}{XB}\right)$

Now, making use of the balance interaction equations presented in subsection 4.1 and recognizing that the BIAS is really EUBAL for this calculation, the following three equations can be written:

1. $BIAS.N_1 = EXINT.N_1 + \dfrac{dN_1}{dN_2} \cdot EXINT.N_2 + \dfrac{dN_1}{dA_x} \cdot EXINT.A_x$

2. $BIAS.N_2 = EXINT.N_2 + \dfrac{dN_2}{dN_1} \cdot EXINT.N_1 + \dfrac{dN_2}{dA_x} \cdot EXINT.A_x$

3. $BIAS.A_x = EXINT.A_x + \dfrac{dA_x}{dN_1} \cdot EXINT.N_1 + \dfrac{dA_x}{dN_2} \cdot EXINT.N_2$.

For the ADEN CRUISE 0° configuration, whose model weight was 667 lbf., the results are summarized:

Guage	Bias	EXINT
N_1	−483 lbf	−477 lbf
N_2	−179 lbf	−190 lbf
A_x	+ 6 lbf	0
R82-0928-002W		

Note the sum of $EXINT.N_1$ and $EXINT.N_2$ equals the 667 lbf model weight. As stated before in this subsection, the total bias weight (483 + 179 = 662 lbf) is close

but not equal to the model weight. Also, observe that a small 6 lbf axial bias weight must exist in order for $EXINT.A_x$ to be identically zero, as it physically must.

Concern was exhibited over the impact of an error in determining the bias split ratio $(EXINT.N_1 \doteq EXINT.N_2)$ on axial force. A sensitivity study was done for an arbitrary 600 lbf model whose c.g. was located either forward or aft of the balance center with bias split ratios of 2.5/1 and 6.0/1. The following table summarizes the outcome:

Bias. A_x	C.G. location	Split-ratio
5 3 lbf	Forward	2 5/1
6 8 lbf	Forward	6 0/1
0 9 lbf	Aft	2 5/1
0 4 lbf	Aft	6 0/1
R82-0928-003W		

These results must be interpreted in light of the fact that 1/2% of full scale is 4 lbf. As expected, the axial bias changes whether the c.g. is forward or aft of the balance center. However, for either forward or aft locations, even a large error in the determination of the split ratio has relatively little impact in the axial force output.

As another point of interest, the sensitivity of axial force to a significant 5% error in assessing the model weight was studied. The results are:

BIAS. A_x	Model Weight
6 lbf	100%
5 7 lbf	95%
R82-0928-004W	

Again, since 1/2% of full scale axial force is 4 lbf, it is clear that an error as large as 5% in model weight imparts only a negligible error to axial force ($\alpha = 0°$). Since the weight of all test configurations did not vary by more than 5% (with most much less), it could be argued that the bias weights did not have to be assessed for every configuration. Although this argument is valid, nevertheless, the incremental model weights still would have had to be assessed for the static weight tares where large errors could exist at some conditions. For example, with a 5% error in weight at an attitude of 12°, the difference in $W \sin \alpha$ is significant:

$W \sin \alpha$	Model Weight
140 lbf	100%
133 lbf	95%
R82-0928-005W	

6.7 MAIN BALANCE SHIFT - THRUST CORRECTION

Midway through the test program, a shift in the main balance axial force was observed. The nature of this shift and a correction for it will be presented. Additionally, attempts at understanding this phenomenon will be discussed.

The axial force gage shift resulted in high static thrust data readings (too much thrust). This is typified in Fig. 6-11 where the main balance reads about 4% (of ideal thrust) higher than the nozzle balance. Note that both balances should theoretically measure the same thrust coefficient. At a typical back pressure (P_o) of 1300 psf and at a nozzle pressure ratio of 4.0, this difference is about 15 lbf or almost 2% of full
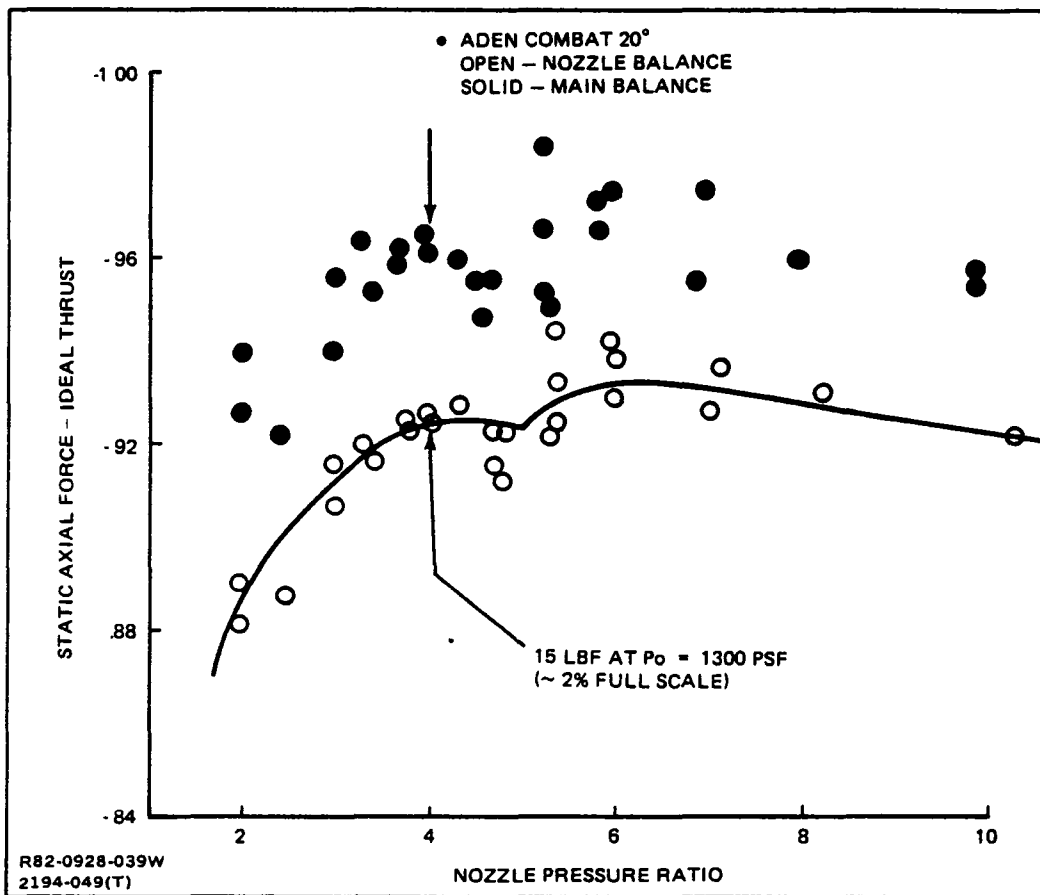

Fig. 6-11 Effect of Main Balance Shift on Static Axial Force

scale. This disparity is considered significant because it is greater than the ± 1/2%
nominal bare balance uncertainty (Ref. 5).

By comparison, a small but perceptible shift was observed in the main balance
normal force output. However, Fig. 6-12 shows that this shift magnitude is typically
1/4% of full scale, and therefore, is to be ignored because it is within the range of
balance normal force repeatability.

By surveying the several static runs of various configurations, the balance
axial force shift appeared to have occurred during run 215 as shown in Fig. 6-13.
The solid line represents a faired curve through four ADEN COMBAT 0° test runs
prior to the shift. As discussed in Ref. 2, the COMBAT 0° and COMBAT 0° ALT.
configurations have exactly the same flow path geometries. Thus, the dashed line
representing the COMBAT 0° ALT. should have duplicated the solid line in Fig. 6-13.
These data for run 215 appear to indicate a balance shift phenomenon.

It was recognized that the possibility existed to correct the main balance data by
using the nozzle balance results. First, however, it must be established that the
nozzle balance functioned properly as shown in Fig. 6-14. Here the resultant static
gross thrust coefficient data from the subject test is compared against the General
Electric Co. data base. Agreement is excellent. Thus, based on this example, in
addition to the more complete nozzle balance discussion of subsection 6.3, it is con-
cluded that the nozzle balance did indeed function properly and, therefore, could be
used as a standard with which to correct the main balance data.

All static runs for each configuration were studied by plotting a main balance
disparity parameter vs. axial load level. The disparity parameter is the difference
between the main and nozzle balance thrust coefficients converted to engineering units
by multiplying by the ideal thrust of both left and right nozzles combined as shown
below:

$$\Delta AF = \left(\frac{T_{SM}}{F_{iM}} - \frac{T_{SN}}{F_{iN}} \right) \times F_{iM} \quad .$$

Fig. 6-15 presents the disparity parameter for a configuration tested prior to the main
balance shift. Since the bulk of the data falls within the ± 1/2% main balance uncer-
tainty, this correlation confirms "zero disparity" because the main and nozzle balances
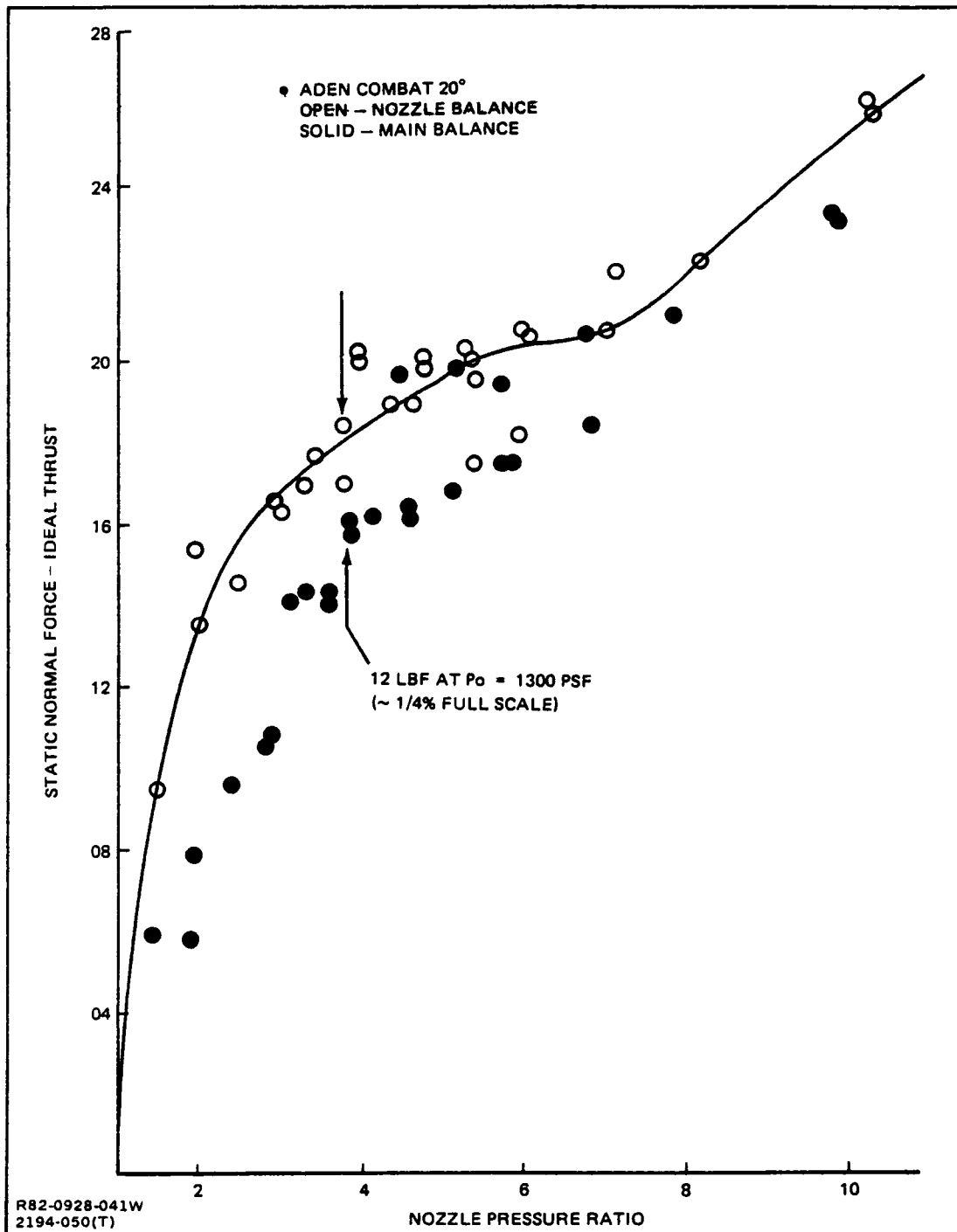agree.

6-16

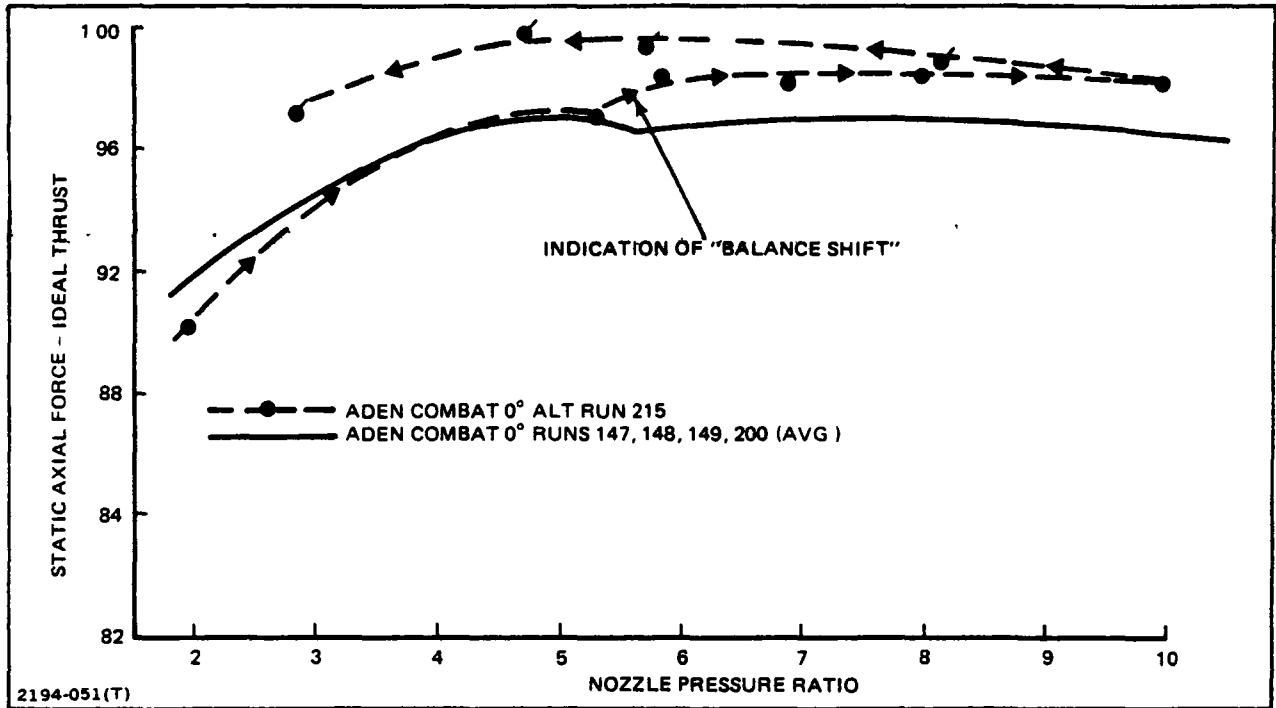Fig. 6-12 Effect of Main Balance Shift on Static Normal Force
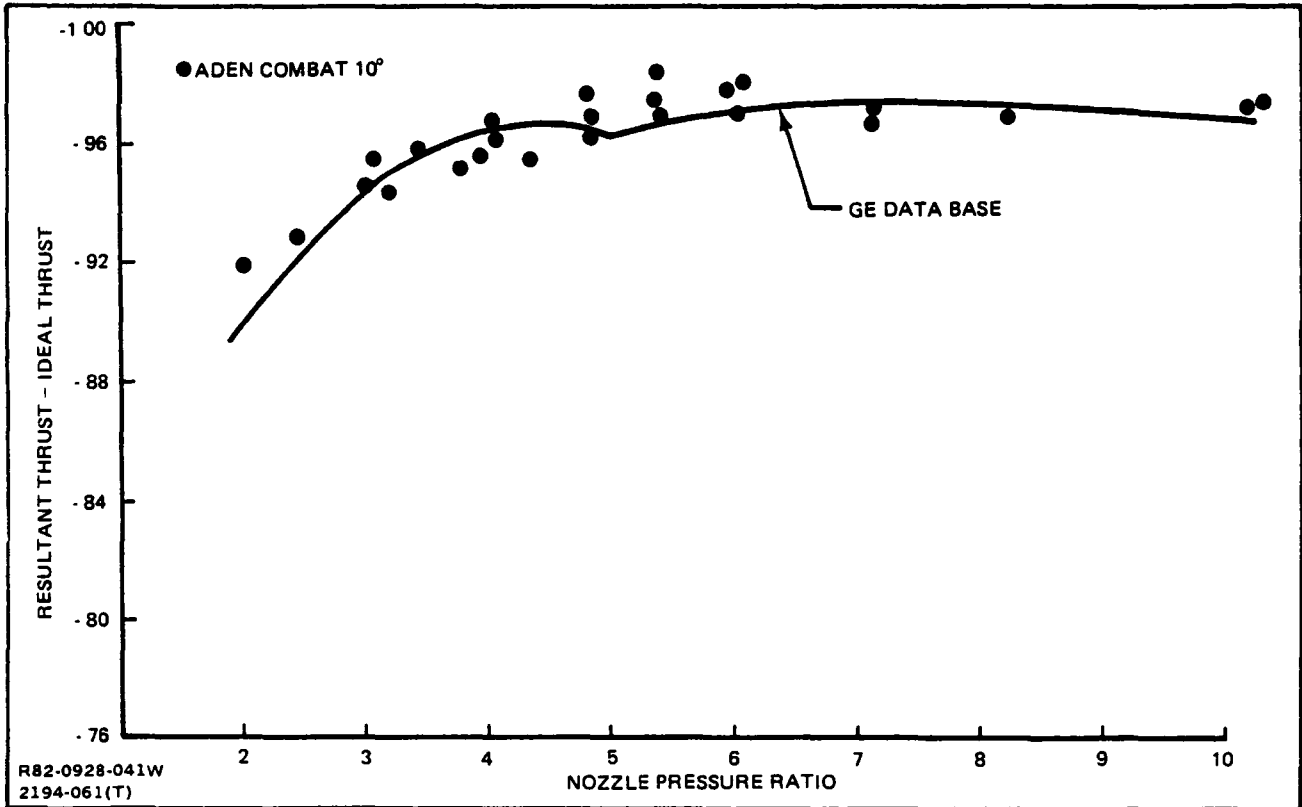
Fig. 6-13 Inception of Main Balance Shift

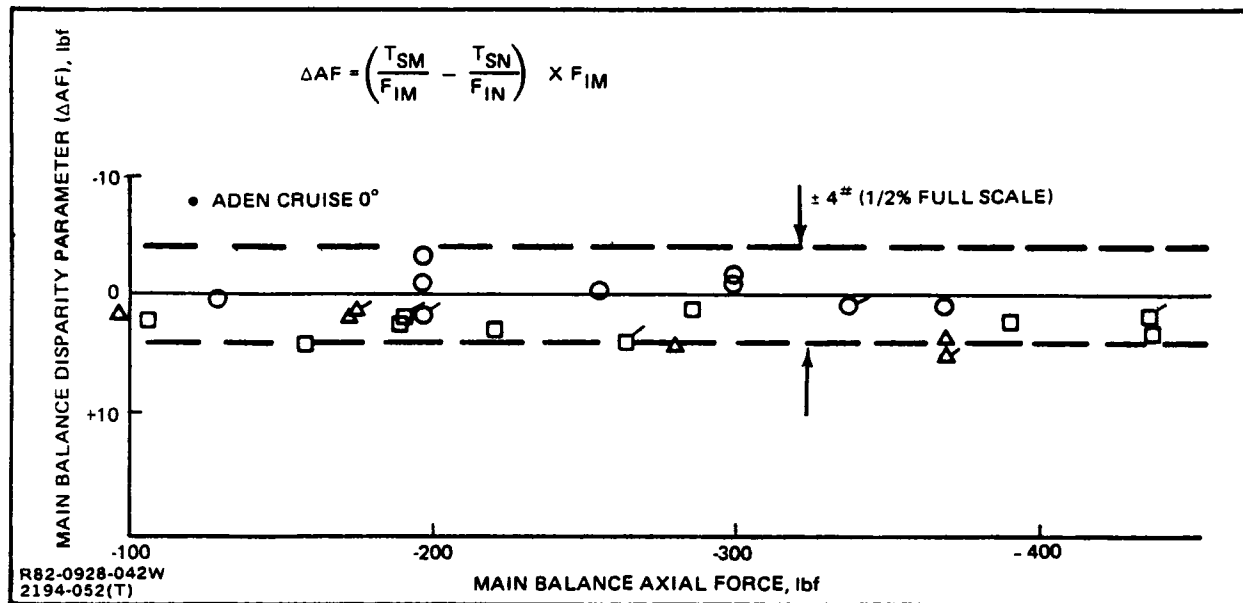Fig. 6-14 Nozzle Balance Resultant Thrust Comparison with GE Data Base

Fig. 6-15 Main/Nozzle Balance Comparison Prior to Balance Shift

On the other hand, Fig. 6-16 presents the disparity parameter for a typical configuration after the main balance shift was observed. Note that the disparity correlates linearly with axial force within the ± 1/2% of full scale tolerance.

A summary of the main balance shift phenomenon at large (300 lbf) and moderate (150 lbf) thrust levels is shown in Figs. 6-17 and 6-18. No disparity between main and nozzle balances is seen prior to the COMBAT 0° ALT. configuration (run 215). After run 215, a disparity exists. The shaded areas indicate a ± 1/2% uncertainty band with the disparity function correlation.

It is not known why the disparity decreases with jet area size. The largest jet area configurations (COMBAT nozzles) display the largest disparity, and as jet area decreases from the DASH configuration to the non-afterburning nozzles (CIRCULAR, CRUISE 0°, ALBEN), the disparity continues to decrease in a regular fashion.

At most conditions of interest, the COMBAT nozzles will be operating at large thrust levels typical of Fig. 6-17. This shows the typical disparity which must be corrected to be about 15 lbf. On the other hand for the non-afterburning nozzles, most conditions of interest are typified by Fig. 6-18 which shows a mean disparity of only 2 lbf. It is, therefore, concluded that for the complete set of non-afterburning nozzles the adjustment required to correct the disparity is either zero (CRUISE 0° ALT., CRUISE 10°) or very small (CIRCULAR, CRUISE 5°, ALBEN).
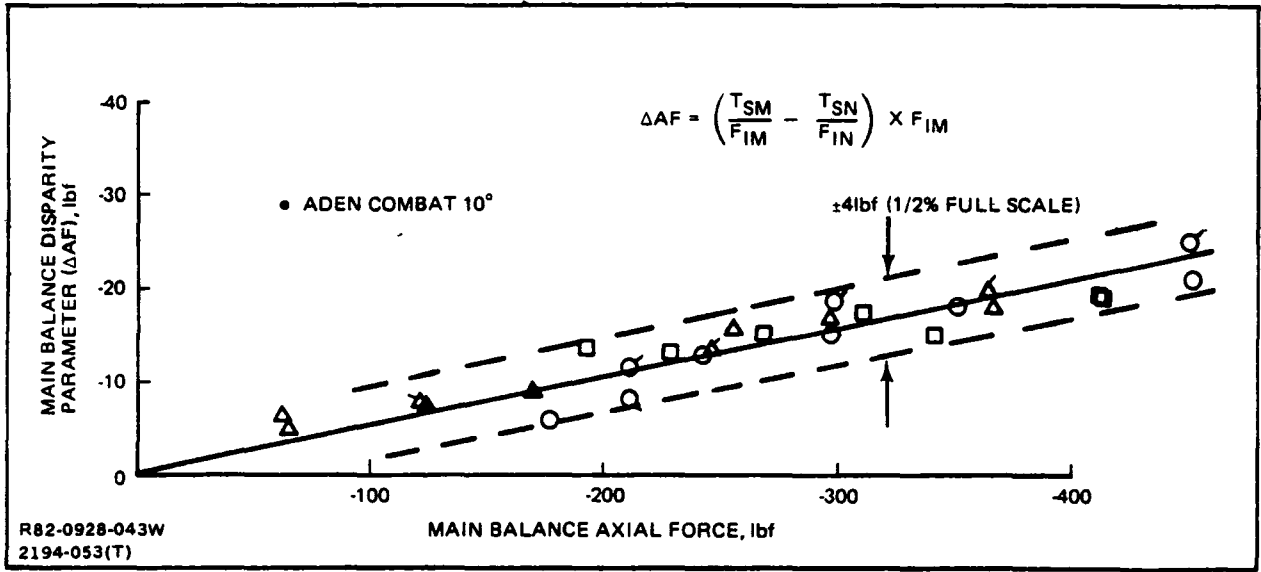
6-19

Fig. 6-16 Main/Nozzle Balance Comparison After Balance Shift
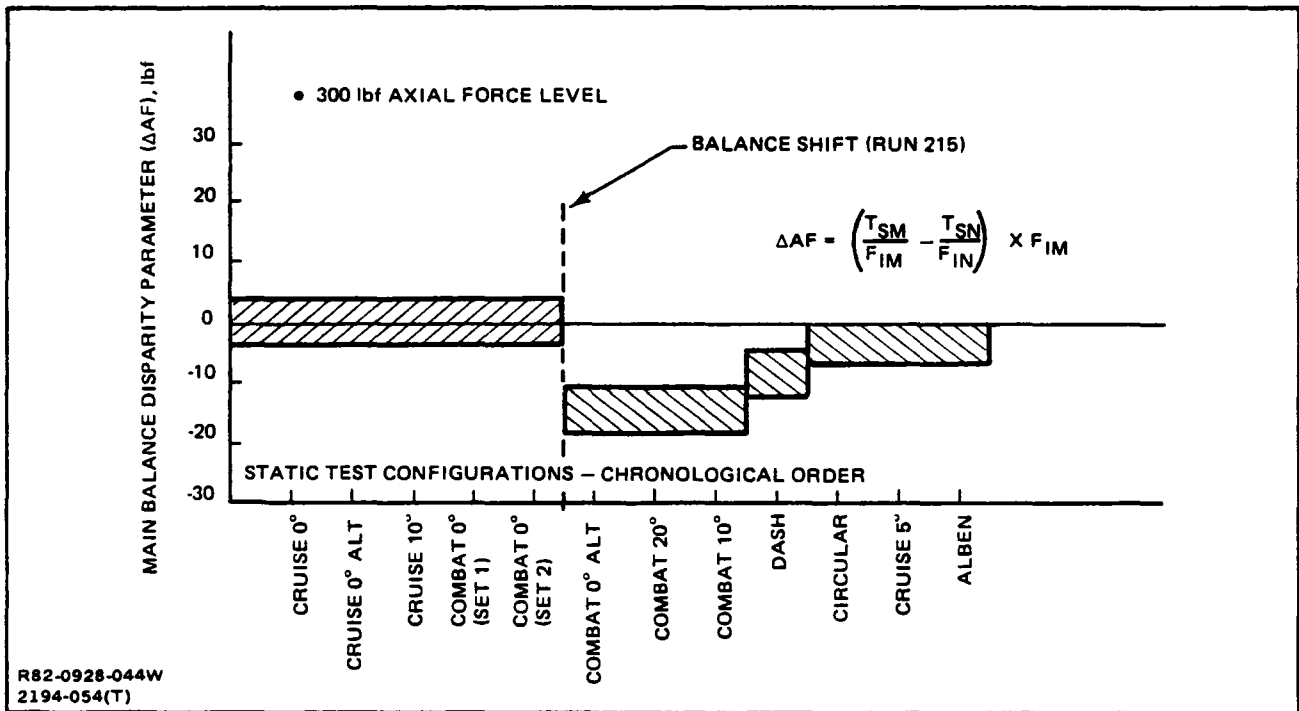

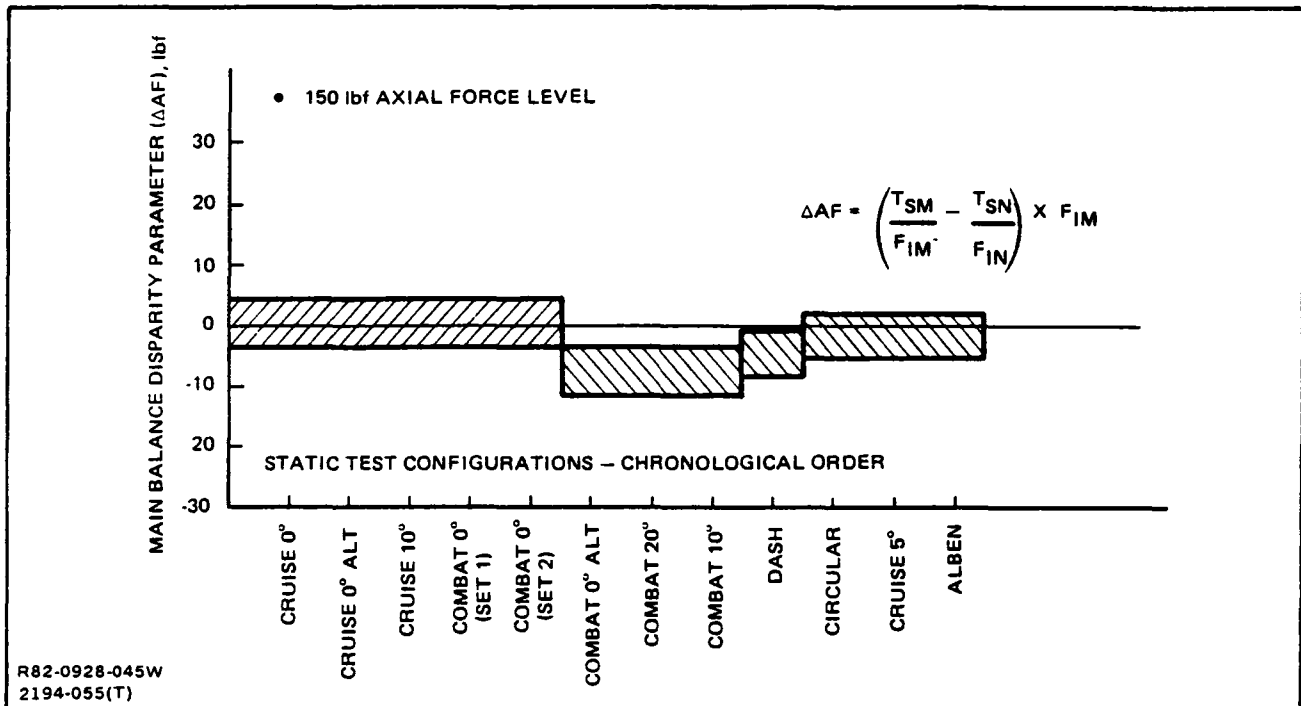Fig. 6-17 Summary of Balance Shift Phenomenon at Large Thrust Levels

Fig. 6-18 Summary of Balance Shift Phenomenon at Moderate Thrust Levels

The correction for the main balance shift was implemented as shown in the following equation:

$$(AF)_{CORR} = (AF)_{UNCORR} - (SLOPE) \times (AF)_{UNCORR} .$$

For each shift-affected configuration, the disparity data was plotted as in Fig. 6-16 and the slope, which is a positive number, was calculated. Since the test program's sign convention dictated thrust to be negative, the effect of this correction is to reduce the thrust magnitude as illustrated below:

$$-97 = (-100) - (0.03) \cdot (-100) .$$

This correction applies when the balance is sensing thrust because the data from which the correction was devised came from thrust runs. The case when the main balance is sensing drag is addressed in subsection 6.8.

It is noted that all static runs after run 215 exhibited the shift phenomenon. Since all wind-on runs were interspersed among the static runs, thus, it must be assumed that the shift phenomenon also existed during the wind-on runs. This is the rationale for correcting the wind-on data in addition to the static data.

Further, it is noted that the principle parameters of this test are the thrust removed parameters as opposed to total parameters. Since the balance shift correction applies to both static thrust and wind-on thrust minus drag, there is a tendency for this correction to cancel (although not completely) in the thrust removed parameters. Thus, the impact of the balance shift correction is diminished on the thrust removed parameters.

A deductive process of elimination was employed to determine that the disparity in static thrust coefficients (measured thrust ÷ ideal thrust) between the two balances was due to the main balance axial gauge measurement. Initially, all possible culprits were explored. These were:

- Nozzle total pressure

- Mass flow

- Dislocated main balance exit flow port

- Momentum tares

- Nozzle balance gauge

- Main balance gauge.

Figs. 6-19 and 6-20 compare the total pressure relationship between the subject Ames program and a previous program at AEDC (Ref. 4). For the right hand nozzle perfect agreement is seen. A slight difference is noticed on the left side. However, this small difference cannot account for the observed thrust coefficient disparity which becomes larger as bellows pressure increases. Note that Fig. 6-20 shows that the total pressure difference diminishes between bellows pressure of 200 to about 500 psia.
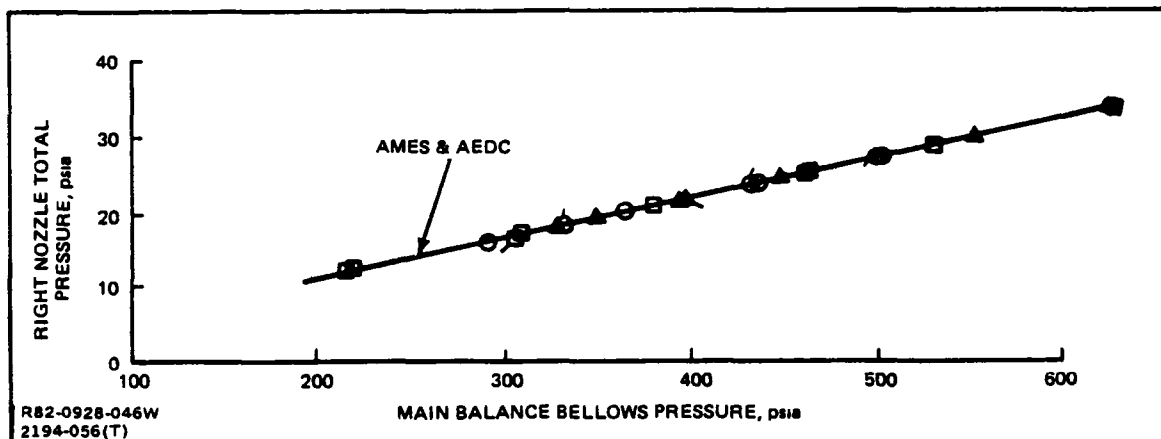

R82-0928-046W
2194-056(T)

Fig. 6-19 Right Nozzle Total Pressure Diagnostic for Balance Shift
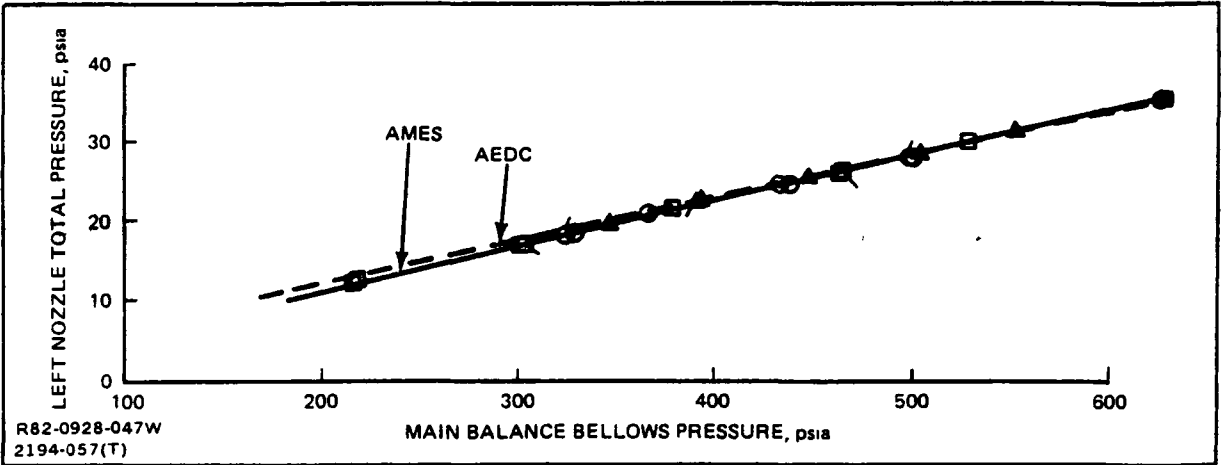
Fig. 6-20 Left Nozzle Total Pressure Diagnostic for Balance Shift

Fig. 6-21 compares the mass flow characteristics before (CRUISE 0°) and after (COMBAT 10°) run 215. No change is seen, so mass flow cannot be the culprit.
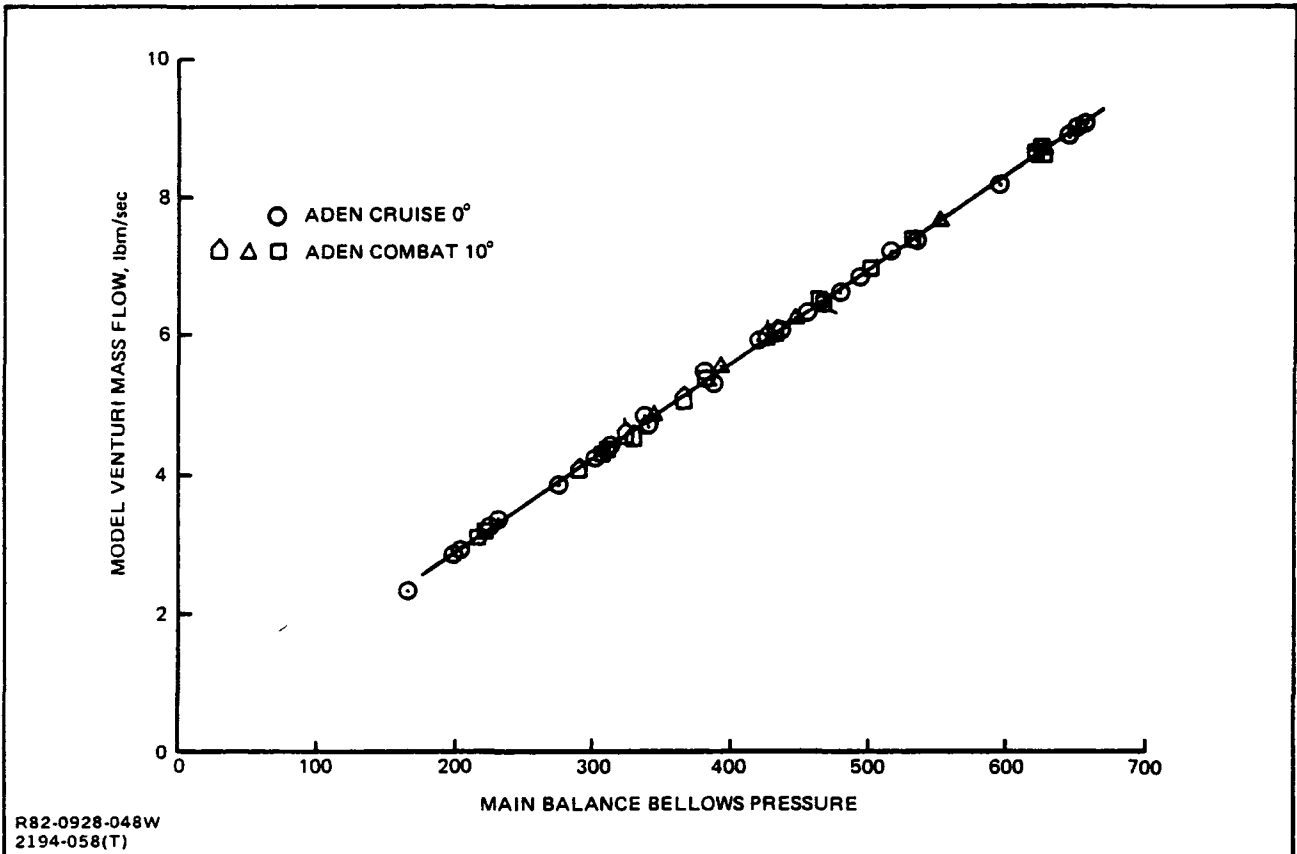
Fig. 6-21 Mass Flow Diagnostic For Balance Shift

After the test during the model tear down phase, it was noticed that the main balance exit flow port (Fig. 2-8) had partially unscrewed. It was hypothesized that this could have upset the relationship between the upstream bellows pressure and the downstream venturi pressure. Fig. 6-22 shows the same flow path characteristic for two runs before and after the thrust coefficient disparity was noticed, thereby disproving this hypothesis.

R82-0928-049W
2194-059(T)

Fig. 6-22 Model Venturi Pressure Diagnostic For Balance Shift

It was also postulated that the thrust coefficient disparity could have been caused by a change in the momentum tare characteristic after run 215 possibly due to the dislocated main balance exit flow port (mentioned above). Such a situation is represented by the sketch below:

R82-0928-006W

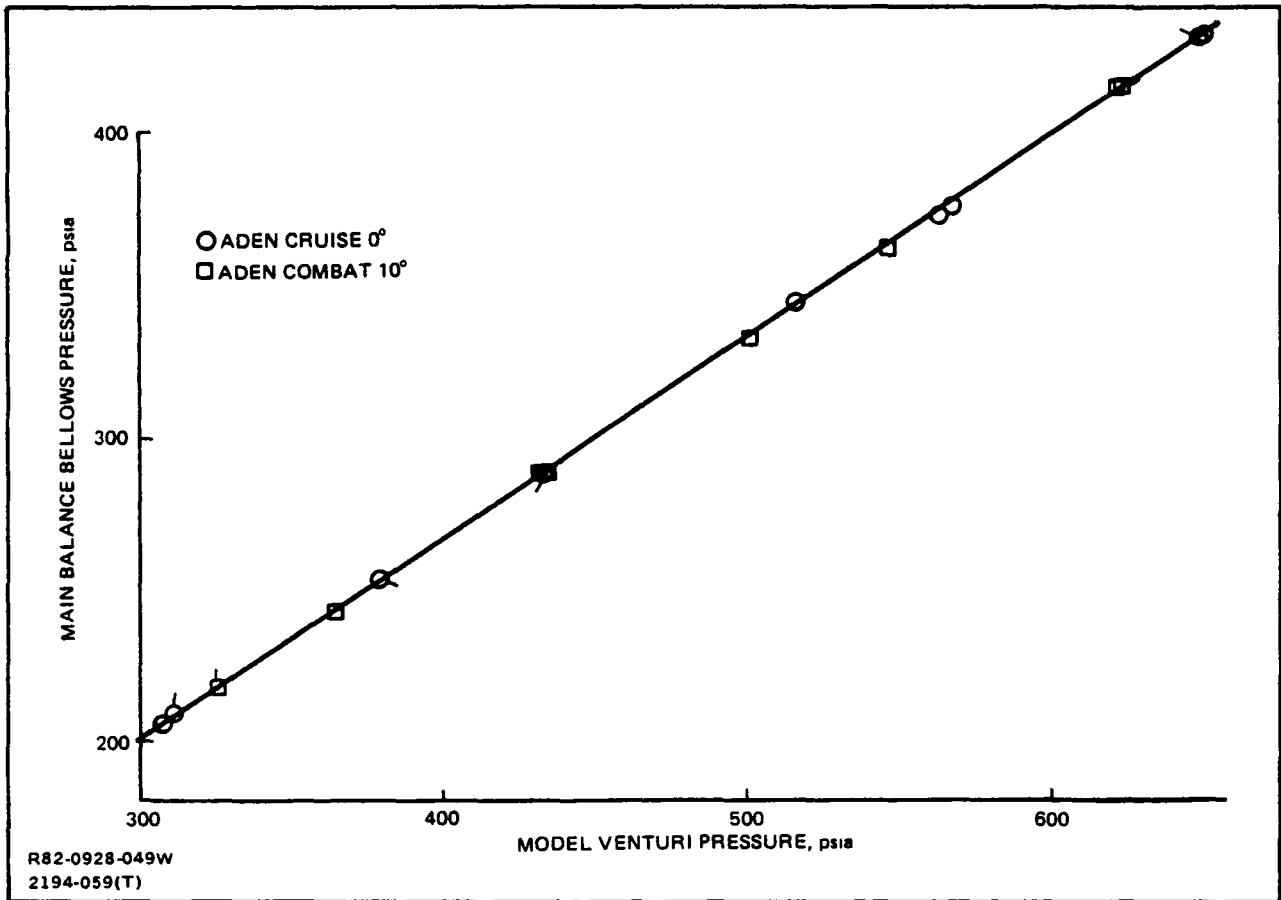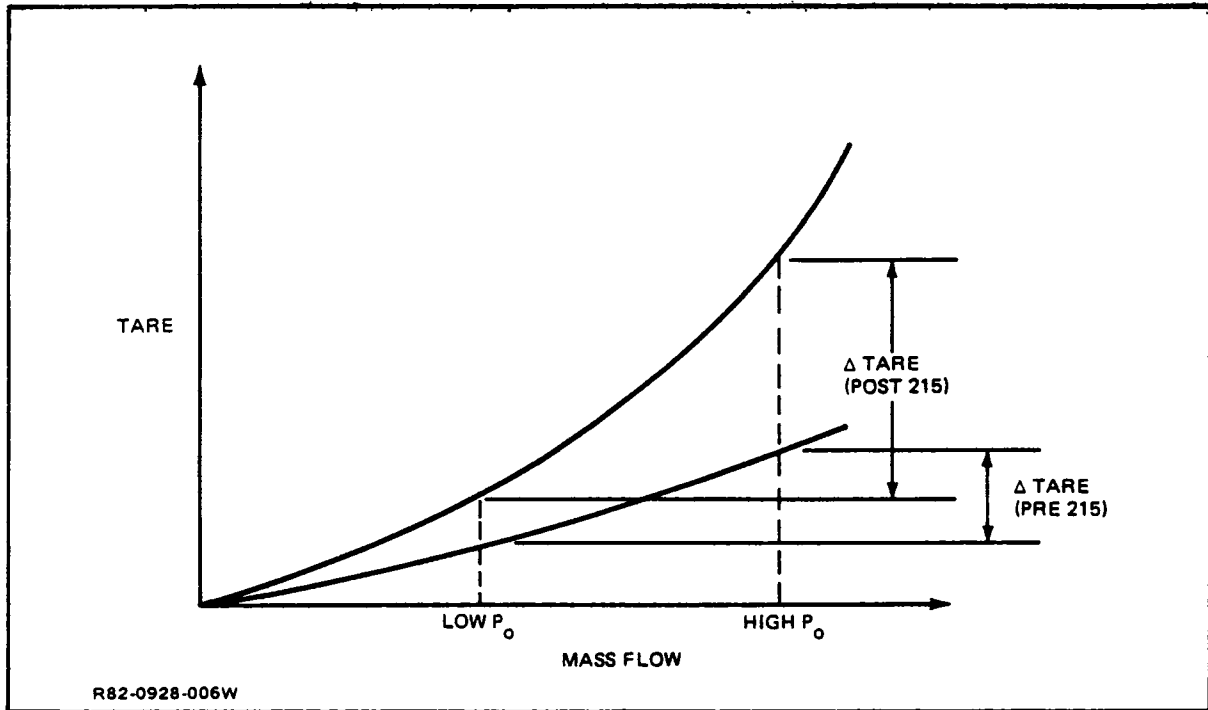Note that this shows how the "delta tare" between two different mass flow levels (at a high and a low back pressure, P_o) could have changed before and after run 215:

$$\Delta \text{ TARE (POST 215)} > \Delta\text{TARE (PRE 215)}$$

Now, let's inspect the static thrust data from a configuration tested after run 215 which utilizes the momentum tares assessed prior to run 215. Fig. 6-23 shows the data for three different P_o levels. Note that at the same NPR, the data which corresponds to different mass flow levels (ie: 4-1/2 vs. 7-1/2 lbm/sec) are in excellent agreement - even better than the usual scatter associated with ± 1/2% of full scale. This could not be so if the momentum tare characteristic changed during the test. Thus, it is concluded that momentum tare phenomena are not responsible for the thrust coefficient disparity.

Fig. 6-14 and subsection 6.3, both discussed previously, eliminate the nozzle balance as being responsible for the thrust coefficient disparity.
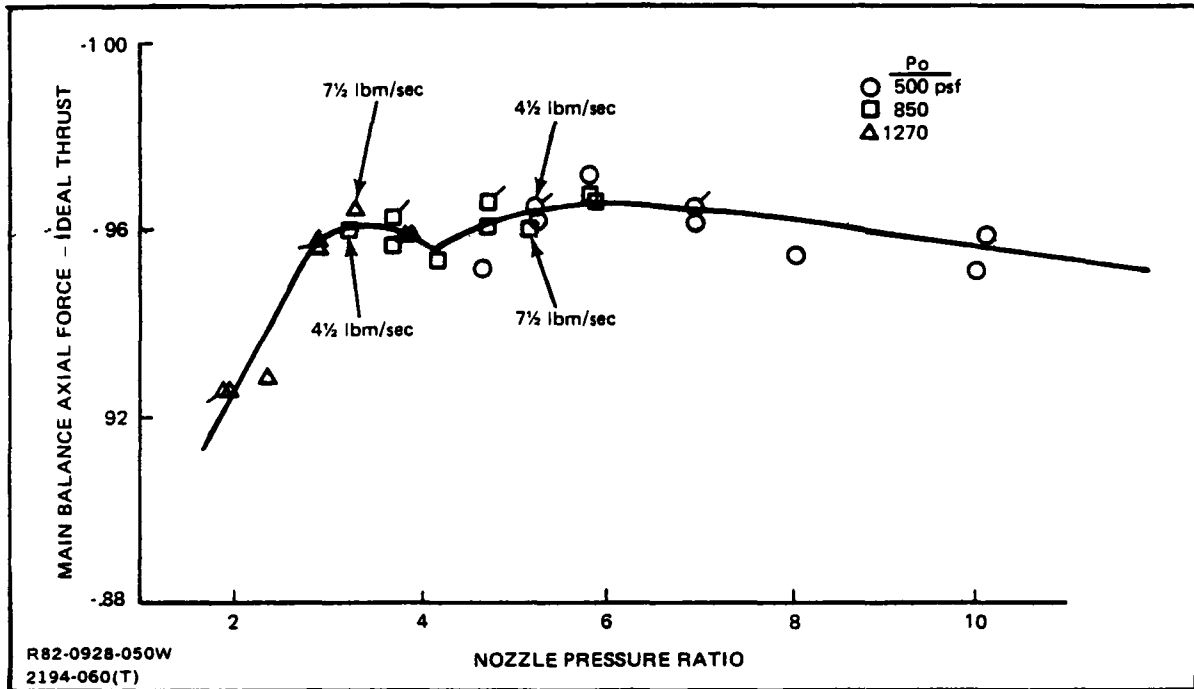
**Fig. 6-23 Momentum Tare Diagnostic For Main Balance Shift**

Thus, it is concluded that the only possibility is that something happened to the main balance midway through the test. Since this balance is not one piece, but instead is composed of several pieces pinned together, it is possible that it took a "different set" thereby stressing the axial gauge differently. This is only one theory; the actual cause remains a mystery.

However, since the static thrust coefficient data disparity did correlate very well with axial load level (as shown in Fig. 6-16) for each affected nozzle configuration, this in itself does provide a measure of confidence in the applied correction.

6.8. MAIN BALANCE SHIFT - DRAG CORRECTION

Experimental substantiation for the balance shift correction existed for the case when the main balance was sensing forces in the thrust direction (the most predominant case) as discussed in subsection 6.7. However, experimental data that would substantiate a correction when the main balance was sensing forces in the drag direction could not practicably be obtained (because static runs are not conducted to obtain drag'). Nevertheless, understanding the mechanism of the balance shift phenomenon provides a rationale to enable the determination of the correction for this "drag dominant" case - in particular, when the jet is off (defined as NPR = 1.0).

A true balance shift phenomenon, that is permanent, must be unidirectional. Using the sketch below, it can be reasoned that if a balance shift increases thrust, it must correspondingly decrease drag when the sense of the applied load is reversed.

R82-0928-007W
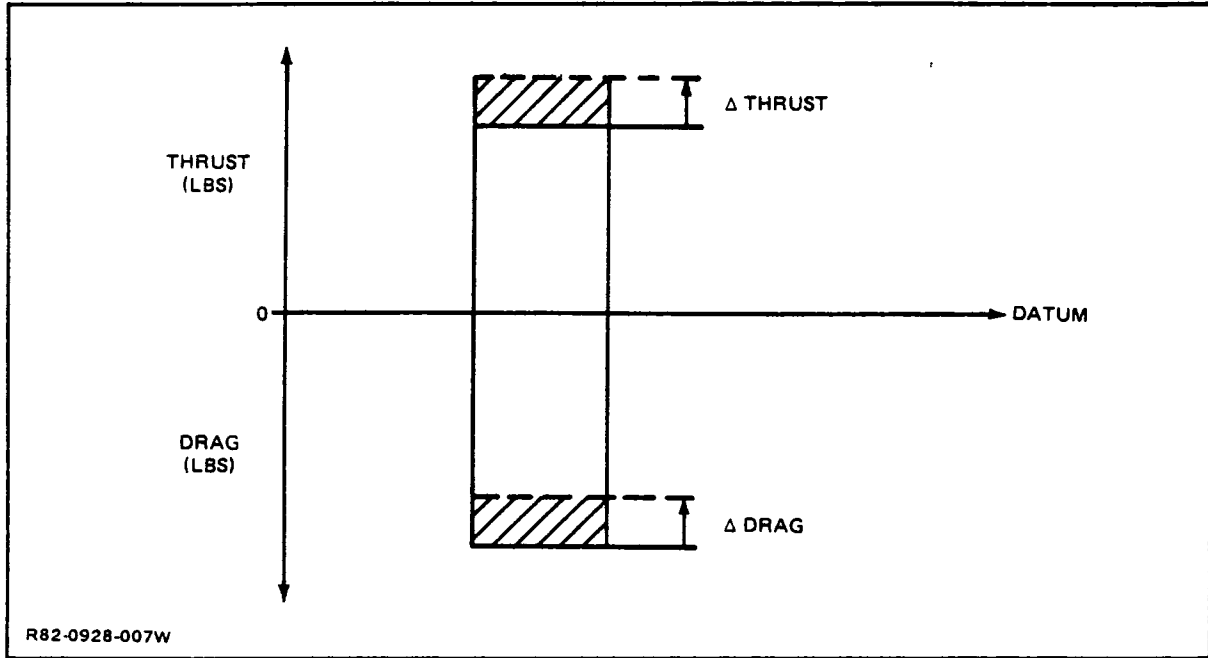
Thus, the correction formulation for the erroneous balance shift must be such that thrust and drag corrections are in opposite directions. Because axial force in the wind direction is defined positive for this test, the correction formulation of subsection 6.7 if applied to the drag dominant case would yield:

$$(AF)_{CORR} = (AF)_{UNCORR} - (SLOPE) \times (AF)_{UNCORR}$$

$$+97 = +100 - (.03) \times (+100)$$

However, a corrected drag value (97) lower than the uncorrected drag value (100) is a contradiction based on the above reasoning. Therefore, it was recognized that the appropriate correction for the drag dominant case must be:

$$(AF)_{CORR} = (AF)_{UNCORR} + (SLOPE) \times (AF)_{UNCORR}$$

This is also discussed in Ref. 1 and applies to all jet-off drag data of Ref. 2. An example of the correction to jet-off drag is shown in Fig. 6-24. Note that the correction resolved an apparent anomaly: "Why did such a large difference exist between the CRUISE and COMBAT nozzle configurations at non-flowing jet-off conditions?" After the correction was applied, both jet-off drag polars were within 10 drag counts as expected.
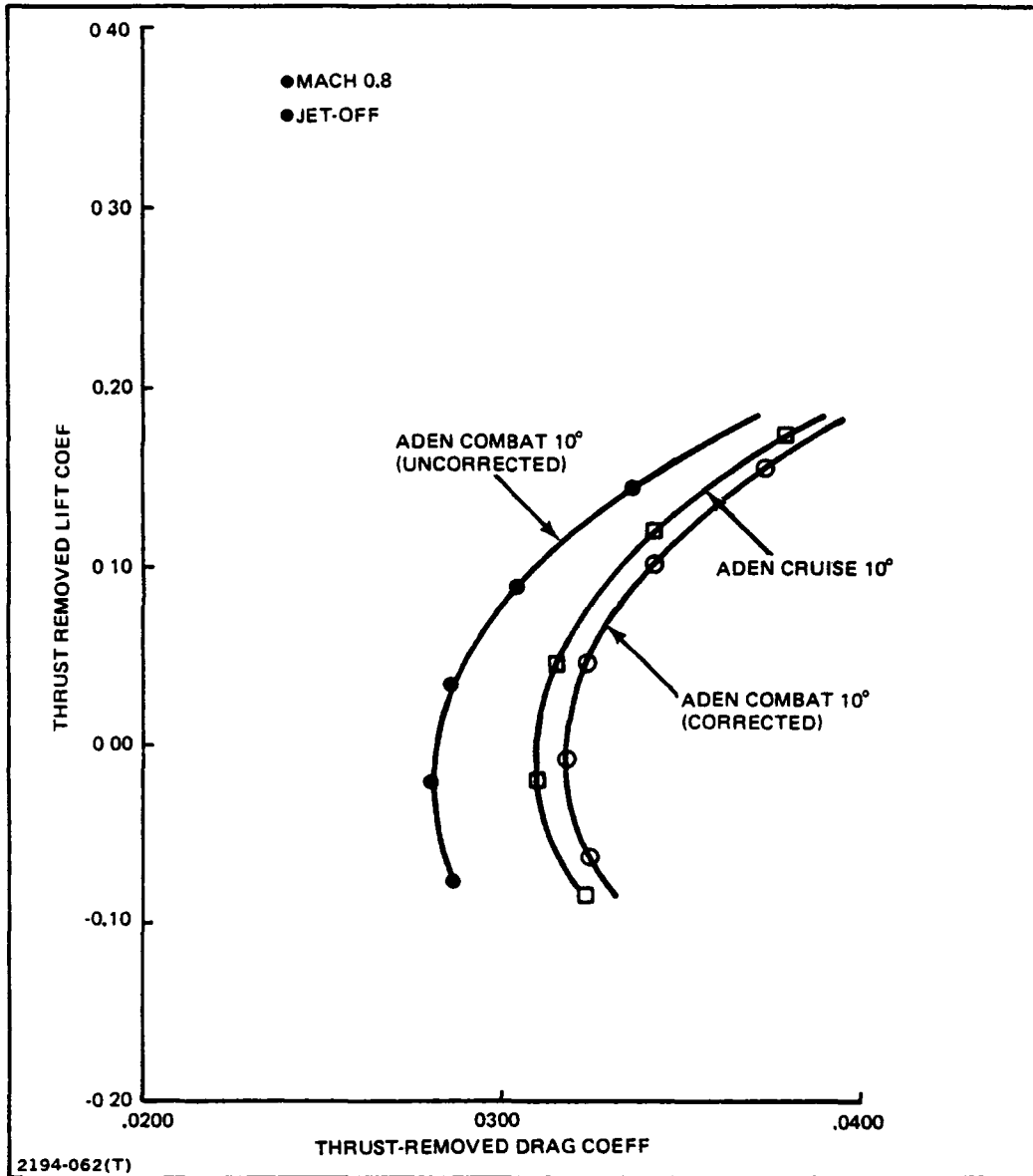

Fig. 6-24 Effect of Main Balance Shift in Drag Direction

6.9 MAIN BALANCE ROLL PIN

Model vibration due to a loose balance can be disastrous during wind tunnel oper-
ation. In the subject test program, a thorough model diagnostic inspection after the
ASME nozzle calibration phase, just prior to the wind-on phase, revealed that the
model was loose on the support sting in roll. Upon tearing down the model it was
discovered that the roll pin diameter was about 0.001 inch too small. Also this pin
was chaffed indicating that it was too soft. The solution of course was to fabricate a
new pin of exactly the correct diameter out of hardened 4340 steel.

This problem is identified in this report to highlight a potentially disastrous
situation that could occur merely due to human error. Fortunately in this program
the loose pin was discovered prior to any occurrence of damage. However, this prob-
lem should have been identified prior to tunnel installation thereby not wasting pre-
cious tunnel occupancy time to resolve the problem. The importance of thorough
model check out during dry-run model builds can never be overemphasized.

6.10 NOZZLE RAKE MANIFOLD LEAK

Initial static thrust data measured on the nozzle balance for the Circular nozzle is
shown in Fig. 6-25. The solid symbols indicate a definite problem because static
thrust coefficients theoretically can not exceed unity. After troubleshooting and
developing a data correction procedure, the final data are shown as the open symbols.
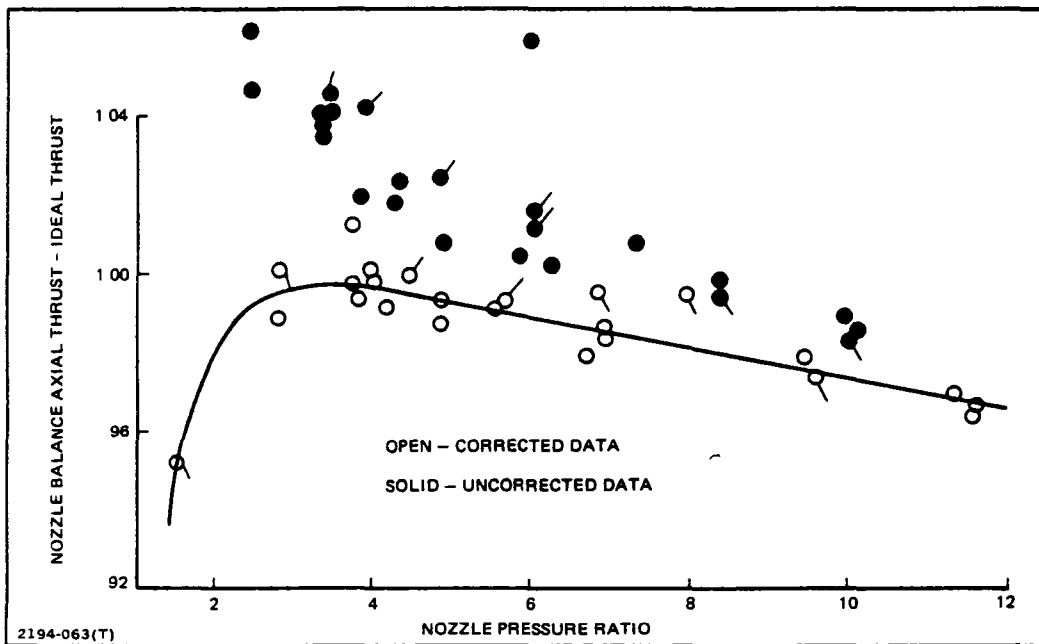The steps leading to this data correction are discussed below.

Fig. 6-25 Effect of Nozzle Total Pressure Error on Thrust

Since the magnitude of the erroneous data of Fig. 6-25 appeared to diminish as nozzle pressure ratio increased, an error in total pressure was suspected. Figure 6-26 presents the left tailpipe total pressure characteristic for the subject test compared to a previous test (Ref. 4). Observe that the Ames data read low. This would cause ideal thrust to also read low and since this quantity is in the denominator a thrust coefficient that reads too high results.

It was decided to also check the right hand tailpipe total pressure relationship to see if agreement could in fact be expected from the two test programs. Fig. 6-27 confirms this, so it was concluded that a problem definitely existed with the left total pressure measurement and it was simply not facility to facility differences.

Further investigation was desirable to determine the exact nature of the problem. Using the continuity equation for choked flow, the total pressure at the nozzle throat could be calculated as follows:

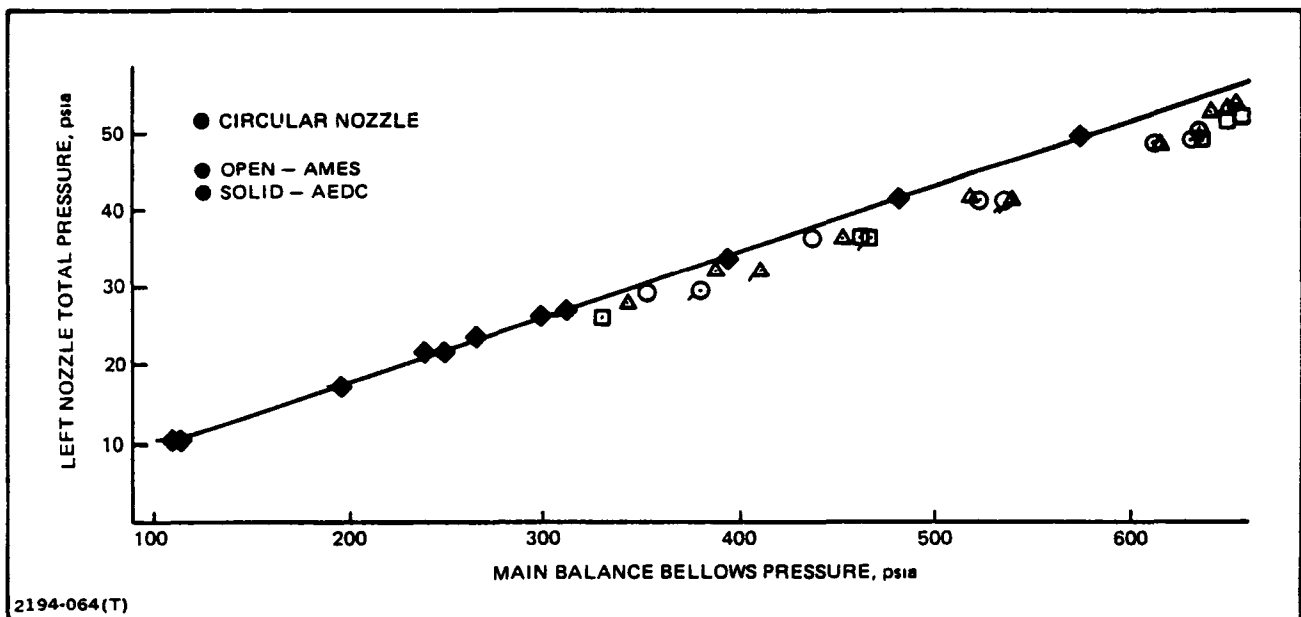$$P_T = (\dot{W} \cdot \sqrt{T_T}) \div (0.5318 \, A_t \cdot C_{DIS})$$

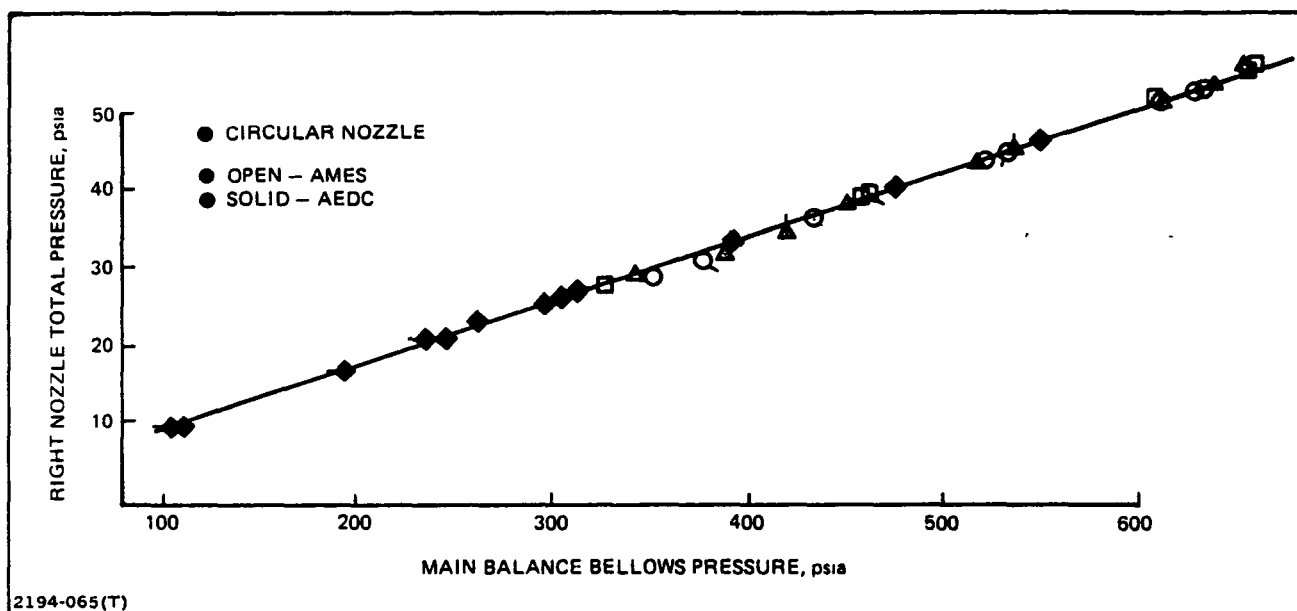Fig. 6-26 Left Nozzle Total Pressure Comparison

6-30

Fig. 6-27 Right Nozzle Total Pressure Comparison

This was done for both left and right nozzles using the following ground rules:

- Total temperature for both left and right nozzles was taken to be the average of the left and right tailpipe thermocouple measurements for consistency

- Both left and right discharge coefficients were assumed equal (as they should be if the nozzles were fabricated identically). A realistic value of 0.99 was selected

- The individual venturi mass flow measurements were used for both left and right hand nozzles

- Individually measured throat areas were employed for both left and right nozzles.

Once the calculated total pressures were obtained they could be compared with the measured total pressures to attempt to explain the phenomenon. This is done in Fig. 6-28 which shows the right nozzle measured to calculated total pressure ratio is constant with flow rate and very close to unity as expected. However, the left total pressure ratio shows a steady and regular decrease (for all test runs) as flow rate is increased. This trend clearly can be the result of only one cause - a leak. Interrogation of the mechanic involved in making the post Circular nozzle model change revealed that several of the plastic tubes on the left hand total pressure rake manifold had "popped-off".

6-31
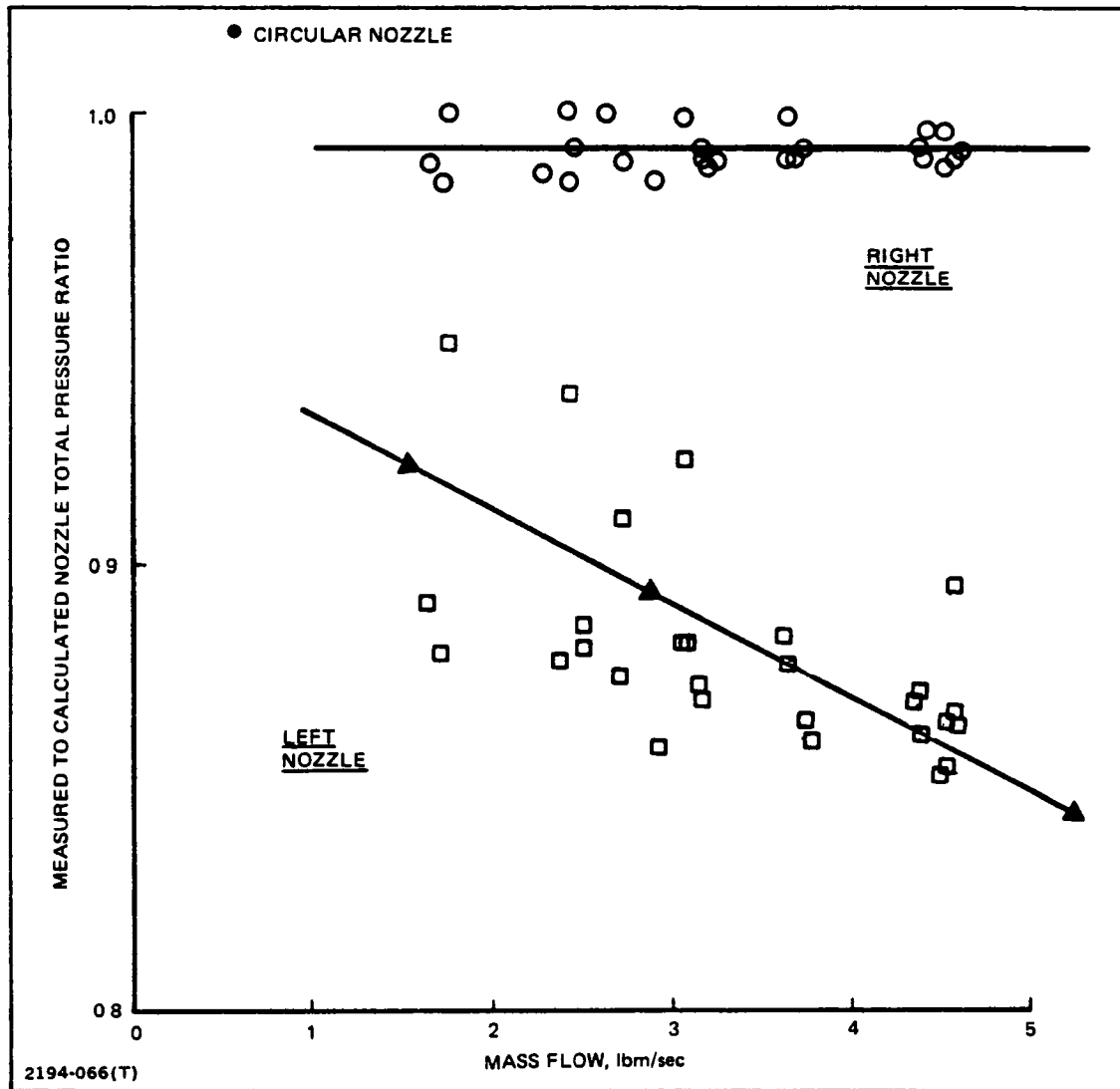
Fig. 6-28 Effect of Leak on Measured Total Pressure

The correction procedure for the erroneous left nozzle total pressure is based on making use of the continuity equation recognizing that left and right nozzles theoretically must have the same Mach number and total temperature conditions. The following relationship is therefore easily derived:

$$P_{TL} = \left(\frac{\dot{W}_L}{\dot{W}_R}\right) \cdot \left(\frac{A_{tR}}{A_{tL}}\right) \times P_{TR}$$

6-32

The venturi measured flow split ratio $(\dot{W}_L/\dot{W}_R)$ for the Circular nozzle configuration is shown in Fig. 6-29. Note that this ratio becomes constant above choking conditions as expected. So, for the entire static and wind-on running of the Circular nozzle the following simple correction to obtain the left nozzle total pressure was implemented in the data reduction program:

$$P_{TL} = 1.0607 \times P_{TR}$$

This adjustment corrected the erroneous static thrust data to the level shown by the faired curve of Fig. 6-25.
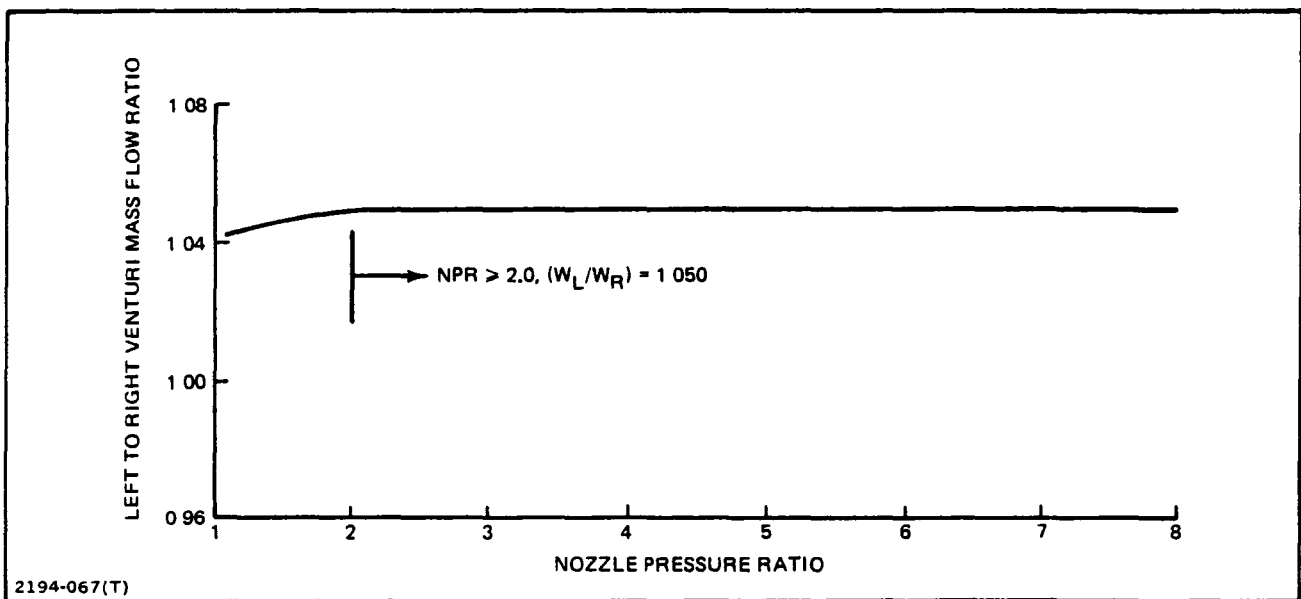
Fig. 6-29 Circular Nozzle Flow Split Determination

2194-067(T)

6.11 ANGLE OF ATTACK ERROR

Prior to the wind-on running of the third test configuration, static calibration runs were conducted. Between two of these static runs (run 106 and run 108) a model leveling check run (107) was made because it was the start of the day shift. During this check run it was observed that the measured static angle of attack had shifted from a nominal -0.7° (for previous static runs) to about -0.4° (an increment of about 0.3°). At this point in the test program, the pressures of limited tunnel occupancy time did not permit an in depth trouble shooting activity to explain the α-shift. Facility test personnel explained that the new angular reference level would be automatically accounted for in the facility data reduction equations.

During the post test analysis of drag polar characteristics for the vectoring configurations, unanticipated data trends suggested that the α-shift problem should be further investigated. A sensitivity study, at a moderate $\alpha = 7°$, using the thrust-removed drag and lift equations:

$$CDTR = CTTR \cdot COS \ \alpha + CNTR \cdot Sin \ \alpha$$
$$CLTR = CNTR \cdot COS \ \alpha - CTTR \ Sin \ \alpha,$$

showed that if the measured α were decreased by 0.3°, then the thrust-removed drag would decrease by about 25 counts (.0025) without any significant "plottable" change in the thrust-removed lift coefficient. At lower angles of attack as zero lift is approached, the error in the thrust-removed drag coefficient, due to an error in the measured α, diminishes to zero. Thus the effect of a constant shift in the measured α is to "rock" the polar to the left as shown in the sketch below.

R82-0928-008W
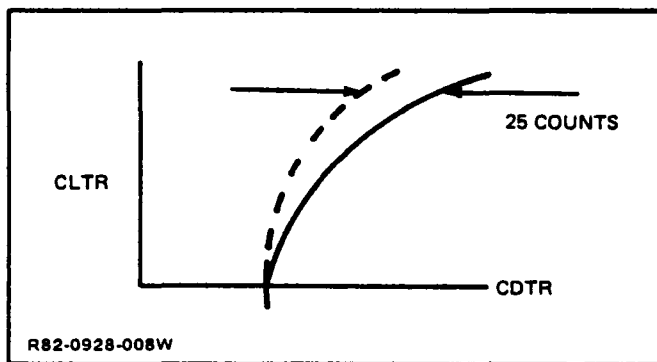
Facility project personnel engaged in a post test trouble shooting effort that confirmed an angle of attack problem. Hand calculations had to be made by facility project personnel to reconstruct the appropriate angle of attack reference level for each configuration. After in depth analysis, the results showed that a very simple correction, within experimental accuracy, could be implemented to correct the data. For all test configurations after run 107, the original α was to be reduced by 0.33°.

$$\alpha_{TRUE} = \alpha_{ORIG} - 0.33°$$

Note that this correction, independently deduced, agrees extremely well with the observed shift of 0.30° discussed above.

All wind tunnel data were recomputed by implementing the above correction. Accordingly, additional data analysis activity had to be expended to re-plot all the corrected data. The graphical presentations of Ref. 1 and 2 show the α-corrected data only.

6.12 STATIC THRUST SELECTION FOR THRUST-REMOVED PARAMETERS

As explained in the "Data Reduction Methodology" section of Ref. 2, four methods existed in this test program to determine the static thrust components employed to obtain the thrust-removed parameters. These methods make use of either the nozzle or main balance static thrust measurements in the numerator and either P_o or F_i in the denominator of a normalized static thrust parameter.

A decision had to be made regarding which method to officially select for data analysis and presentation of the thrust-removed aeropropulsion parameters. Of the four alternate calculation methods discussed in Ref. 2, three have been written into the data reduction procedure of this test program. They are:

1. NBTP - Nozzle Balance (Static) Thrust; P_o-Method

2. NBTF - Nozzle Balance (Static) Thrust; F_i-Method

3. MBTP - Main Balance (Static) Thrust; P_o-Method

These three methods are compared at a subsonic non-afterburning and a supersonic afterburning condition. Figure 6-30 shows no difference exists among the methods for lift coefficient. Any differences in normal force ($\sim$ lift) due to measurement uncertainty or human error (data fairing) are so small that they are imperceptible on this standard lift coefficient scale (0.10 per inch). This was generally true for all nozzles so that lift coefficient need not be considered in the process of selecting a particular data reduction method.

On the other hand the drag coefficient did display significant differences for all nozzles. Figure 6-31 shows a comparison of the three methods in the drag direction for the ADEN Cruise 0° nozzle. This disparity was typical although some configurations exhibited slightly less and/or somewhat greater differences between methods. Since lift is literally independent of method type, the drag differences are directly reflected in the polar differences of Fig. 6-32. A typical maximum disparity, depending on lift coefficient (or angle of attack), is 10 to 20 drag counts.
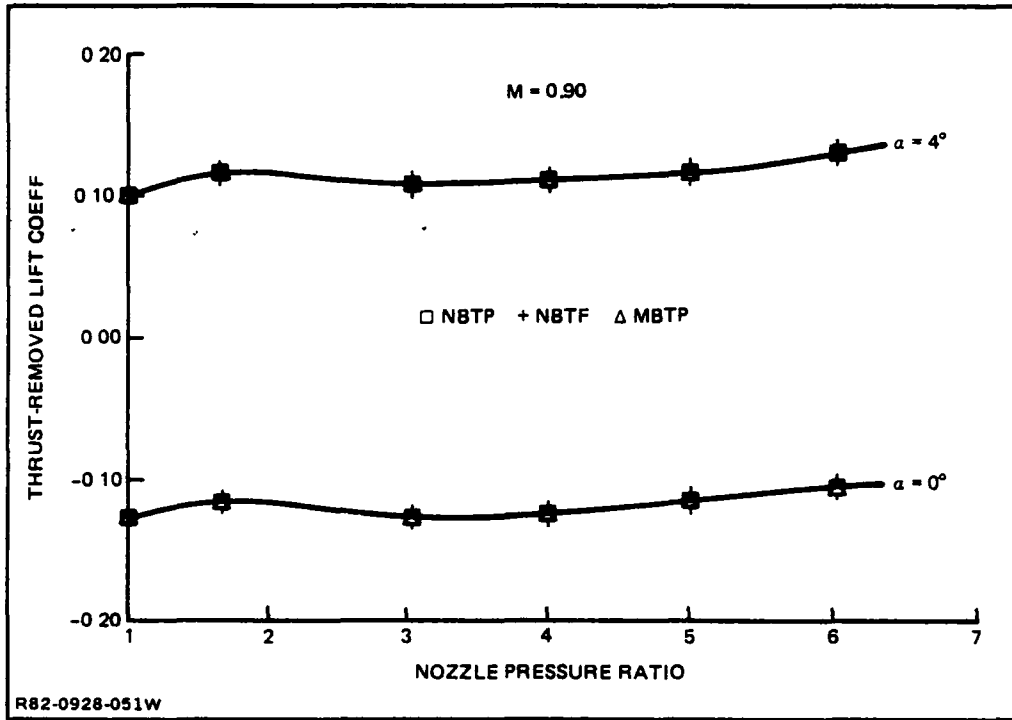
Fig. 6-30 ADEN Cruise 0° Lift Comparison
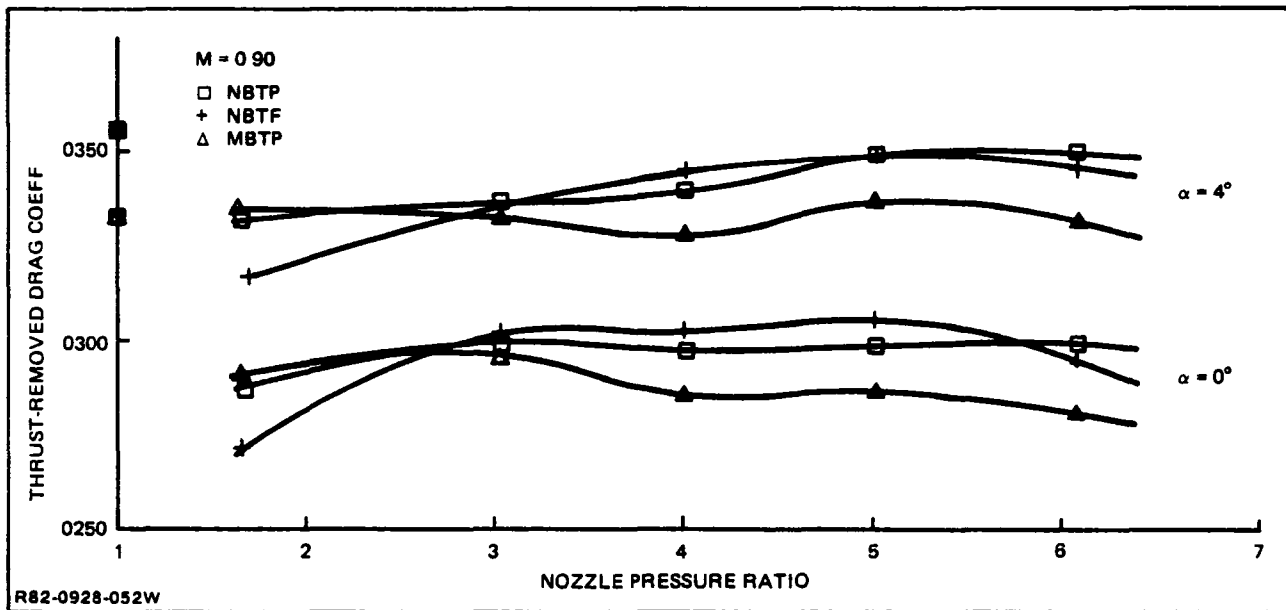
Fig. 6-31 ADEN Cruise 0° Drag Comparison

6-36
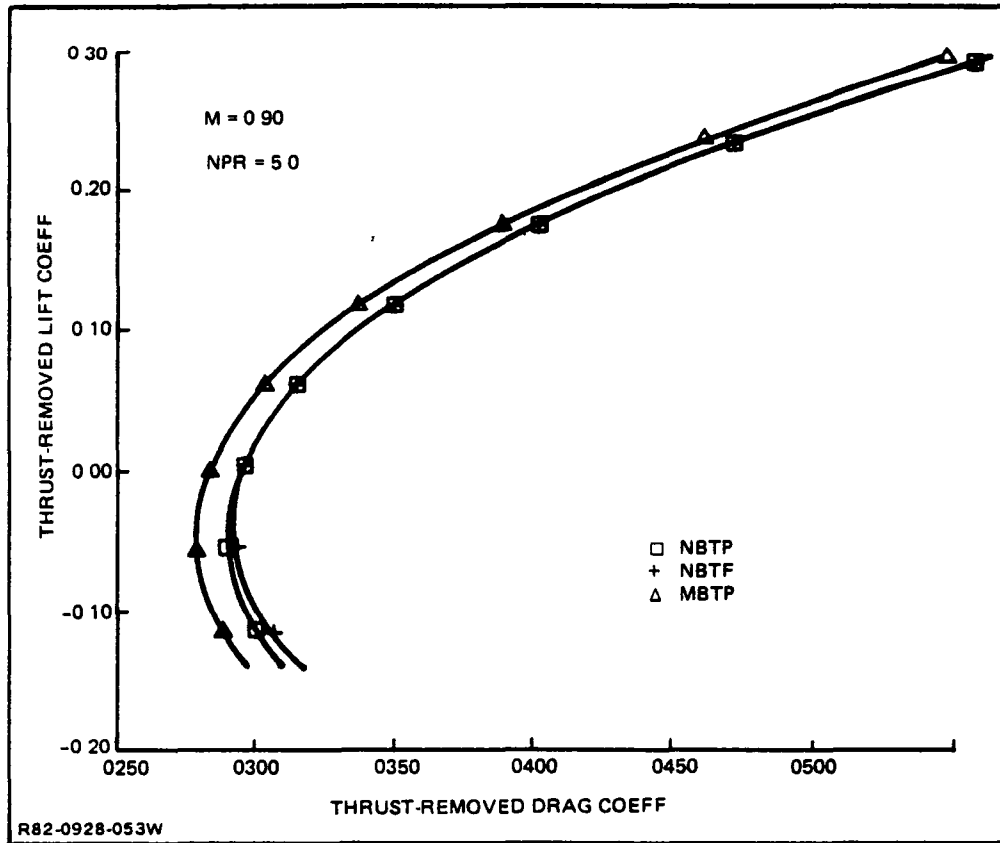
Fig. 6-32 ADEN Cruise 0° Polar Comparison

Similarly, at M = 1.4 the same presentation is made for the ADEN Dash nozzle for thrust-removed drag (Fig. 6-33) and the drag polar (Fig. 6-34). The typical maximum disparity is approximately 15 drag counts over the angle-of-attack range.

Using this type of polar comparison, many charts for all nozzles were prepared that summarize the differences between the three methods for various combinations of Mach number, nozzle pressure ratio and lift coefficient. A typical example is shown in Fig. 6-35 for four configurations at Mach 0.9 and two configurations at M = 1.4. This figure represents six of almost 100 combinations that were studied.

Fig. 6-33 ADEN Dash Drag Comparison

Fig. 6-34 ADEN Dash Polar Comparison

Fig. 6-35 Comparison of Data Reduction Methods

R82-0928-056W

One criterion for selecting the favored data reduction method could be based on the percentage of occurences that this particular method featured drag levels in between the other two methods. The chart below summarizes the statistics.
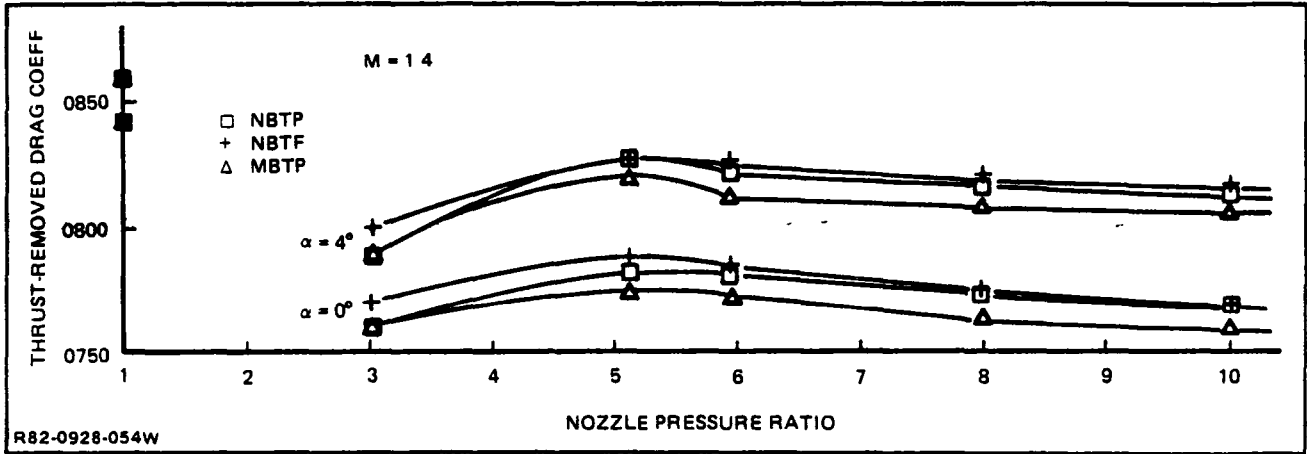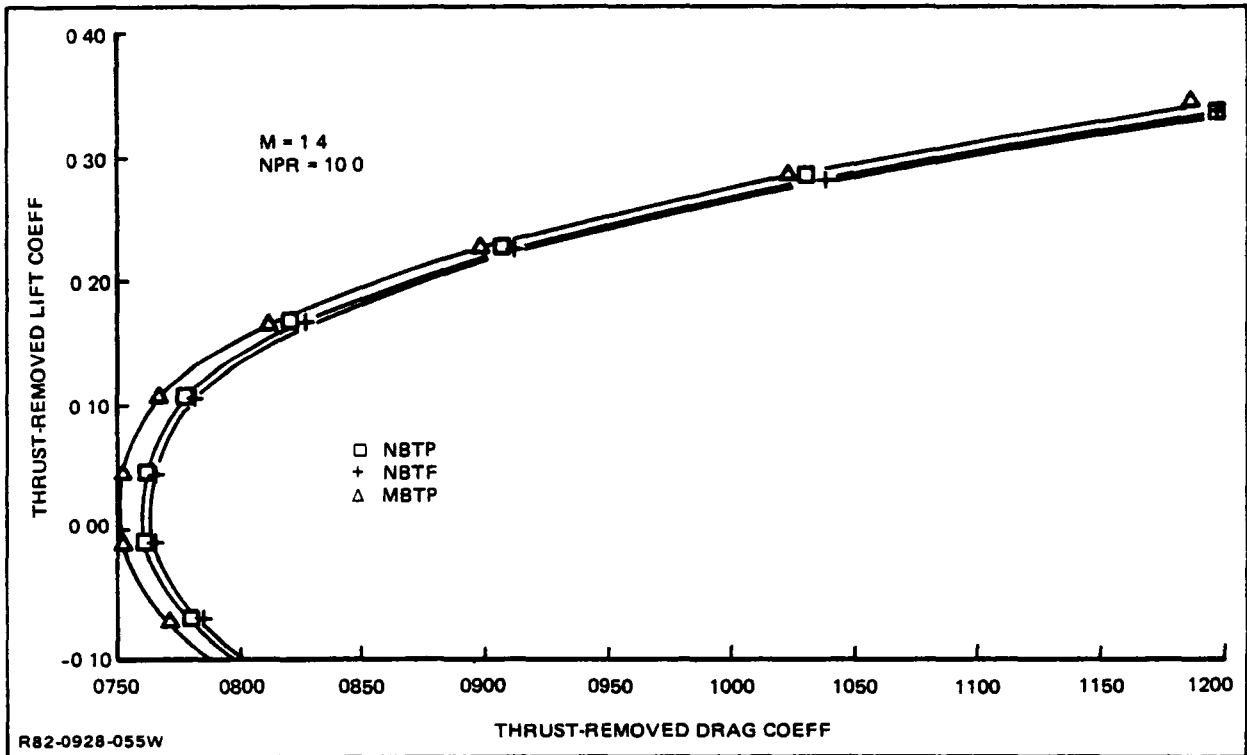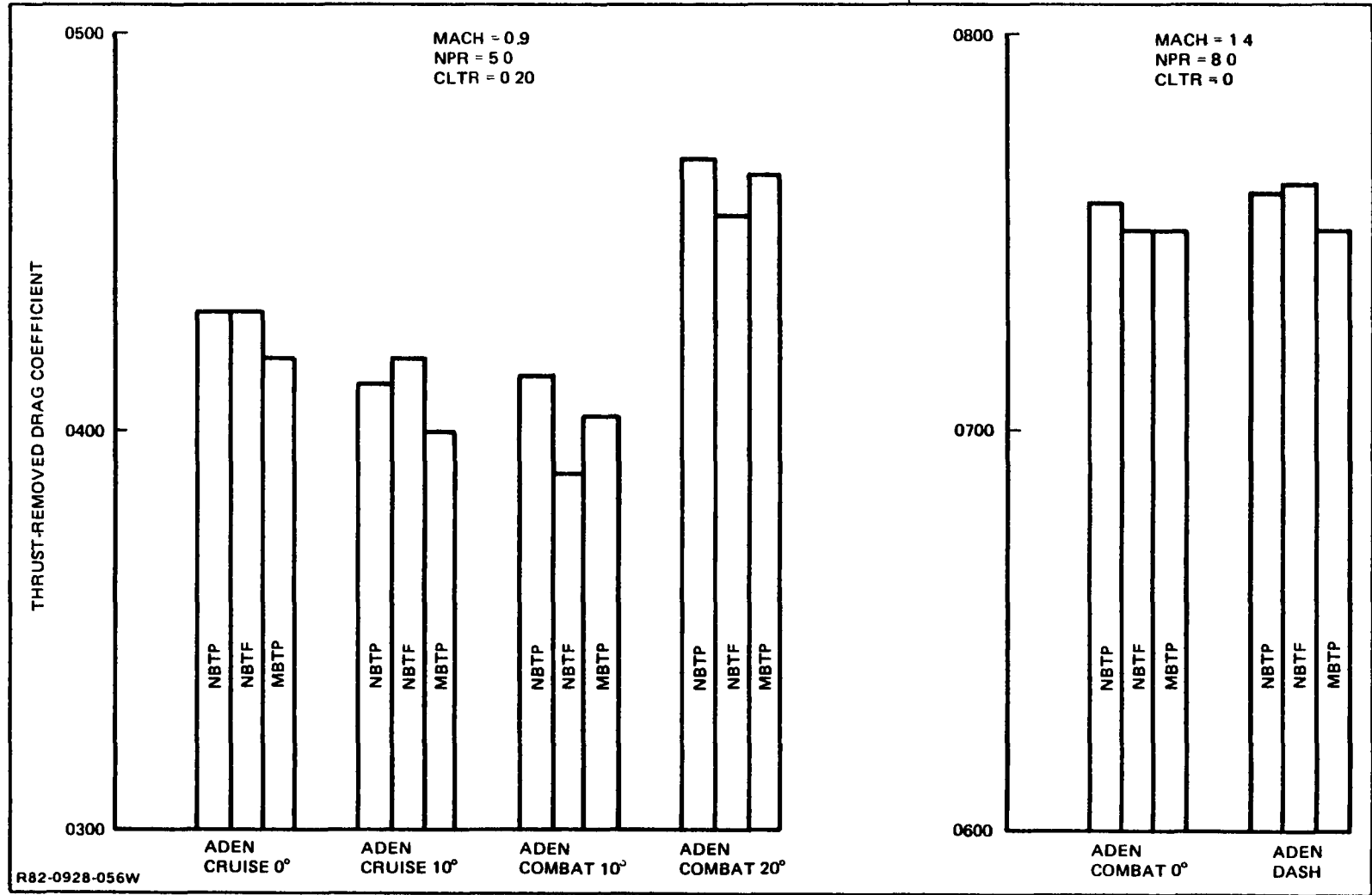
Drag	Method		
Position	NBTP	NBTF	MBTP
Lowest	16%	41%	43%
Middle	32%	22%	46%
Highest	52%	37%	11%
R82-0928-009W			

It could be concluded that the single F_i-Method (NBTF) should immediately be discarded because only 22% of the time does its drag appear in the desired middle position. Of the other two P_o-Methods, the one using the main balance (MBTP) clearly is the winner for it occupies the middle position much more frequently (46% vs 32%) and holds its worst extreme position less frequently (43% vs 52%).

This rudimentary analysis was only one element in the selection process. Other considerations are discussed below.

1. Method NBTF introduces large error at low nozzle pressure ratios (Ref. 2) due to the difficulty in fairing the very steep-sloped thrust characteristic (non-dimensionalized with ideal thrust) as nozzle pressure ratio is decreased towards unity.

2. In addition to the balance measurement, the NBTF method relies on the measurement of jet total pressure, jet total temperature, tunnel static pressure, and most important, mass flow. On the other hand, the two P_o -Methods only require a corresponding single measurement: tunnel static pressure. Thus the NBTF method can suffer from an accuracy problem. For example, the repeatability error in mass flow, typically exceeds ± 1%.

3. Utilization of the single nozzle balance hinges on the implicit assumption that the non-dimensional thrust characteristic developed by the left nozzle is applicable to the right nozzle. This is a good assumption as long as the nozzle flow paths are fabricated identically. But throat area measurements of some nozzles differed by up to 2 1/2% between left and right hand sides.

4. Good experimental practice dictates that the thrust which is removed should be measured by the same physical instrument as the thrust-minus-drag from which it is removed. Note that the NBTP and NBTF methods remove a static thrust that is based on nozzle balance measurements from the thrust-minus-drag measurement of the main aircraft balance. This allows for the possible existence of bias errors.

5. Furthermore, as explained in detail in subsection 6.7, the main balance axial force measurements required a post test correction for some configurations. Since this correction affected both static and wind-on runs, its effect tends to cancel in the MBTP method of calculating the thrust-removed parameters. Thus less risk is associated with the selection of the main balance static thrust rather than the nacelle balance thrust.

Based on the above observations in conjunction with the statistical study described previously it was concluded to utilize the MBTP method for final data reduction. Accordingly, all the data presented in Ref. 1 and 2 are based on main aircraft balance measurements using the P_o-Method.

6.13 IMPACT OF STATIC THRUST INPUT ERROR

The procedure to remove the static thrust components from the wind-on total parameters utilized "table look-ups". Extensive data files of almost 3000 individual numbers had to be developed for each of the 11 unique static thrust configurations involving three static thrust components and three static thrust methodologies (subsection 6.12) each. The clerical task involved in accurately handling and controlling such a huge data matrix posed a significant challenge because the potential for human error was high.

For example, a seemingly small error in inputting numbers from a faired static thrust curve into the table look-up could easily lead to large errors in the thrust-removed parameters. This is illustrated in Fig. 6-36 where less than a 0.01 error in normalized nozzle balance axial force (lbf per psfa) led to a .0070 error in drag coefficient (70 aircraft drag counts) as shown in Fig. 6-37. This is observed by comparing the erroneous drag based on nozzle balance thrust with the correct drag level based on main balance thrust.
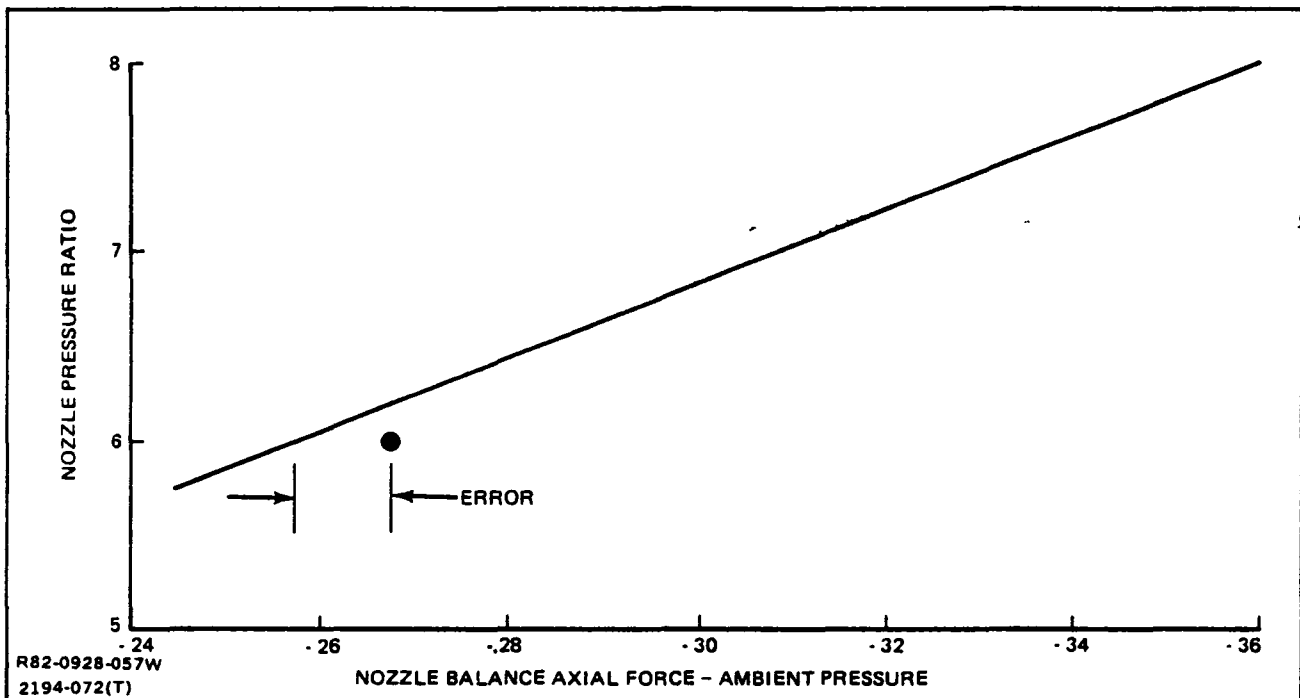
Fig. 6-36 Static Thrust Input Error Example

Such potential errors were completely eliminated from the final test results of Ref. 1 and 2 by developing a "triple-check" bookkeeping procedure and exercising great care in the development and implementation of the table look-ups.

6.14 TOTAL TEMPERATURE MEASUREMENT

A thermocouple was installed in both left and right hand nacelle ducts. The flow environment downstream of the tailpipe choke plates was very turbulent, and additionally the thermocouple wires were very thin gauge - at least two reasons making accurate total temperature measurements difficult.

Theoretically both left and right hand tailpipes must produce the same exhaust flow temperature because there is no thermodynamic mechanism to create an imbalance. These two thermocouple readings were not in agreement throughout the test generally differing by 0° - 40°R. Since neither measurement could be determined absolutely to be in error, it was decided that this disparity be resolved by averaging the two measurements so that the theoretical equality between left and right tailpipes was preserved.

6-42
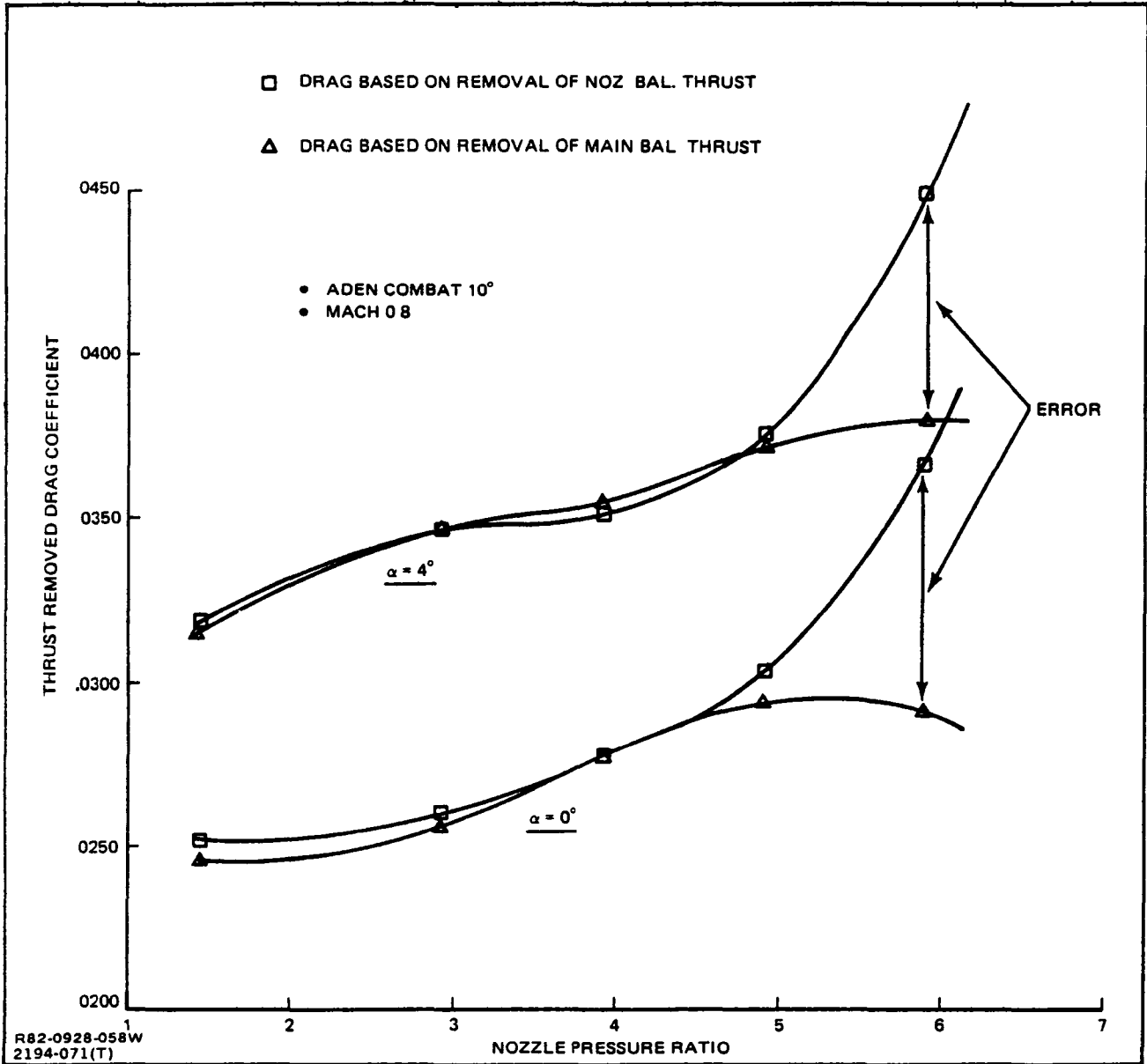
Fig. 6-37 Impact of Static Thrust Error on Drag

6-43

It is noted that for this test program the measurement of nozzle total temperature is secondary, being used only for ideal thrust and ideal mass flow. As explained in Ref. 2, the key thrust-removed parameters are obtained by employing the "P_o-Method" which is not dependent on ideal thrust and total temperature. Thus, this total temperature problem was of only minor significance.

7 - CONCLUDING REMARKS

This report emphasized the experimental aspects of the static and wind-on testing of V/STOL vehicle design jet-effects scale model employing a dual flow-through balance system. Some of the key items discussed are:

- Flow-through balance calibrations including bellows pressure tare corrections

- ASME nozzle thrust and mass flow calibrations including the assessment of force balance momentum tare corrections

- Static thrust calibrations of test nozzle configurations

- Alternative methodologies employed to obtain thrust-removed parameters

- Jet-effects test operation guidelines

- Data reduction procedures

- Test and data trouble-shooting techniques

- Test problems and solutions.

In particular, some of the major problem areas requiring solutions were:

- Total pressure measurement

- Force balance grounding

- Model weight bias determination and implementation in data reduction

- Force balance shift assessment.

This experimental investigation, which has contributed to the aeropropulsion V/STOL data base, has also led to the documentation of significant jet-effects testing techniques that will be useful to future investigations.

8 - REFERENCES

1. Schnell, W. C., and Ordonez, G. W., "Axisymmetric and Non-Axisymmetric Exhaust Jet Induced-Effects on a V/STOL Vehicle Design" (Part I: Data Presentation), NASA CR 166146, May 1981.

2. Schnell, W. C., "Axisymmetric and Non-Axisymmetric Exhaust Jet Induced-Effects on a V/STOL Vehicle Design" (Part II: Analysis of Results), NASA TM 1344 July 1982.

3. Hoff, G., "Installed Performance of the 2-D ADEN on an Advanced Multimission V/STOL Fighter Aircraft Model", General Electric Co. Report No. R76AEG468.

4. Schnell, W. C., and Grossman, R. L., "Wind Tunnel Test of a Propulsive Lift Enhancement Model", AFFDL-TR-78-104, August 1978.

5. Baker, D. C., "Asymmetric Nozzle Performance Data at Mach Numbers from 0.6 to 1.5," Arnold Engineering Development Center Report No. AEDC-DR-77-88, September 1977.

1 Report No. NASA CR 166147	2. Government Accession No	3 Recipient's Catalog No
4 Title and Subtitle AXISYMMETRIC & NON-AXISYMMETRIC EXHAUST JET INDUCED-EFFECTS ON A V/STOL VEHICLE DESIGN (PART III: EXPERIMENTAL TECHNIQUE)		5. Report Date June 1982
		6. Performing Organization Code
7 Author(s) William C. Schnell		8. Performing Organization Report No
9 Performing Organization Name and Address Grumman Aerospace Corporation Bethpage, NY 11714		10 Work Unit No
		11 Contract or Grant No NAS2-9887
12 Sponsoring Agency Name and Address National Aeronautics and Space Administration Washington, D.C. 20546		13 Type of Report and Period Covered Contract Report
		14 Sponsoring Agency Code

15. Supplementary Notes

Point of Contact: D. B. Smeltzer, M.S. 227-2, NASA Ames Research Center Moffett Field, CA 94035
Phone: FTS 448-5858, 415-965-5858

16 Abstract

A wind tunnel investigation, sponsored by the NASA Ames Research Center, was conducted to determine the jet induced effects of several exhaust nozzle configurations (axisymmetric, and vectoring/modulating varients) on the aeropropulsive performance of a twin-engine V/STOL fighter design. A 1/8 scale model was tested in the NASA Ames 11 ft transonic tunnel at static conditions and over a range of Mach numbers from 0.4 to 1.4. This report is the third in a series of three reports covering this comprehensive wind tunnel investigation of approximately 2.000 test points. The first report, Part I: Data Presentation (Ref. 1), presents the model geometry and the entire set of test data (static and wind-on) in graphical form. The second report, Part II: Analysis of Results (Ref. 2), thoroughly analyzes and interprets the test results and presents highlights of each major data study. This third report, Part III - Experimental Technique, discusses the experimental aspects of the static and wind-on test programs. In particular the following subjects are emphasized: jet-effects test techniques in general, flow-through balance calibrations and tare force corrections, ASME nozzle thrust and mass flow calibrations, test problems and solutions.

17 Key Words (Suggested by Author(s)) Exhaust Nozzle Jet-induced Effects Vectoring (thrust)	18. Distribution Statement Unlimited Subject Category 02
19 Security Classif (of this report) Unclassified	20. Security Classif (of this page) Unclassified

19 Security Classif (of this report) Unclassified	20. Security Classif (of this page) Unclassified	21 No of Pages	22. Price*

End of Document